11114

NATIONAL LIBRARY
OTTAWA

BIBLIOTHÈQUE NATIONALE
OTTAWA

CANADA

NAME OF AUTHOR... *George J. Besserer*

TITLE OF THESIS... *THE USE OF REFRACTIVE INDEX MEASUREMENTS... IN HIGH PRESSURE VAPOR-LIQUID EQUILIBRIUM STUDIES*

UNIVERSITY.. *UNIVERSITY OF ALBERTA*

DEGREE FOR WHICH THESIS WAS PRESENTED...... *Ph. D.*

YEAR THIS DEGREE GRANTED........ *1972*

Permission is hereby granted to THE NATIONAL LIBRARY

OF CANADA to microfilm this thesis and to lend or sell copies

of the film.

The author reserves other publication rights, and

neither the thesis nor extensive extracts from it may be

printed or otherwise reproduced without the author's

written permission.

(Signed) *George J. Besserer*

PERMANENT ADDRESS:

#112 7835 159 ST

Edmonton, Alberta

DATED. *May 3* 19 *72*

NL-91 (10-68)

THE UNIVERSITY OF ALBERTA

THE USE OF REFRACTIVE INDEX MEASUREMENTS

IN HIGH PRESSURE VAPOR-LIQUID

EQUILIBRIUM STUDIES

by

Ⓒ GEORGE RAYMOND JOSEPH BESSERER

A THESIS

SUBMITTED TO THE FACULTY OF GRADUATE STUDIES AND RESEARCH

IN PARTIAL FULFILMENT OF THE REQUIREMENTS FOR THE DEGREE

OF DOCTOR OF PHILOSOPHY

DEPARTMENT OF CHEMICAL AND PETROLEUM ENGINEERING

EDMONTON, ALBERTA

SPRING, 1972

UNIVERSITY OF ALBERTA

FACULTY OF GRADUATE STUDIES AND RESEARCH

The undersigned certify that they have read, and recommend
to the Faculty of Graduate Studies and Research for acceptance, a thesis
entitled THE USE OF REFRACTIVE INDEX MEASUREMENTS IN HIGH PRESSURE VAPOR-
LIQUID EQUILIBRIUM STUDIES submitted by GEORGE RAYMOND JOSEPH BESSERER in
partial fulfilment of the requirements for the degree of Doctor of
Philosophy.

....
Supervisor

....

....

....

....

....

Date...Jan. 7, 1972...

ABSTRACT

A high pressure apparatus has been developed for measuring refractive indices and compositions of coexisting phases in vapor-liquid equilibrium. The mixture to be studied is contained between two pistons which are connected hydraulically to an opposed transmission motorized Ruska pump. This allows the pistons to be moved up and down simultaneously while maintaining the volume between them constant. In the center of the cell a pyrex window and a steel mirror form a $30°$ prism shaped cavity. The refractive index of the fluid in the cavity is measured by knowing the prism angle and measuring the deviation angle of a beam of light from an autocollimating telescope. The optical system design is such that the only moving part is the telescope and the deviation angle is automatically the minimum deviation angle. Small samples are taken from either of two micrometering sampling valves and analyzed by gas chromatography.

The equipment and method were evaluated by comparison of the molar volumes calculated from the refractive index with those obtained by direct volumetric measurement for the n-butane-carbon dioxide system at $100°F$.

The compositions and refractive indices of the coexisting vapor and liquid phases of the i-butane-carbon dioxide and i-butane-ethane systems were determined in the temperature range $100°F$ to $250°F$. The pressure range extended from the vapor pressure of i-butane to the critical regions of the systems. The molar volumes of the phases were calculated from their measured refractive indices and their molar average refractivities. The thermodynamic consistency of the data was tested.

The refractive indices of carbon dioxide, ethane and liquid i-butane were determined in the temperature range 100° to 250°F up to a pressure of 1500 psia.

TO MY WIFE

STARLEEN

ACKNOWLEDGEMENTS

TABLE OF CONTENTS

Table of Contents (cont'd)

LIST OF TABLES

List of Tables (cont'd)

LIST OF FIGURES

List of Figures (cont'd)

I - INTRODUCTION

Data on the composition of equilibrium vapor and liquid phases of hydrocarbon and many other systems have been obtained by several different methods in a variety of different experimental cells. Only rarely, however, have data on phase compositions been obtained simultaneously with density data. Aside from being of interest in themselves, the coexisting phase density data are useful in several other ways. They are a valuable asset in the evaluation of vapor-liquid equilibrium prediction methods. With equations of state, for example, the phase density data are used to calculate the component fugacities and partial molar volumes. Also, the phase density data are an intrinsic part of the enthalpy and entropy departure calculations.

The residual transport properties, residual thermal conductivity and residual viscosity, appear to be well correlated to density. Therefore, knowledge of coexisting phase densities can be used to estimate their viscosities and thermal conductivities. This work was undertaken therefore to produce a convenient and accurate method for obtaining both composition and density data at elevated pressures on coexisting vapors and liquids.

The refractive index was chosen as a means for accomplishing this because this property can be measured easily and accurately, and it is related quantitatively to the density. Accordingly, a cell was designed which was capable of attaining equilibrium and of allowing the compositions and the refractive indices of the phases to be measured with convenience and accuracy.

The n-butane-carbon dioxide system at 100°F was chosen to evaluate the performance of the cell and the method. Two previously

unreported systems, the i-butane-ethane system and the i-butane-carbon dioxide system, were then studied in the temperature range 100°F to 250°F at pressures extending from the vapor pressure of i-butane to the critical regions of the systems. The densities of the phases were calculated from their measured compositions and refractive indices.

The cell may also be used to determine single phase refractive indices. The refractive indices of carbon dioxide, ethane and liquid i-butane were determined in the temperature range 100° to 250°F up to a pressure of 1500 psia.

II - RELATIONSHIP OF REFRACTIVE INDEX TO DENSITY

For a given substance the refractive index is a property which is closely related to the density. The first formula expressing this relationship was put forward by Newton in 1704, and since then a number of empirical and semi-empirical formulae have been proposed. Both Batsanov[1] and Partington[2] have reviewed this historical development. Hill, Vaughan, Price and Davies[3] have presented a comprehensive treatment of how dielectric properties and refractive index are related to molecular behavior.

A list of the more important refractivity formulae is given below:

1) Newton-Laplace (1704,1806)

$$\frac{1}{\rho} \cdot (n^2 - 1) = \text{constant} \qquad 1.01$$

2) Beer-Gladstone-Dale (1853,1863)

$$\frac{1}{\rho} \cdot (n - 1) = \text{constant} \qquad 1.02$$

3) Lorentz-Lorenz (1880)

$$\frac{1}{\rho} \cdot \frac{n^2 - 1}{n^2 + 2} = \text{constant} \qquad 1.03$$

4) Edwards (1894)

$$\frac{1}{\rho} \cdot \frac{n - 1}{n} = \text{constant} \qquad 1.04$$

3

5) Zecchini (1895)

$$\frac{1}{\rho} \cdot \frac{n^2 - 1}{n^3 + 2} = \text{constant} \qquad \qquad 1.05$$

6) Eykmann (1895)

$$\frac{1}{\rho} \cdot \frac{n^2 - 1}{n + 0.4} = \text{constant} \qquad \qquad 1.06$$

7) Lichtenecker (1926)

$$\frac{1}{\rho} \cdot (\log n) = \text{constant} \qquad \qquad 1.07$$

8) Macdonald (1926)

$$\frac{1}{\rho} \cdot \frac{n^2 - 1}{n} = \text{constant} \qquad \qquad 1.08$$

The simplest formula, Beer-Gladstone-Dale, holds reasonably well over a wide density range. This is exemplified in Figure 1 which shows a plot of refractive index versus density for the data of Michels et al on ethylene[4], carbon dioxide[5], and nitrogen[6] at pressures up to 2000 atm. The Lorentz-Lorenz refractivity, however, is the soundest expression relating the refractive index to the density because it is the only formula which can be related to the polariz-ability of the molecule.

If an electric field, F, acts on a molecule the average moment induced will be proportional to the field provided that the field is not extraordinarily large.
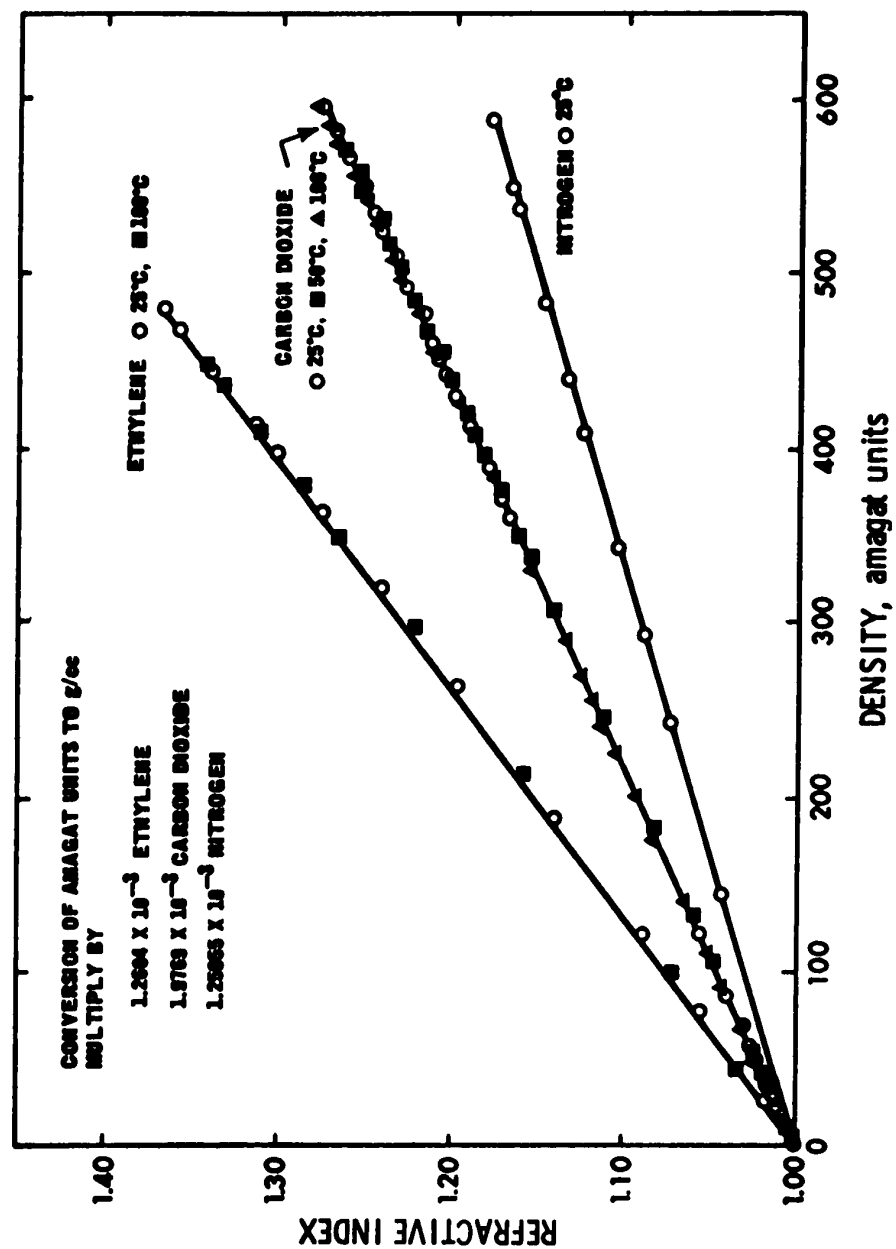
FIG. 1   RELATIONSHIP OF REFRACTIVE INDEX TO DENSITY FOR ETHYLENE, CARBON DIOXIDE AND NITROGEN

$$m = \alpha_T F \qquad\qquad 1.09$$

The constant of proportionality is called the polarizability of the molecule and is the sum of the electronic, the atomic, and the orientation polarizabilities.

$$\alpha_T = \alpha_e + \alpha_a + \alpha_o \qquad\qquad 1.10$$

The electronic contribution arises from the electric field causing a displacement of the electrons relative to the nucleus in each atom; the atomic contribution from a displacement of the atomic nuclei relative to one another; and the orientation contribution from the tendency of the electric field to align molecules with permanent dipole moments parallel to itself.

Each of the three types of polarizability is a function of the frequency with which the applied field is altered. In a steady field all three types are at their equilibrium values. When the field is altered with a frequency in the range of 10^{10} to 10^{12} cycles per second the orientation polarizability fails to attain its equilibrium value and at higher frequencies no longer contributes to the total polarizability. At infra-red frequencies, 10^{13} to 10^{14} cycles per second, the atomic polarizability fails to attain its equilibrium value leaving only the electronic polarizability effective in the visible and ultraviolet regions of the spectrum, 10^{14} to 10^{15} cycles per second.

The Lorentz-Lorenz formulation is given by Equation 1.11

$$R_{LL} = \frac{M}{\rho} \frac{n^2 - 1}{n^2 + 2} = \frac{4\Pi N}{3\epsilon} \alpha_e = \text{constant} \qquad 1.11$$

Experimentally the Lorentz-Lorenz refractivity is not exactly constant but increases slightly with increasing density passing through a maximum and declining thereafter. This behavior is exemplified in Figure 2 which shows a plot of R_{LL} versus density for Michels and Hamers'[5] data on carbon dioxide at 99.7°C.

Several theories have been put forward to account for these variations. For anisotropic molecules Raman and Krishnan[7] deduced that there would be an asymmetric distribution of the polarizable matter surrounding any given molecule in the medium, rather than a spherical one as assumed in Lorentz-Lorenz formulation. As a consequence, the anisotropic nature of the polarization field will increase with the molar density causing a progressive variation of R_{LL}. Kirkwood[8] and Yvon[9] showed that even for spherical molecules the polarization field fluctuates with the thermal motion of the molecules and produces a fluctuating induced moment the magnitude of which increases with increasing density.

Mazur and Mandel[10] and Jansen and Mazur[11] used a quantum mechanical approach and found that the polarizability should vary with density, increasing when attractive forces are dominant and decreasing when repulsive forces are dominant. Buckingham and Pople[12] also used a quantum mechanical approach and proposed that R_{LL} could be represented by a virial expansion in molar volume, namely

$$R_{LL} = R_{LL}^0 + B/V + C/V^2 \qquad 1.12$$
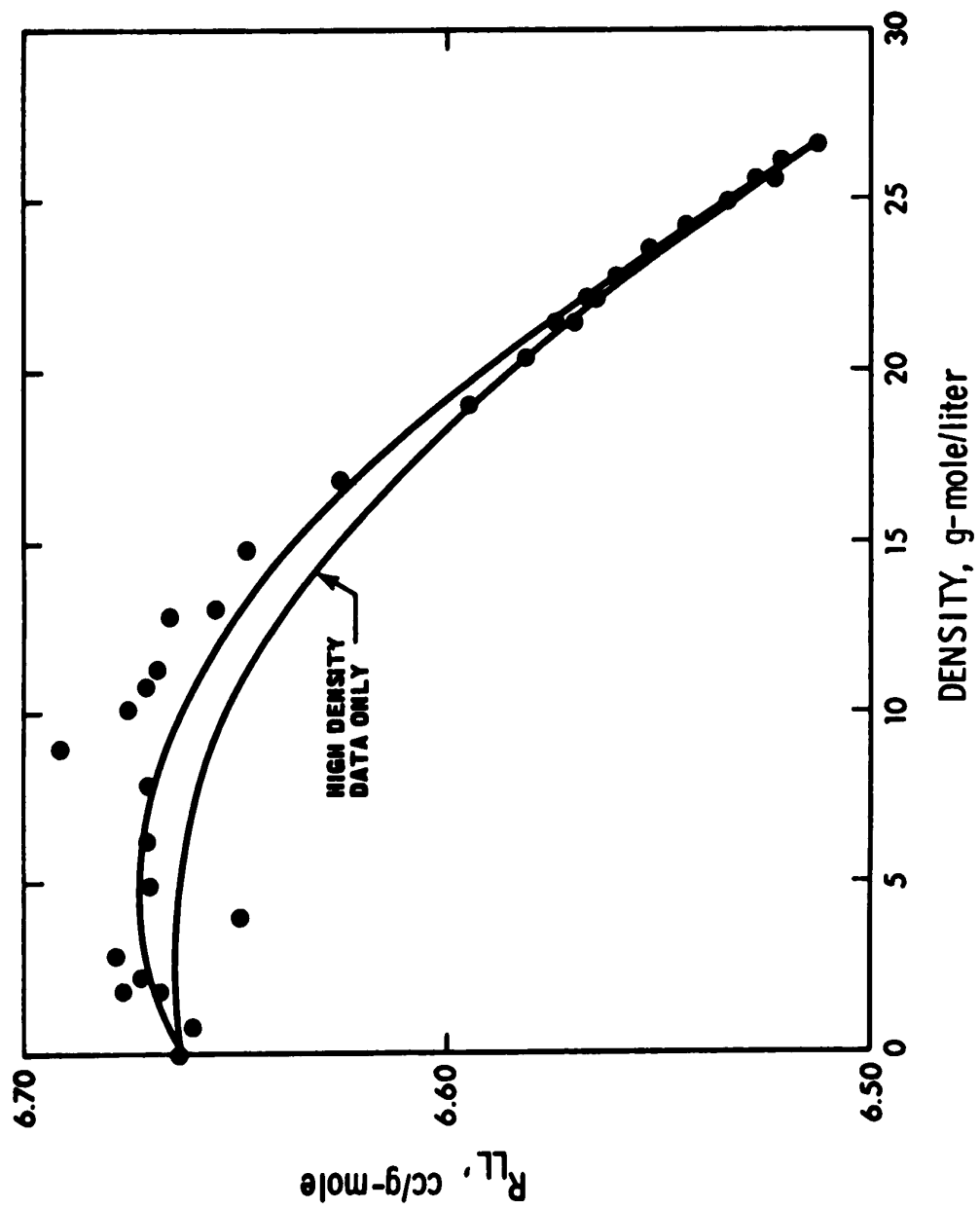
FIG. 2   VARIATION OF THE LORENTZ-LORENZ REFRACTIVITY WITH DENSITY FOR
CARBON DIOXIDE AT 99.7°C

where R_{LL}^0 is the limit of the molar refractivity at zero density, and B and C are the second and third virial refractivity coefficients respectively. A plot of $(R_{LL}-R_{LL}^0)V$ versus $1/V$ of Michels and Hamers[5] data for carbon dioxide is shown in Figure 3, where R_{LL}^0 for carbon dioxide was obtained from Stoll's[13] low pressure data. B and C are obtained from the intercept and slope respectively.

In the visible region of the spectrum the effect of frequency on R_{LL} can be adequately represented by making only R_{LL}^0 a function of wavelength, since, within experimental error, B and C are independent of wavelength. Figure 4 shows the effect of wavelength on R_{LL}^0 for CO_2.
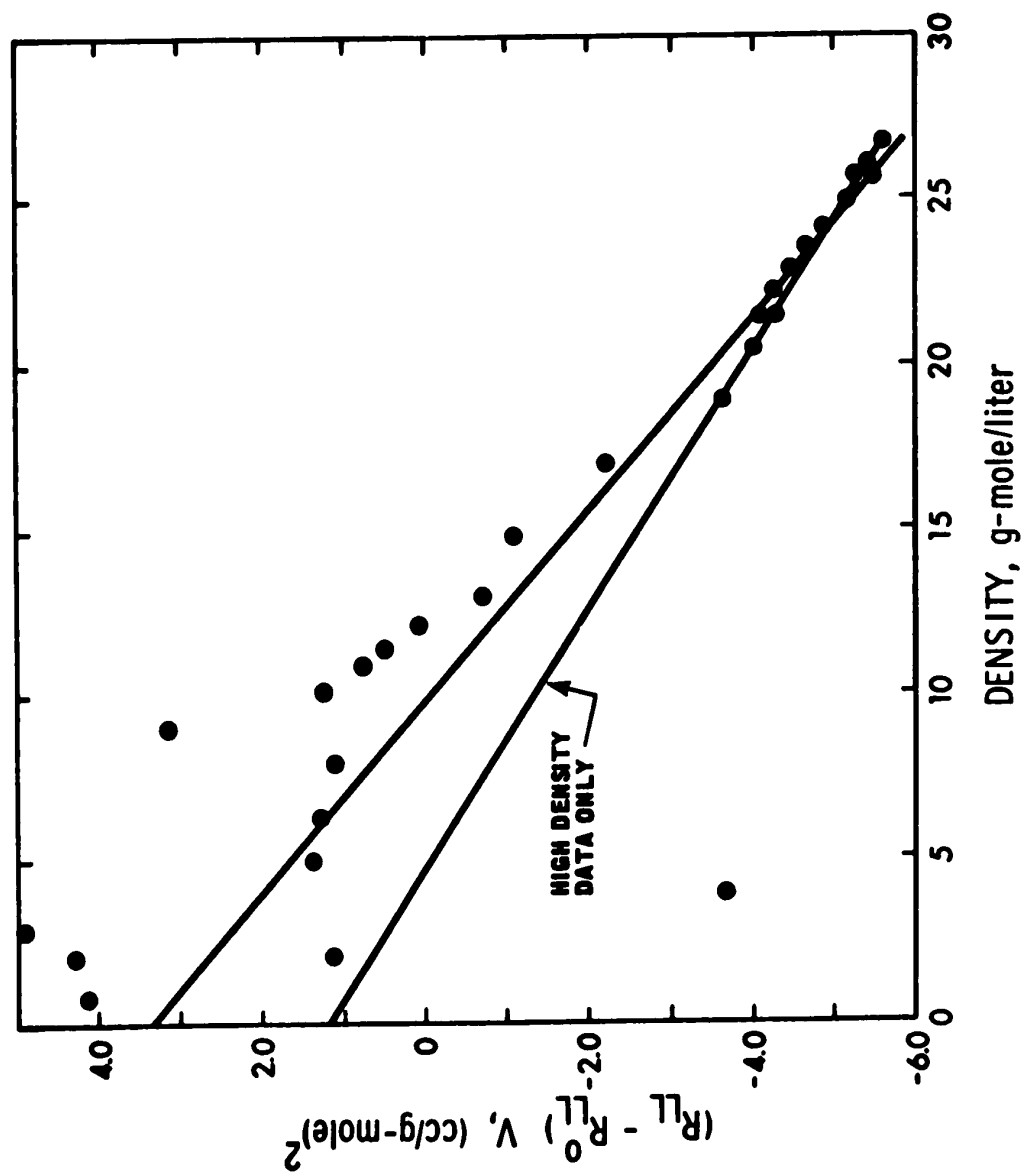
FIG. 3   DETERMINATION OF THE SECOND AND THIRD REFRACTIVITY VIRIAL
COEFFICIENTS FOR CARBON DIOXIDE AT 99.7°C
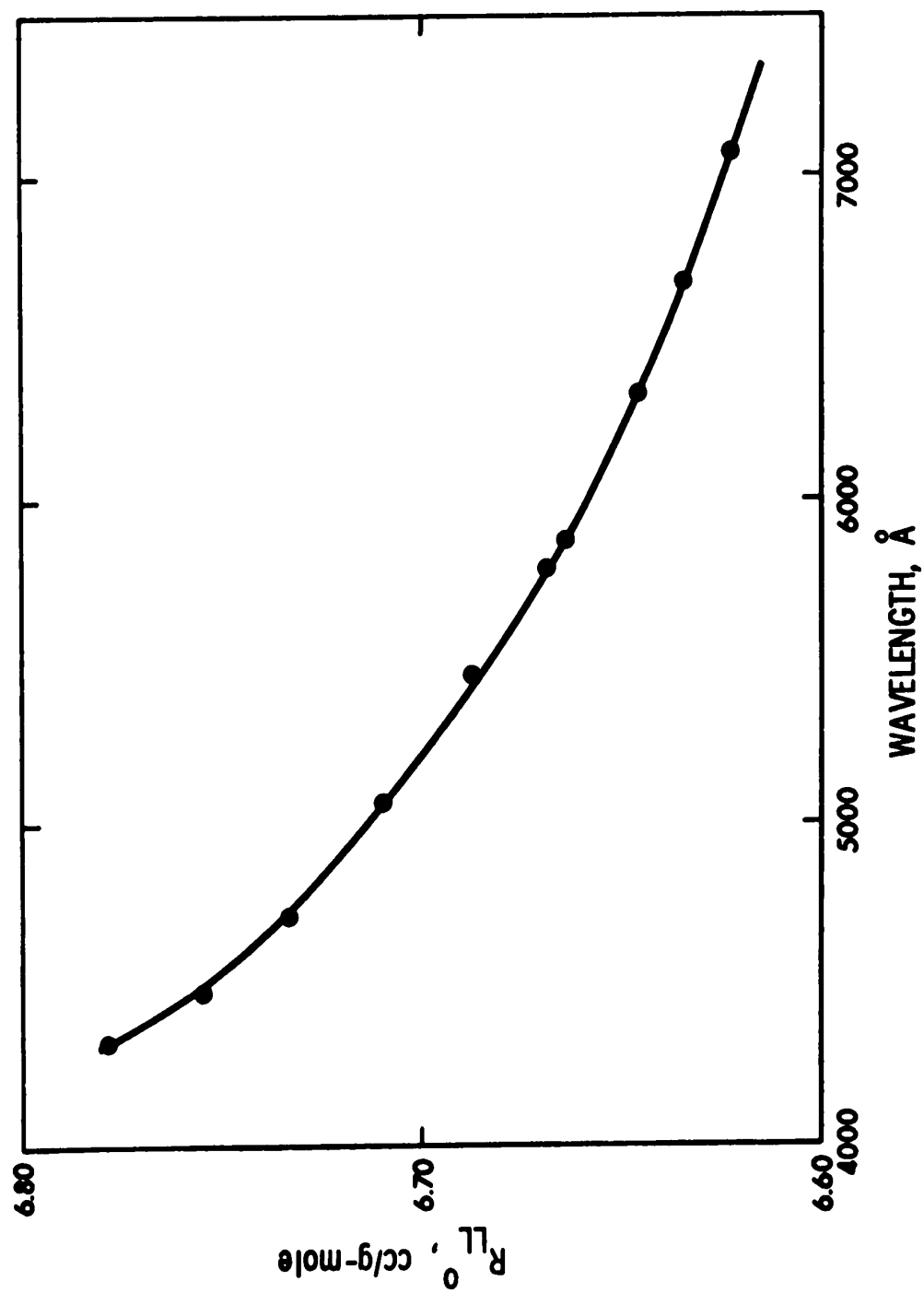
FIG. 4   VARIATION OF THE CARBON DIOXIDE LOW DENSITY REFRACTIVITY WITH WAVELENGTH

III - METHODS OF MEASURING REFRACTIVE INDEX

There are four means by which the refractive index of a fluid can be measured:

    a. Spectrometry

    b. Interferometry

    c. Critical angle refractometry

    d. Immersion

Spectrometers

A spectrometer is used to measure the minimum angle through which a beam of monochromatic light is deviated by a prism shaped sample of the fluid. Figure 5 shows a prism in the position of minimum deviation. In this position the angle of incidence and the angle of emergence are equal:

$$i_i = i_o = i \qquad\qquad 3.01$$

The refraction angles are equal to each other and one half the prism apex angle, A:

$$r_i = r_o = A/2 \qquad\qquad 3.02$$

The angle of incidence is equal to one half the apex angle plus the minimum deviation angle, D:

$$i = 1/2 \ (A + D) \qquad\qquad 3.03$$

From Snell's law of refraction

12
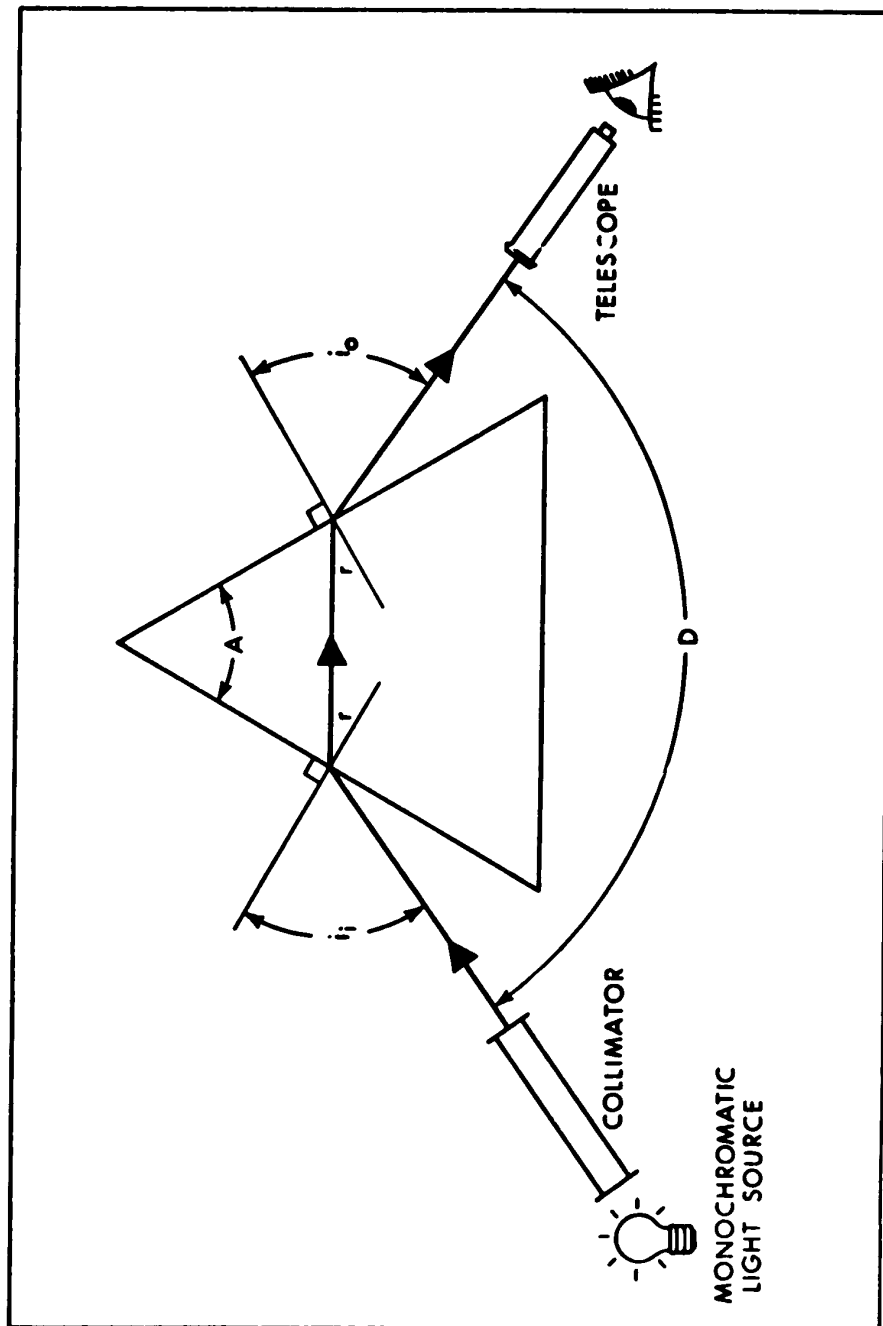
FIG. 5   SCHEMATIC REPRESENTATION OF A SPECTROMETER IN THE POSITION OF MINIMUM DEVIATION ANGLE

$$n_1 \sin i = n_2 \sin r \qquad\qquad 3.04$$

where n_1 is the refractive index of air and n_2 the refractive index of the prism material, it follows that

$$n_2 = n_1 \frac{\sin 1/2(A + D)}{\sin 1/2(A)} \qquad\qquad 3.05$$

Interferometers

An interferometer or étalon consists of two thin plates separated by a distance d. A slitted beam of monochromatic light of wavelength λ is sent to the interferometer and the interference rings produced are observed in the focal plane of the objective lens of a telescope.

The measurement of the refractive index is usually carried out in the following manner. The space between the plates is first evacuated and the interference pattern observed. The gas whose refractive index is to be measured is slowly let into the region containing the étalon. The number of interference fringe shifts, k, are counted. The refractive index of the gas between the plates can thus be obtained from the formula

$$n - 1 = \frac{k\lambda}{2d} \qquad\qquad 3.06$$

Critical Angle Refractometers

The Abbe and Pulfrich refractometers are two types of commercial refractometer which use the angle at which total internal reflection

occurs for light passing from glass to a liquid on its surface. From Snell's law and Figure 6 it follows that:

$$n_3 = n_2 \frac{\sin B}{\sin \pi/2} = n_2 \sin B \qquad 3.07$$

where n_3 is the refractive index of the liquid n_2 the refractive index of the glass and B the critical angle.

Immersion Methods

The immersion method is based on the disappearance of an interface between two immiscible fluids or a fluid and a solid when their refractive indices are equal. If the refractive index of one of the phases is known then the other is also known.
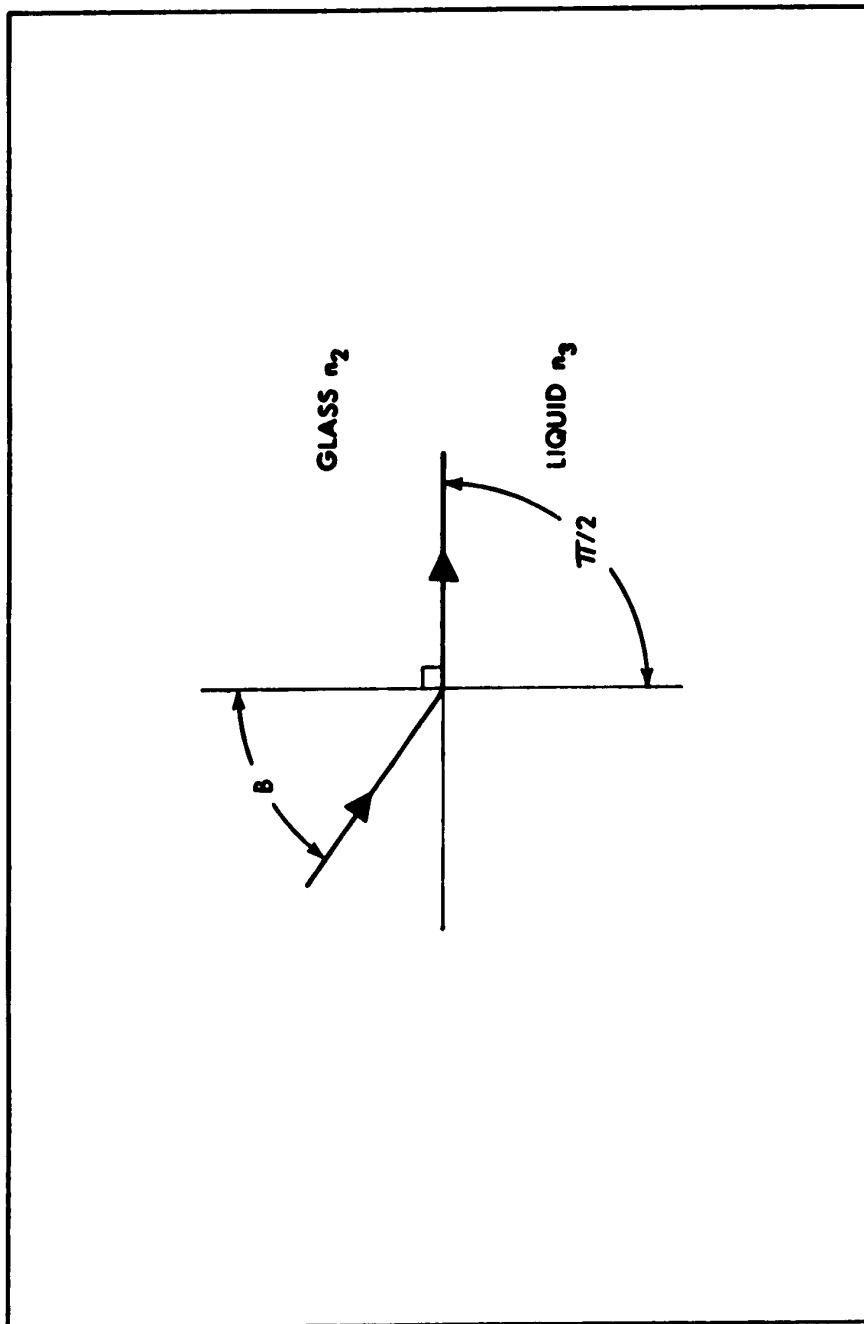
FIG. 6   SCHEMATIC REPRESENTATION OF THE CRITICAL ANGLE OF REFRACTION

IV - HIGH PRESSURE REFRACTOMETERS

Several high pressure refractometers have been built using the minimum deviation angle principle. Examples of these are described by Lyons and Poindexter[14], Poulter et al[15], Smith[16], Schmidt and Thomas[17], and Teague and Pings[18]. In all cases a separate collimator and telescope were used and no means of mixing the cell contents were employed.

Interferometers have been used frequently to measure refractive indices at high pressures. Examples of these are described by Siertsema[19], Ayres[20], Phillips[21], Himstedt and Wertheimer[22], Eisele[23], Opladen[24], Michels et al[4,5,6], Belonogov and Gorbunkov[25,26], Diller[27,28], and Sliwinski[29].

The critical angle and immersion techniques have had limited application at elevated pressures. Bellingham and Stanley Limited (London, England) have a pipe refractometer which is capable of operating at pressures up to 150 psi. Francis[30] used the immersion principle to obtain refractive indices of many liquified gases at elevated pressures. He determined the iso-optic temperature of the liquified gas and an immiscible fluid, such as brine, sealed in a thick-wall glass tube. The refractive index of the immiscible fluid was known or could be measured easily and therefore the refractive index of the liquified gas at the iso-optic temperature was known.

Several unique high pressure refractometer designs have been described in the literature. The optical system for measuring the refractive index of a fluid in a capillary tube was described by Melville and Watson[31]. A similar type of system, the capillary projection method, was later used by Deryagin et al[32] and Konstantinov

et al[33]. A refractometer consisting of a coiled pyrex rod, a constant intensity light source, and a photoelectric detector was described by Shaw and Johnson[34]. The loss of intensity of the light shone in one end of the rod and measured at the other was found to be directly proportional to the refractive index of the fluid in which the coiled rod was immersed. A high pressure refractometer design employing an internal rotating glass prism and no other moving parts has been described by Vukalovich et al[35].

In this study, a high pressure refractometer was designed based on the minimum deviation angle principle. The optical system differs somewhat from previous designs in that the only moving part is an autocollimating telescope and the measured angle is automatically the minimum deviation angle.

V - PREVIOUS WORK

A number of experimental studies have been made to determine the relationship between density and refractive index. These studies have frequently involved a lighter gaseous substance which is confined and then compressed so that the refractive index can be obtained over a range of densities. Measurements of this kind have been carried out on hydrogen[20,25,27], deuterium[28], helium[36], argon [18,37-42], xenon[43], krypton[44], nitrogen[6,20], oxygen[20], air[19,24,45], carbon dioxide[5,17, 19-21,24,30,35,38,45-47], ethylene[4,25,48,49], methane[37,49], tetra-fluoromethane[37], water[32,50,51], ammonia[25,52], ethane[29,30,53], propane [29,30,53-55], butane[29,30,53,54], hydrogen sulfide[30,39], and 1-pentane[56].

The refractive index and density of compounds which are liquids at or near ambient conditions has been studied extensively. A good review of these has been presented by Timmermans[57,58].

VI - MIXTURES AND THE ADDITIVITY OF THE
LORENTZ-LORENZ REFRACTIVITIES

The assumption that the Lorentz-Lorenz refractivities are additive in mixtures can be justified by the near additivity found in a large number of mixtures and by the manner in which atomic and radical refractivities can be summed to give molecular refractivities. Smyth, Engel, and Wilson[59] studied the refractive index and density of twelve binary liquid mixtures. Their study included systems such as carbon tetrachloride-acetone and n-heptane-ethyl iodide, covering their full compositional ranges. In every case the maximum deviation from additivity was less than 0.1 percent. Bloom and Rhodes[60] showed that the refraction of molten salts are close to the refraction of the salts in aqueous solution and also that the refraction of molten mixtures follow the law of additivity within experimental error. Young and Finn[61] found that in glasses the refractivities are additive to within $\pm$ 0.1 percent.

Recently Burfield, Richardson and Guereca[62] used dielectric constant measurements and a molar average Clausius-Mosotti function (the dielectric constant replaces n^2 in Equation 1.03) to calculate coexisting phase densities in the helium-carbon dioxide system. Their results compared favorably with previous volumetric measurements.

Keilich[63] in a theoretical study of molar refractivities of dense mixtures has shown that R_{LL} is strictly additive only in the case of perfect gases. The non-additive terms were found to be functions of the polarizabilities, molecular symmetry and dipole moment of the molecules and the density of their mixture.

Although the existence of non-additive terms appears to be well founded in theory, experimentally these terms have been shown to be rather small. In the study of high pressure phase equilibria the compositions of the phases can usually be measured to within $\pm$ 0.3 mole percent, with some improvement at the extreme composition ends. When the refractive index is used to calculate the equilibrium phase molar volumes, this and the associated errors in the measurement of temperature and pressure will make the error due to the non-additive terms small in comparison. Also, the measurement of the refractive indices of the equilibrium phases can be made conveniently and accurately which is generally not the case when direct volumetric measurements are attempted.

VII - EQUIPMENT DESIGN

A schematic diagram of the apparatus and its associated equipment is shown in Figure 7 and the essential features of the cell design are shown in Figure 8. It has an overall length of 48 cm. and was machined from a 10 cm. diameter type 316 stainless steel cylinder. The cell proper consists of three parts, two cylinder-piston end sections and a central windowed section. The three sections are bolted together with the high pressure seals between them made by flattened teflon O-rings. Each piston has a 10 cm. travel and is confined to its respective cylinder. The function of the pistons is to isolate the cell contents from the hydraulic fluid, a low viscosity silicone oil, and to provide a means for varying the cell volume. The piston seal is effected by four O-rings, one teflon and three neoprene.

The horizontal section A-A through the center of the cell shows how the window, a pyrex glass disk 2.9 cm. in diameter and 2.5 cm. thick with its faces flat and parallel to $\pm 10^{-4}$ cm., and a type 316 stainless steel mirror form the boundaries of a 30° prism. The window and mirror are held in place by bolted cover plates and sealed against lapped surfaces with 1.5 mm. thick glass-filled teflon gaskets. A 316 stainless steel sheathed iron-constantan thermocouple has its tip exposed to the fluid forming the prism.

A second horizontal section B-B shows one of the sampling valves, the pressure transducer port and the circulation line outlet. The sampling valves are internally mounted Circle Seal MV-92 micro-metering valves with provision made for flushing out and evacuation of the low pressure sampling lines. The circulation system used to

23
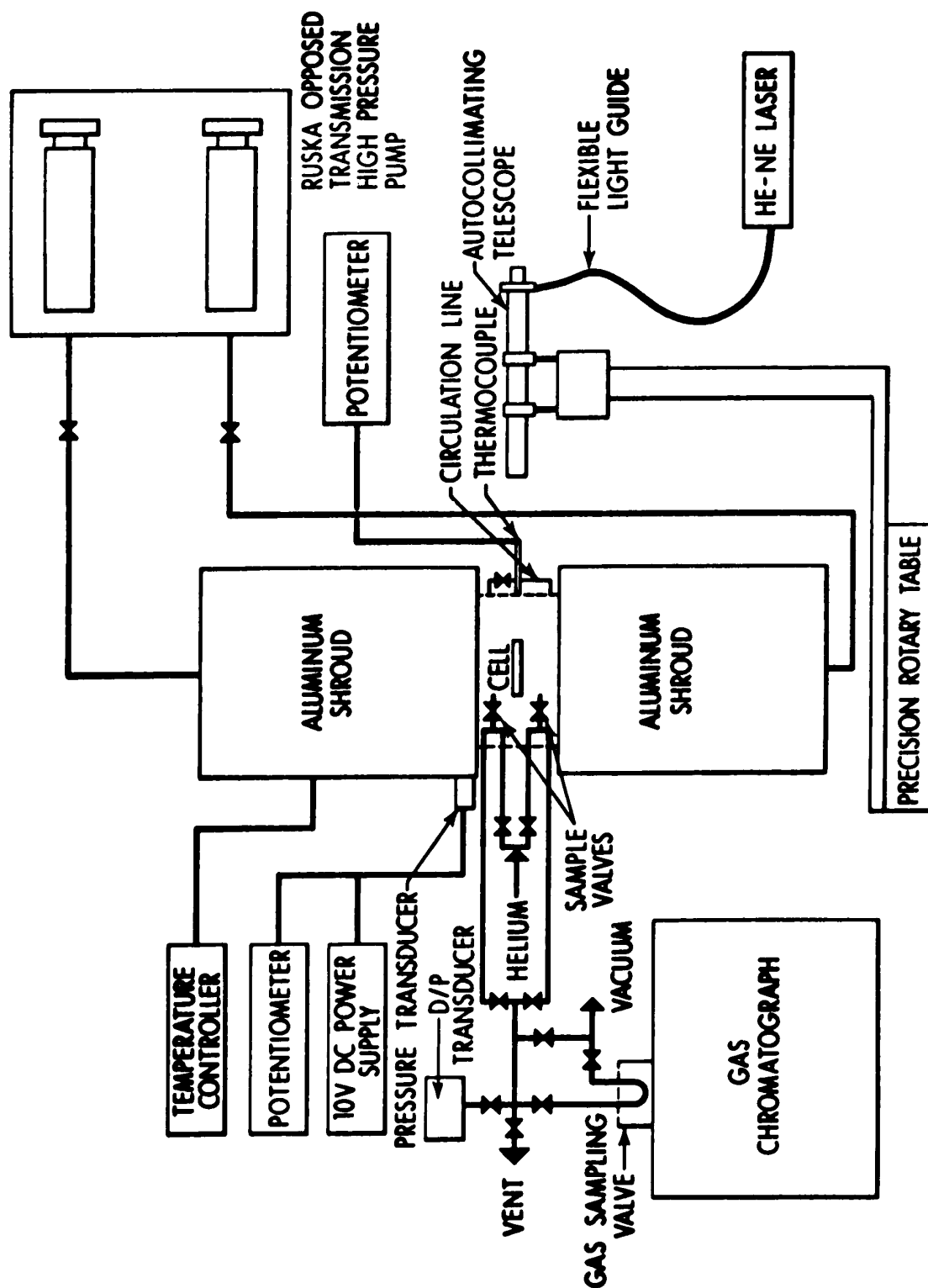
FIG. 7   SCHEMATIC DIAGRAM OF THE EQUILIBRIUM CELL AND ITS ASSOCIATED EQUIPMENT

COOLING COIL

STRIP HEATER

ALUMINUM ENVIRONMENTAL SHROUD

MOUNTING BOLT SLOT

UPPER PISTON

HYDRAULIC FLUID CONDITIONING COIL

SAMPLE LINE

CIRCULATION LINE INLET

SAMPLE VALVE

PRESSURE TRANSDUCER

SAMPLE LINE

SECTION B-B

UPPER CYLINDER

SAMPLE VALVE

PRESSURE TRANSDUCER

CENTRAL WINDOWED SECTION

THERMOCOUPLE

SAMPLE VALVE

EXTERNAL CIRCULATION LINE

INTERNAL CHECK VALVE

ALUMINUM ENVIRONMENTAL SHROUD

LOWER PISTON

CYLINDER

MOUNTING BOLT SLOT

LINE 0.7 cm OFF CYLINDER AXIS

WINDOW COVER PLATE

PYREX WINDOW

STRIP HEATER

THERMOCOUPLE

STEEL DISK WITH POLISHED SURFACE

COOLING COIL

DISK COVER PLATE

HYDRAULIC FLUID CONDITIONING COIL

CENTRAL TO AXIS

SECTION A-A

FIG. 8 ESSENTIAL FEATURES OF THE EQUILIBRIUM CELL DESIGN

FIG. 8 ESSENTIAL FEATURES OF THE EQUILIBRIUM CELL DESIGN

attain equilibrium consists of an internal check valve in the central section and an external 3.3 mm. diameter stainless steel line with a shut-off valve.

Cell Temperature Control

The temperature of the equilibrium cell is maintained by two 15 cm. diameter aluminum environmental control shrouds which are placed over the ends of the cell as shown in Figure 8. Each shroud has four 150 watt strip heaters and a 6 meter cooling coil. A thermocouple proportional band temperature controller (Thermoelectric 400) operates the heaters in both shrouds and controls the cell temperature to within $\pm$ .05°C of the setpoint.

Operational Procedure

The two pistons are hydraulically driven by a motorized dual cylinder high pressure pump with an opposed transmission (Ruska model 2248 WII). This allows both pistons to be move simultaneously up or down maintaining the volume between them constant. The possible working volume ranges from 10 cc. to 175 cc.

Mixing and equilibration are attained by running the pistons up and down. On the upstroke, the internal check valve closes and the fluids are forced through the external circulation line and sprayed into the upper cylinder. On the downstroke the circulation line valve is closed and the fluids pass through the check valve. Five to ten cycles are usually sufficient to attain equilibrium.

The point at which equilibrium is achieved is obvious since the reflected light image becomes stable in each phase. The refractive

index of each phase is easily measured by moving it into the prism and measuring the deviation angle, γ. The temperature is measured with an iron-constantan 316 stainless steel sheathed thermocouple with its tip exposed to the fluid in the prism and the pressure is measured with a strain gauge pressure transducer (Consolidated Electronics) calibrated against the vapor pressure of carbon dioxide at 20°C, and is believed known to $\pm$ 0.2 atm.

Samples of liquid and vapor are expanded to a pressure of 0.2 atm through the micro-metering valves into the evacuated line connected to the gas chromatograph gas sampling valve. The pressure in the sampling line is measured with a differential pressure transducer (Pace Wianko). Two samples of each phase are taken and triplicate chromatographs are run on each sample. The average size of each sample is 10^{-3} g-moles corresponding to a 0.2 percent depletion of an average load. The pressure drop associated with a sample taking was always less than 0.1 atm. The gas chromatograph (Hewlett-Packard Model 700) equipped with a thermal conductivity cell and an appropriate column was calibrated with the pure components over a sample loop pressure range of 0.05 to 0.7 atm. The sample pressures were adjusted so that the peak areas of the components were within the calibrated intervals.

The hydraulic fluid is preconditioned before it enters the cell by 2.5 meters of high pressure tubing which has been coiled into each shroud. The whole apparatus is insulated by a double layer of

Armoflex foam rubber insulation.

Optical System

A telescope (Gaertner M523 aperture 28 mm., f.1. 250 mm.)
with an Abbe-Lamont autocollimating eyepiece (Gaertner L372) is
mounted on a 25 cm. diameter precision rotary table (Karl Kneise
RTHP-10) with a two second vernier hand wheel and a maximum table
error of 10 seconds in 360 degrees of rotation. The table is centered
under a point on the front surface of the pyrex cell window. Mono-
chromatic light at a wavelength of 6328 $\overset{o}{A}$ is provided by a Helium-
Neon gas laser (Spectra Physics Model 132) and is transmitted to the
eyepiece by a glass fiber light guide.

Figure 9 is a schematic representation of the angle measure-
ment involved in the determination of the refractive index. The angle
γ is measured by autocollimation and from Snell's law it follows that

$$n_1 \sin \gamma = n_2 \sin \beta \qquad 7.01$$

$$n_2 \sin \beta = n_3 \sin \delta \qquad 7.02$$

$$\therefore \quad n_3 = n_1 \sin \gamma / \sin \delta \qquad 7.03$$

where n_1 is the refractive index of the ambient air, n_2 the refractive
index of the glass, and n_3 the refractive index of the fluid forming
prism. The angle δ is the prism angle and is equal to the measured
angle γ when $n_1 = n_3$, that is, the cell contains ambient air. The
measured angles have a repeatability of $\pm$ 4 seconds and a table error
of $\pm$ 2 seconds over the measured range. The refractometer has an over-
all possible error of $\pm$ 6 x 10^{-5} in the refractive index and a possible
range of 1.0 to 1.7.
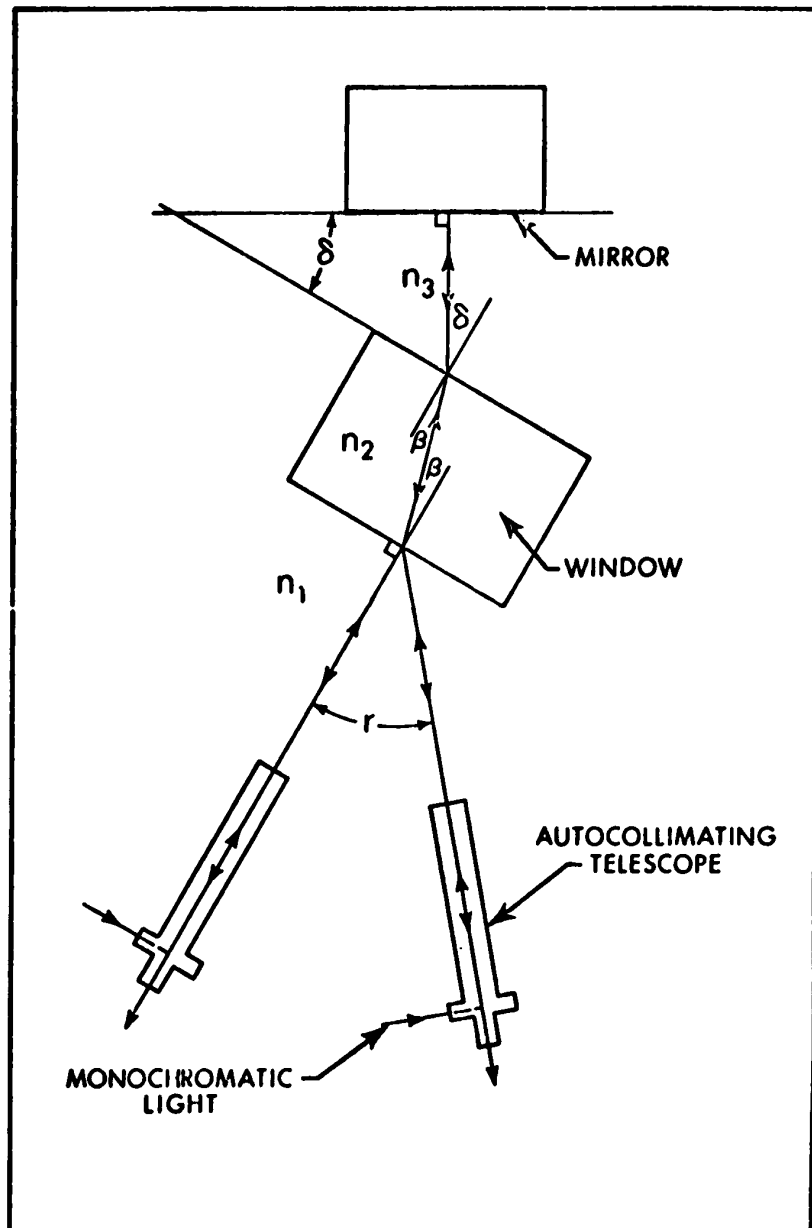
FIG. 9   SCHEMATIC REPRESENTATION OF THE ANGLE MEASUREMENT INVOLVED
IN THE DETERMINATION OF THE REFRACTIVE INDEX

This optical system has three advantages over a conventional spectrometer which normally consists of a 60° prism with a separate collimator and telescope[64].

1. The time required to make a measurement is reduced from the usual five to ten minutes to less than one minute because the minimum deviation angle is obtained without trial and error and without movement of the prism, in this case the cell.

2. Only one high pressure window with flat and parallel faces is required as opposed to two of equal thickness.

3. The rotary table can be centered under any point on the front surface of the glass window rather than the optical center of the prism as in a conventional spectrometer.

VIII - EQUIPMENT EVALUATION

The carbon dioxide-n-butane binary was studied at 100.0°F and compared with the data of Olds, Reamer, Sage and Lacey[65] and Poettmann and Katz[66]. The n-butane used in this study was Matheson instrument grade. A chromatographic analysis of this material showed it to contain 99.5 mole percent n-butane, 0.4 mole percent propane, 0.03 mole percent i-butane and 0.07 mole percent nitrogen and/or methane. The carbon dioxide was obtained from Canadian Liquid Air Ltd. and contained better than 99.9 mole percent carbon dioxide.

Figure 10 shows the experimental compositional isothermal data and those of the above authors. It will be noted that the present data and the data of Olds et al[65] show some significant differences when compared to the earlier work of Poettmann and Katz[66].

Figure 11 shows the refractive index (6328$\overset{o}{A}$) of n-butane, carbon dioxide, and the coexisting liquid and gas phases of their mixture at 100.0°F in the pressure range 4 to 80 atm. In order to calculate the density from the refractive index and the composition the molar refractivities of the pure components were required.

The refractive index of carbon dioxide has been studied by Michels and Hamers[5] in the temperature range 25 to 100°C and at pressures up to 2400 atm., and by Phillips[21] at 34°C at pressures up to 100 atm. Stoll[13] determined the refractive index of carbon dioxide at 20°C and 1 atm. pressure for wavelengths from the ultraviolet to the infrared. The first term in the virial expansion of Equation 1.12 for R_{LL} of carbon dioxide at 6328$\overset{o}{A}$ was obtained from Stoll's data and the second and third terms were obtained from a plot of $(R_{LL}-R_{LL}°)V$
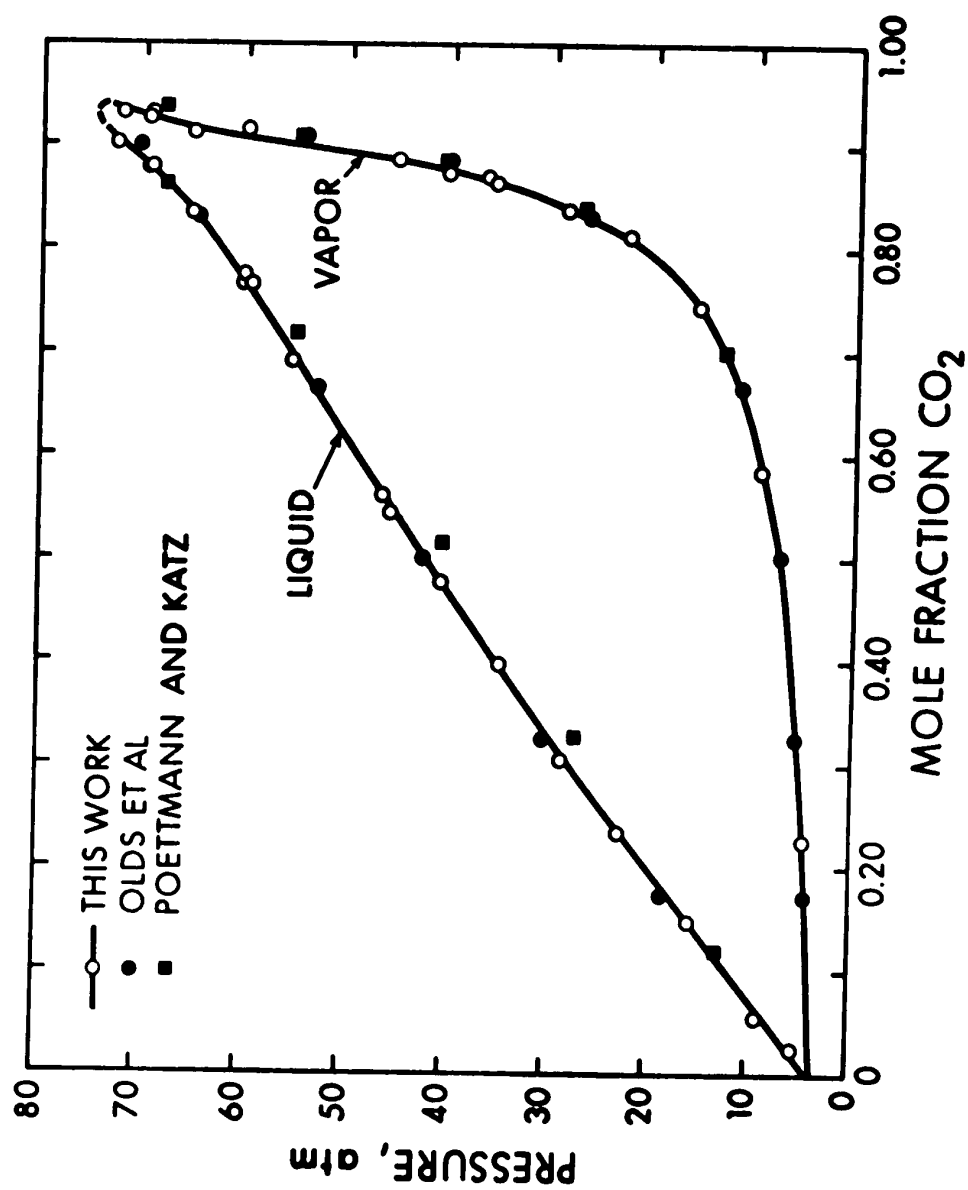
FIG. 10   PRESSURE-EQUILIBRIUM PHASE COMPOSITION DIAGRAM FOR THE n-BUTANE-CARBON
DIOXIDE SYSTEM AT 100°F
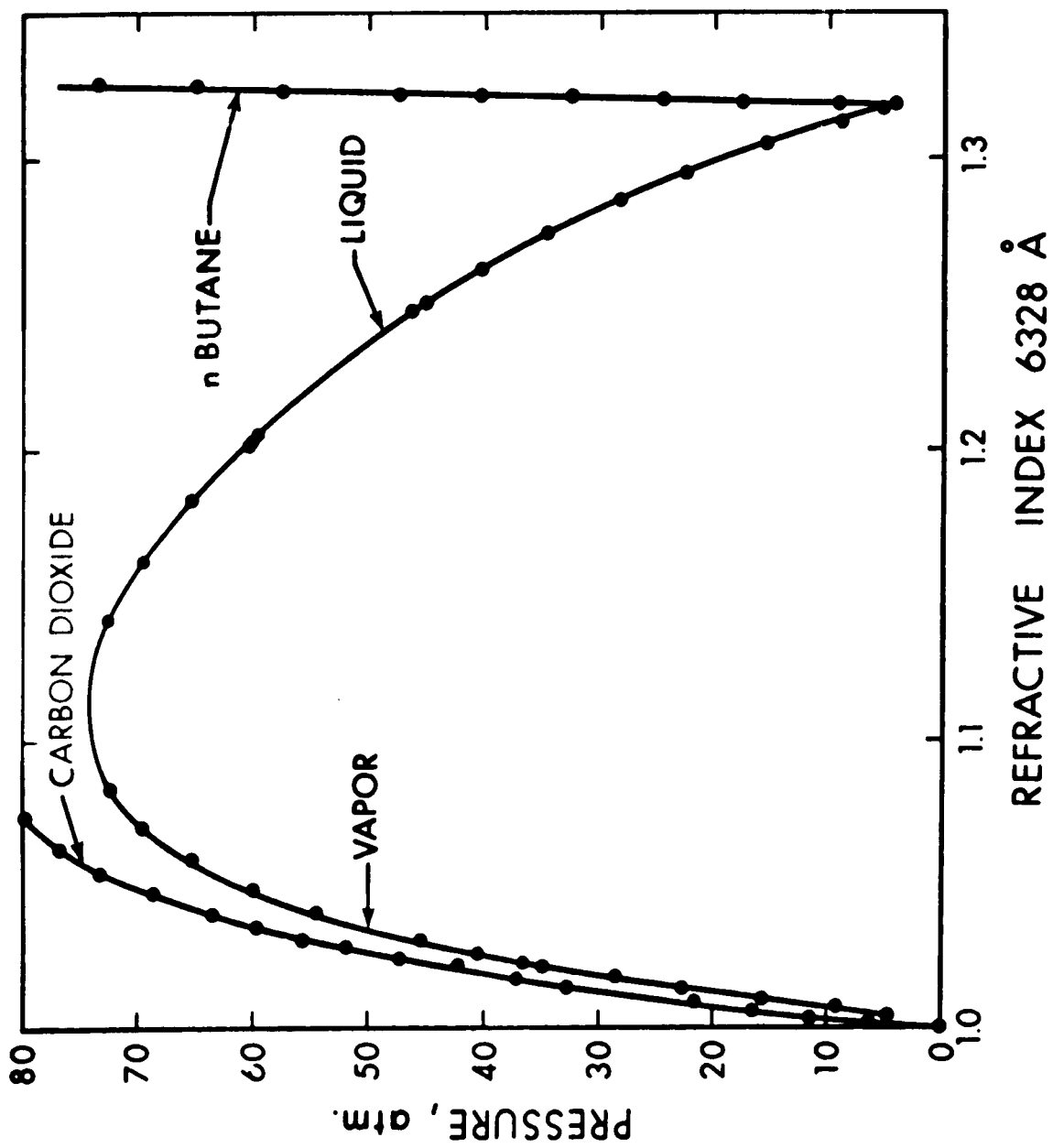
PRESSURE-REFRACTIVE INDEX DIAGRAM FOR THE n-BUTANE-CARBON DIOXIDE SYSTEM AT 100°F

FIG. 11

versus 1/V of Michels and Hamers' high density data. The lower density data could not be used because of the excessive scatter on this very sensitive plot.

For n-butane, several measurements have been reported, all at 5893$\overset{o}{A}$. Grosse[53] determined the refractive index of the liquid at low temperatures and atmospheric pressure using a modified Abbe refractometer. Francis[30] determined the iso-optic temperature of the liquified gas and an immiscible fluid or solution for which the refractive index was known as a function of temperature. Sliwinski[29] measured the refractive index and density of the coexisting liquid and vapor phases in the temperature range 0° to 94°C.

The refractive index of carbon dioxide and n-butane were measured at 100.0°F and pressures up to 100 atm. The molar refractivity of n-butane was calculated using molar volumes obtained from Sage Webster and Lacey[67]. The smoothed data are given in Table 1.

The mixture refractivity, $(R_{LL})_m$ was calculated by using a molar average mixing rule

$$(R_{LL})_m = \sum_i x_i (R_{LL})_i \qquad 8.01$$

where x_i is the mole fraction of each component. The molar volume of the mixture can then be obtained from the refractive index of the phase and the mixture refractivity. The experimental refractive indices (6328$\overset{o}{A}$), the compositions, and the calculated refractivities and molar densities of the coexisting phases in the carbon dioxide-n-butane binary are given in Table 2.

Figure 12 shows the calculated densities of the coexisting

TABLE 1

REFRACTIVE INDICES OF CARBON DIOXIDE AND n-BUTANE AT 100.0°F

Pressure atm.	n-Butane Refractive[a] index	R_{LL} cc/g-mole	Carbon Dioxide Refractive[a] index	R_{LL} cc/g-mole
10	1.3195	20.44	1.0042	6.64
20	1.3205	20.43	1.0086	6.65
30	1.3215	20.42	1.0136	6.65
40	1.3226	20.41	1.0192	6.65
50	1.3236	20.40	1.0265	6.65
60	1.3247	20.39	1.0353	6.64
70	1.3258	20.38	1.0478	6.64
80	1.3267	20.37	1.0738	6.64
90	1.3277	20.36	1.1393	6.61
100	1.3287	20.35	1.1565	6.60

[a] relative to vacuum at 6328Å.

Table 2. Coexisting Vapor and Liquid Phase Properties in the Carbon Dioxide-n-Butane System at 100.0°F

Pressure atm.	VAPOR				LIQUID			
	Y_{CO_2} mole Frac.	Refractive[a] Index	ρ[b] g mole/liter	R_{LL}[c] cc/g-mole	X_{CO_2} mole Frac.	Refractive[a] Index	ρ[b] g-mole/liter	R_{LL}[c] cc/g-mole
72.8	-	-	-	-	0.904	1.1421	11.56	7.96
72.2	0.934	1.0838	7.284	7.55	-	-	-	-
69.7	0.927	1.0704	6.060	7.65	0.879	1.1633	12.68	8.30
65.2	0.913	1.0584	4.916	7.83	0.836	1.1838	13.26	8.89
60.0	0.916	1.0483	4.089	7.80	0.768	1.2037	13.23	9.83
54.3	0.898	1.0404	3.249	8.24	0.691	1.2243	13.09	10.89
45.2	0.888	1.0306	2.475	8.18	0.544	1.2508	12.26	12.92
40.3	0.878	1.0264	2.100	8.33	0.480	1.2626	11.97	13.80
34.8	0.866	1.0222	1.739	8.49	0.399	1.2747	11.55	14.92
28.4	0.839	1.0178	1.339	8.86	0.307	1.2866	11.07	16.19
22.7	0.813	1.0144	1.038	9.22	0.236	1.2957	10.74	17.18
15.7	0.744	1.0105	0.684	10.17	0.149	1.3054	10.34	18.38
9.1	0.587	1.0080	0.434	12.34	-	-	-	-
8.9	-	-	-	-	0.058	1.3131	9.905	19.63
5.2	-	-	-	-	0.026	1.3172	9.797	20.08
5.0	0.228	1.0050	0.194	17.29	-	-	-	-

a   relative to vacuum at 6328Å

b   calculated from refractive index

c   molar average of pure refractivities
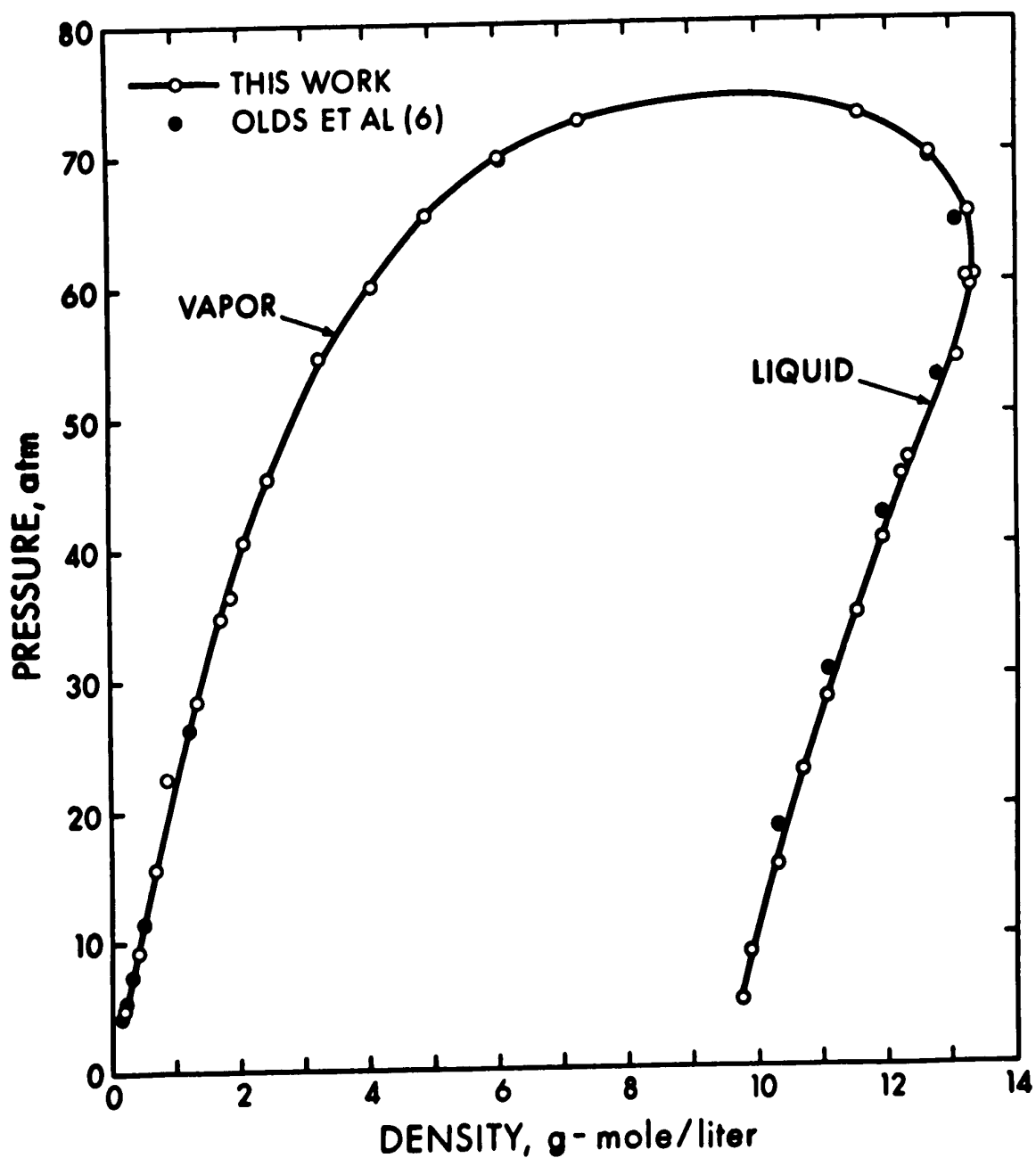
FIG. 12   PRESSURE-EQUILIBRIUM PHASE DENSITY DIAGRAM FOR THE n-BUTANE-CARBON DIOXIDE
            SYSTEM AT 100°F

liquid and vapor phases and also the data of Olds et al[65] which were
obtained by direct volumetric measurement for the binary system at
100°F. The average deviation of the calculated density minus that
of Olds is +1.1 percent for the liquid and -1.8 percent for the vapor.
The standard deviation of all the points is $\pm$ 1.5 percent.

The molar refractivities of the liquid and vapor phases were
calculated from the compositions of the phases using the refractivities
of the component substances in their natural state at the operating
temperature and pressure. For example, at 100°F and 40 atm. the carbon
dioxide exists as a gas and has a refractivity of 6.65 cc/g-mole while
the n-butane exists as a liquid and has a refractivity of 20.41 cc/g-mole.
The molar refractivities of the coexisting liquid and vapor were cal-
culated using these values. Having obtained the refractivities sub-
stitution of the refractive indices yields their molar densities.

In the section which follows the same procedure is used to
calculate the molar densities of the coexisting phases for the i-butane-
carbon dioxide system and the i-butane-ethane system. The pure component
data can be obtained from the experimental data listed in Appendix D or
can be calculated using the refractivity virial coefficients listed in
Appendix E.

IX - EXPERIMENTAL DATA

Two binaries are reported in this work, the i-butane-ethane system and the i-butane-carbon dioxide system. The i-butane-ethane system has recently been studied by Skripa et al[68] in the temperature range -94°F to 32°F. The i-butane-carbon dioxide system has not previously been reported in the literature.

In this work both of the above systems were studied at 100°, 160°, 220°, and 250°F at pressures from the vapor pressure of i-butane to the critical region of the system. The refractive indices of the coexisting phases were measured and the molar volumes calculated using a molar average Lorentz-Lorenz refractivity. The refractive indices of i-butane, ethane, and carbon dioxide were measured at 100°, 160°, 220° and 250°F at pressures from atmospheric to 1500 psia.

Apparatus

The apparatus used was the windowed double piston cell described in Chapter VII. It was found that the hydraulic fluid preheating coils were not long enough for operations at temperatures above 200°F. The oil was therefore initially passed through a coil immersed in a 200°F bath before entering the preheat coils in the shroud. The large temperature difference between the oil in the pump and the oil in the cell caused a small change in the working volume of the cell when the pistons were being moved simultaneously up or down. This situation was remedied by connecting a 10 cc. displacement pump to one of the oil lines. The pressure in the cell was easily maintained constant manually to 0.2 psi.

The temperature was measured with an iron-constantan thermocouple sheathed in 316 stainless steel with its reference junction in an ice bath and its measuring junction in the cell contents. The thermocouple was calibrated at the triple point and steam point of water. The cell temperature was controlled to within $\pm$ 0.1°F of the set operating temperature.

The pressure was measured with a 0-1500 psi pressure transducer calibrated at atmospheric pressure and the vapor pressure of carbon dioxide at 20°C. The maximum combined non-linearity and hysteresis of the transducer was $\pm$ 3 psi.

The phase compositions were determined by gas chromatography as described earlier. The thermal conductivity cell was maintained at 200°C and 150 ma current with a Helium flow rate of 25 cc/min. For the i-butane-carbon dioxide system a six foot 10 percent UC-W98 80-100S column maintained at 20°C was used. For the i-butane-ethane system a six foot Porapak Q column maintained at 100°C was used.

The refractive indices of the phases were determined by measuring the minimum deviation angle of a prism of the fluid as described earlier.

Materials

Matheson instrument grade i-butane was used. It was analyzed and found to contain 99.9 mole % i-butane, the major impurity being propane. The ethane used was Phillips research grade with a reported analysis of 99.94 mole % ethane. The carbon dioxide was obtained from Canada Liquid Air Ltd. It was analyzed and found to contain better than 99.9 mole % carbon dioxide.

Results

A. Refractive Indices of Ethane, Carbon Dioxide and i-Butane

The smoothed refractive indices of ethane, carbon dioxide, and i-butane at pressures up to 1500 psia in the temperature range 100°F to 250°F are given in Tables 3, 4 and 5, respectively. Figures 13, 14, and 15 show the experimentally determined refractive index data, which are also tabulated in the Appendix. The molar refractivities of i-butane were calculated by using the volumetric data of Sage and Lacey[69] and the measured refractive indices. The molar refractivities used for ethane were those reported by Sliwinski[29] with R_{LL}^o corrected to the He-Ne lazer frequency. For carbon dioxide the values obtained from Michels and Hamers[5] high density data were used.

B. Coexisting Phase Properties of the i-Butane-Carbon Dioxide System

Plots of the experimentally determined phase compositions and refractive indices and the calculated volumetric data for the i-butane-carbon dioxide system are shown in Figures 16, 17 and 18, respectively. These data are also tabulated in the Appendix. The smoothed data are given in Table 6 and the K-factor versus pressure curves are shown in Figure 19.

C. Coexisting Phase Properties of the i-Butane-Ethane System

Plots of the experimentally determined phase composition, refractive index and volumetric data for the i-butane-ethane systems are shown in Figures 20, 21 and 22, respectively. These data are also tabulated in the Appendix. The smoothed data are given in Table 7 and the K-factor versus pressure curves are shown in Figure 23.
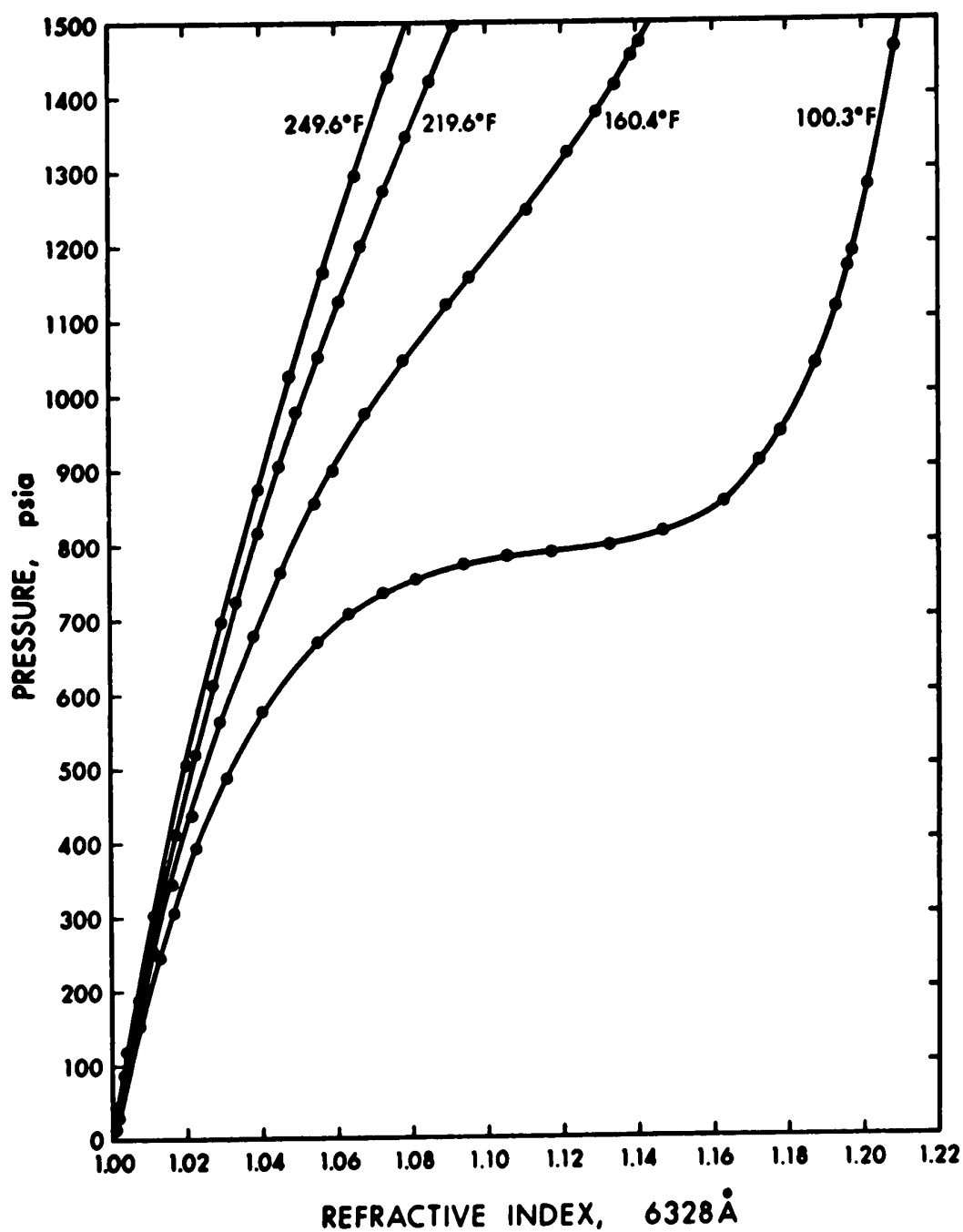
FIG. 13 EFFECT OF TEMPERATURE AND PRESSURE ON THE
REFRACTIVE INDEX OF ETHANE

Table 3. Effect of Temperature and Pressure on the

Refractive Index of Ethane

Pressure psia	Refractive Index* 100.3°F	160.4°F	219.6	249.6
100	1.0047	1.0043	1.0039	1.0037
200	1.0100	1.0089	1.0080	1.0075
300	1.0159	1.0138	1.0122	1.0115
400	1.0230	1.0191	1.0166	1.0157
500	1.0315	1.0251	1.0212	1.0199
600	1.0438	1.0318	1.0264	1.0245
700	1.0611	1.0395	1.0319	1.0295
750	1.0788	1.0440	1.0348	1.0321
800	1.1365	1.0490	1.0378	1.0348
850	1.1620	1.0540	1.0410	1.0375
900	1.1712	1.0591	1.0443	1.0402
1000	1.1835	1.0716	1.0514	1.0461
1100	1.1916	1.0865	1.0587	1.0521
1200	1.1979	1.1023	1.0665	1.0585
1300	1.2025	1.1180	1.0747	1.0652
1400	1.2063	1.1321	1.0831	1.0723
1500	1.2100	1.1440	1.0919	1.0795

*Relative to vacuum at 6328$\overset{o}{A}$
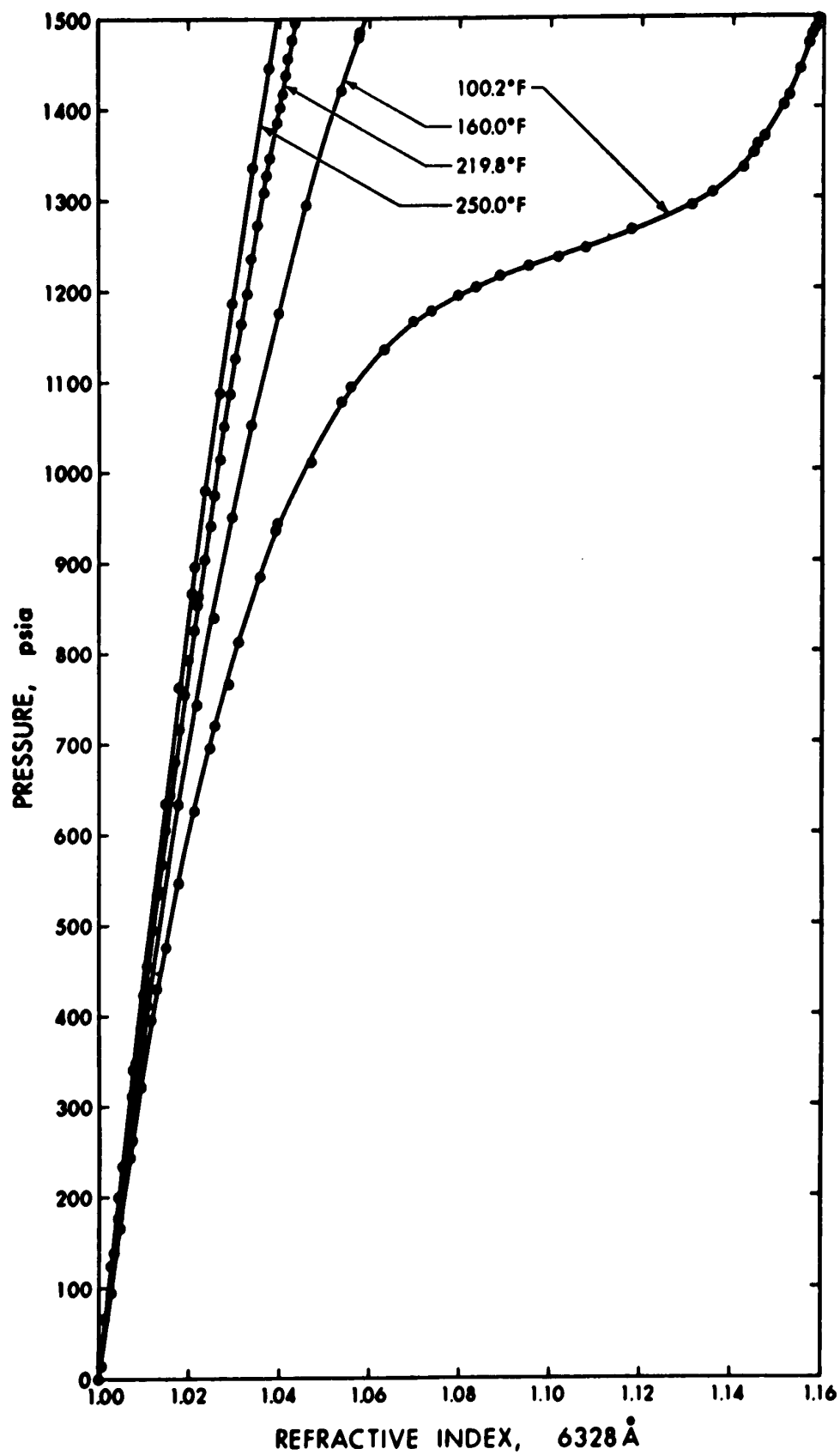
FIG. 14   EFFECT OF TEMPERATURE AND PRESSURE ON THE REFRACTIVE
INDEX OF CARBON DIOXIDE

Table 4. Effect of Temperature and Pressure on the

Refractive Index of Carbon Dioxide

Pressure psia	Refractive Index*			
	100.2°F	160.0°F	219.8°F	250.0F
100	1.0027	1.0025	1.0023	1.0021
200	1.0055	1.0050	1.0046	1.0042
300	1.0086	1.0077	1.0069	1.0064
400	1.0120	1.0104	1.0093	1.0087
500	1.0158	1.0134	1.0118	1.0110
600	1.0199	1.0165	1.0144	1.0135
700	1.0246	1.0199	1.0172	1.0161
800	1.0299	1.0235	1.0201	1.0187
900	1.0364	1.0274	1.0231	1.0214
1000	1.0454	1.0314	1.0261	1.0241
1050	1.0508	1.0336	1.0276	1.0255
1100	1.0570	1.0358	1.0292	1.0269
1150	1.0657	1.0382	1.0308	1.0283
1200	1.0805	1.0408	1.0324	1.0298
1250	1.1105	1.0434	1.0341	1.0312
1300	1.1333	1.0462	1.0358	1.0327
1350	1.1438	1.0492	1.0376	1.0342
1400	1.1499	1.0520	1.0395	1.0358
1500	1.1580	1.0587	1.0432	1.0390

*Relative to vacuum at 6328$\overset{o}{A}$
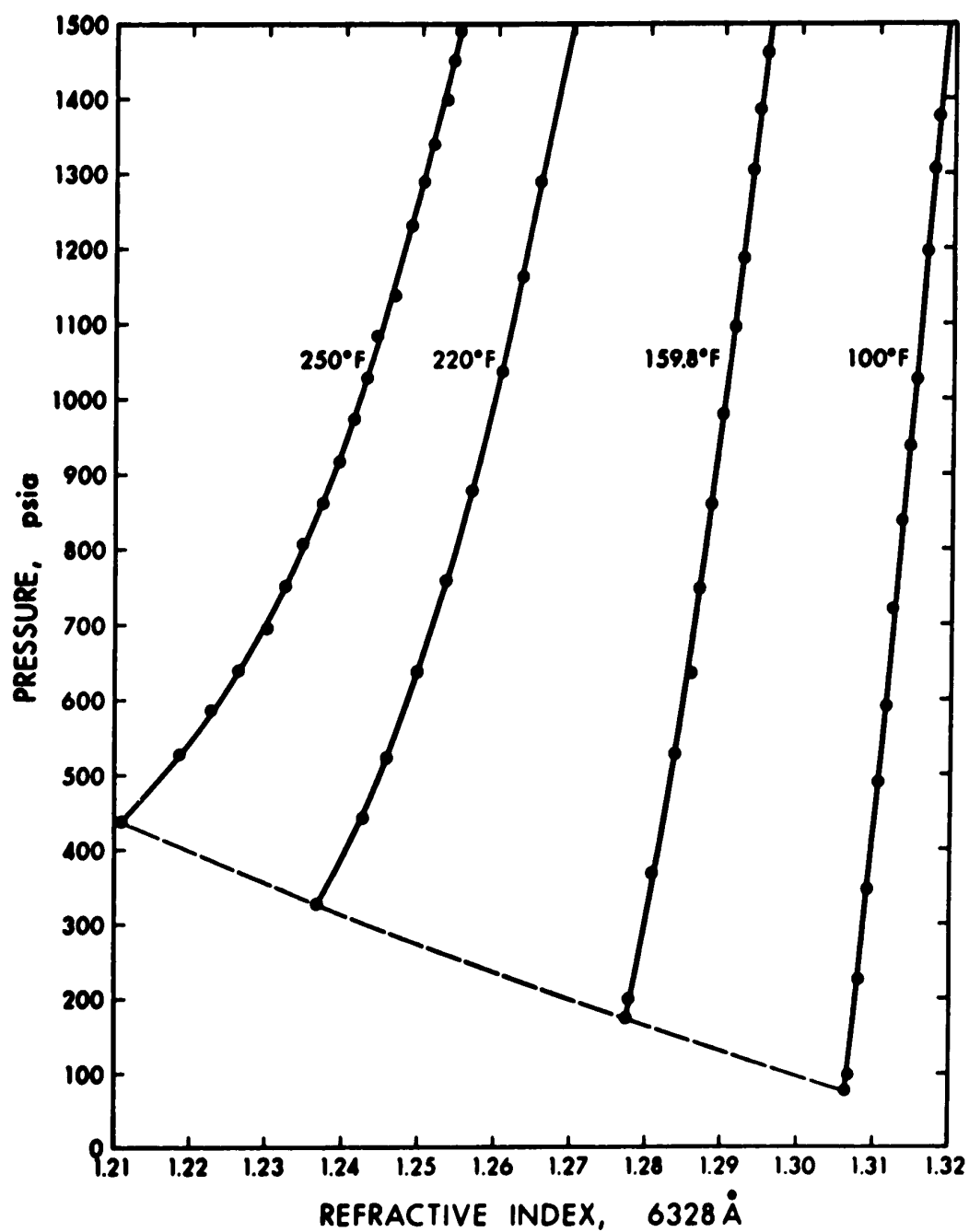
FIG. 15   EFFECT OF TEMPERATURE AND PRESSURE ON THE REFRACTIVE
INDEX OF LIQUID I-BUTANE

Table 5. Effect of Temperature and Pressure on the
Refractive Index of Liquid i-Butane

Pressure psia	Refractive Index*			
	100.0F	159.8F	220.0F	250.0F
100	1.3068	-	-	-
200	1.3078	1.2779	-	-
300	1.3088	1.2800	-	-
400	1.3097	1.2820	1.2406	-
500	1.3107	1.2838	1.2449	1.2166
600	1.3117	1.2852	1.2486	1.2239
700	1.3125	1.2866	1.2519	1.2300
800	1.3132	1.2878	1.2548	1.2349
900	1.3141	1.2889	1.2576	1.2389
1000	1.3149	1.2901	1.2599	1.2422
1100	1.3158	1.2913	1.2620	1.2452
1200	1.3165	1.2925	1.2641	1.2480
1300	1.3173	1.2937	1.2661	1.2506
1400	1.3181	1.2948	1.2680	1.2530
1500	1.3190	1.2960	1.2700	1.2553

*Relative to vacuum at 6328$\overset{o}{A}$
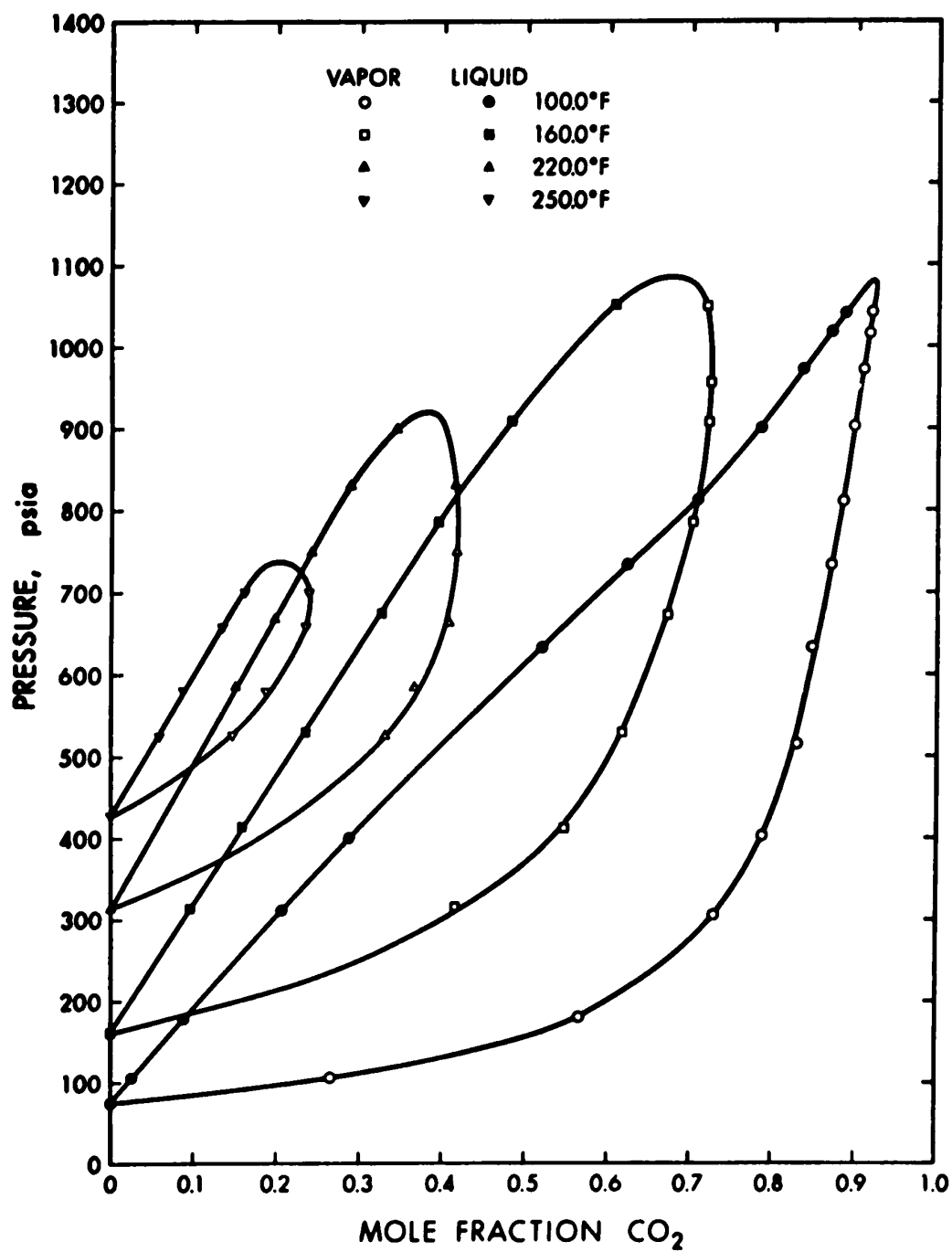
FIG. 16 PRESSURE-EQUILIBRIUM PHASE COMPOSITION
DIAGRAM FOR THE i-BUTANE-CARBON DIOXIDE SYSTEM
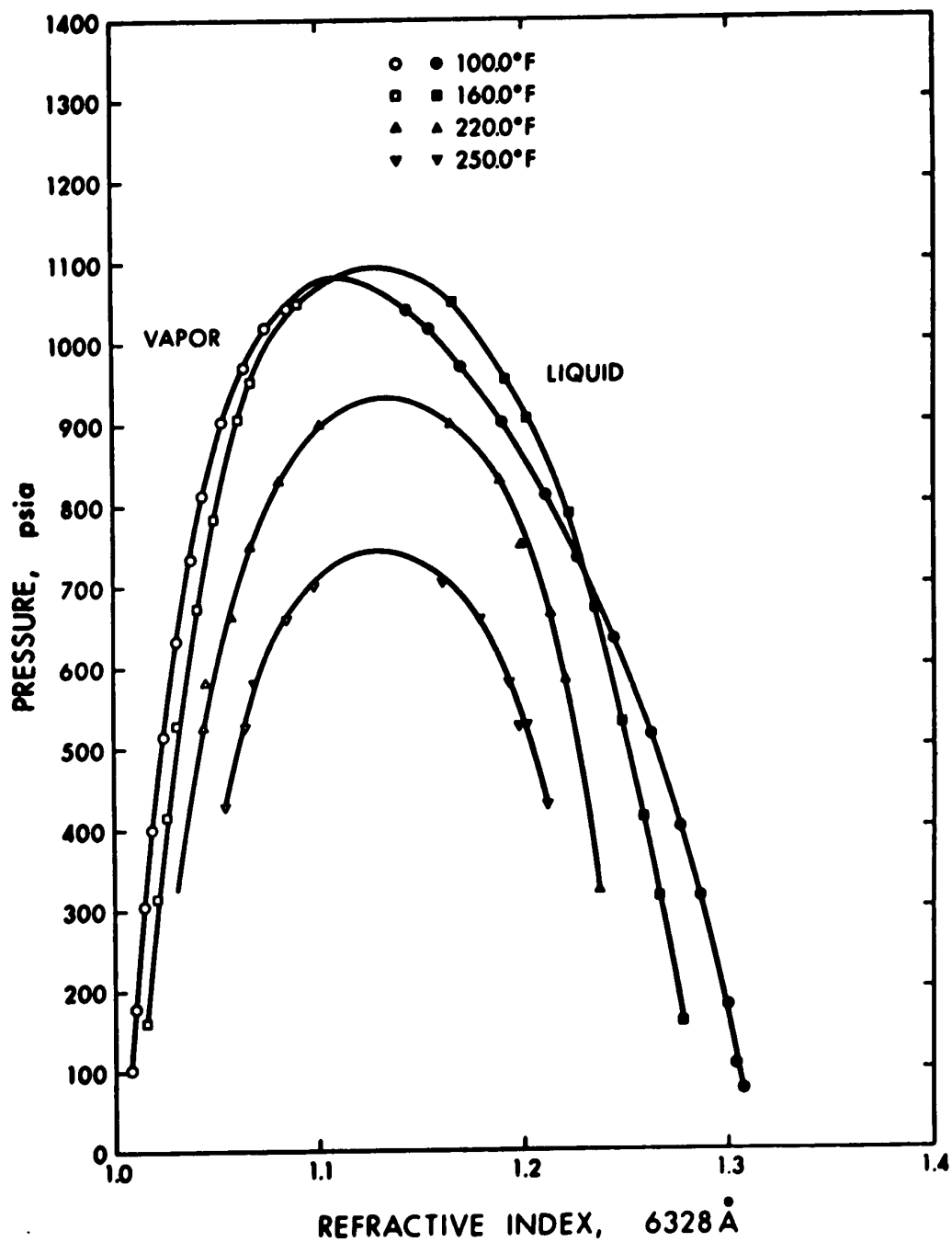
FIG. 17   PRESSURE-EQUILIBRIUM PHASE REFRACTIVE INDEX DIAGRAM
FOR THE i-BUTANE-CARBON DIOXIDE SYSTEM
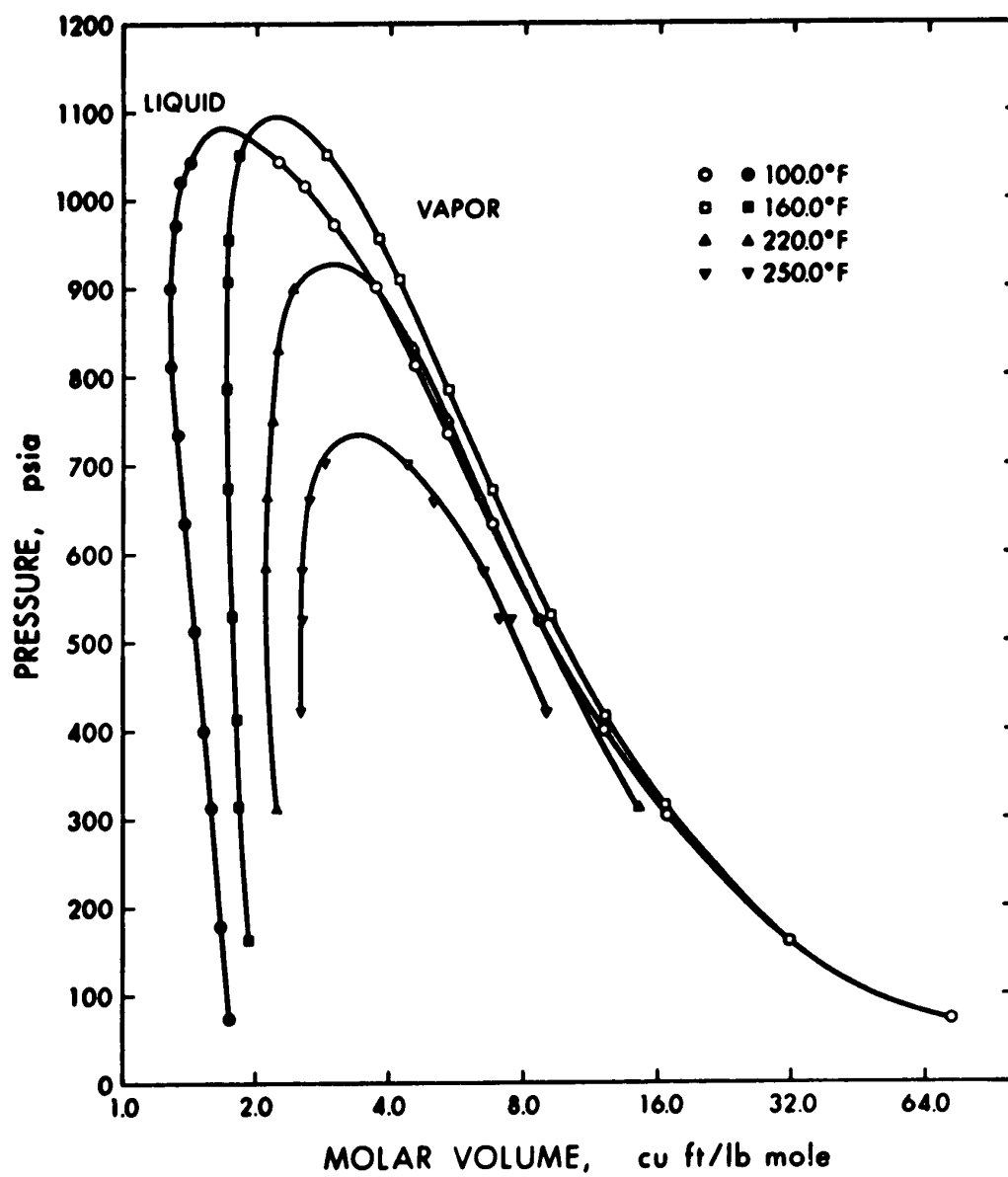
FIG. 18   PRESSURE-EQUILIBRIUM PHASE MOLAR VOLUME
DIAGRAM FOR THE i-BUTANE-CARBON DIOXIDE SYSTEM.

Table 6. Smoothed Vapor-Liquid Equilibria Data for the
i-Butane-Carbon Dioxide System

100.0°F

Pressure psia	Composition mole frac. CO_2		Refractive Index		Molar Volume cu.ft./lb-mole	
	Liquid	Vapor	Liquid	Vapor	Liquid	Vapor
100	0.021	0.228	1.3077	1.0078	1.74	49.5
150	0.064	0.477	1.3031	1.0094	1.71	34.0
200	0.107	0.600	1.2982	1.0112	1.67	26.0
250	0.150	0.677	1.2935	1.0129	1.64	20.7
300	0.195	0.723	1.2881	1.0149	1.60	17.0
350	0.241	0.758	1.2829	1.0169	1.56	14.1
400	0.287	0.786	1.2770	1.0190	1.53	12.0
500	0.382	0.821	1.2644	1.0238	1.46	9.10
600	0.482	0.843	1.2500	1.0293	1.40	7.18
700	0.586	0.862	1.2331	1.0358	1.35	5.77
800	0.691	0.879	1.2138	1.0437	1.30	4.68
900	0.782	0.895	1.1903	1.0539	1.28	3.67
1000	0.854	0.910	1.1610	1.0700	1.33	2.70
1050	0.890	0.916	1.1409	1.0935	1.44	2.14
1080	0.918	0.918	1.110	1.110	1.68	1.68

160.0°F

Pressure psia	Composition mole frac. CO_2		Refractive Index		Molar Volume cu.ft./lb-mole	
	Liquid	Vapor	Liquid	Vapor	Liquid	Vapor
200	0.023	0.154	1.2752	1.0169	1.90	26.0
250	0.055	0.303	1.2719	1.0189	1.87	21.1
300	0.088	0.400	1.2683	1.0210	1.85	17.5
350	0.119	0.471	1.2643	1.0231	1.82	14.7
400	0.149	0.530	1.2603	1.0254	1.80	12.6
450	0.181	0.569	1.2562	1.0279	1.78	11.0
500	0.213	0.600	1.2570	1.0302	1.76	9.71
600	0.275	0.645	1.2423	1.0357	1.74	7.77
700	0.338	0.678	1.2320	1.0420	1.72	6.38
800	0.403	0.703	1.2195	1.0500	1.72	5.21
900	0.472	0.718	1.2033	1.0606	1.72	4.24
950	0.513	0.720	1.1930	1.0675	1.73	3.78
1000	0.561	0.720	1.1794	1.0818	1.76	3.31
1050	0.618	0.711	1.1590	1.0930	1.88	2.83
1082	0.672	0.672	1.129	1.129	2.23	2.23

Table 6. (continued)

220°F

Pressure psia	Composition mole frac. CO_2		Refractive Index		Molar Volume cu.ft./lb-mole	
	Liquid	Vapor	Liquid	Vapor	Liquid	Vapor
350	0.021	0.084	1.2373	1.0347	2.20	13.1
400	0.050	0.179	1.2340	1.0372	2.17	11.5
450	0.078	0.246	1.2304	1.0404	2.13	10.3
500	0.106	0.307	1.2270	1.0438	2.11	9.10
550	0.131	0.349	1.2235	1.0475	2.10	8.18
600	0.159	0.377	1.2192	1.0516	2.10	7.33
650	0.187	0.398	1.2143	1.0561	2.11	6.60
700	0.213	0.410	1.2095	1.0611	2.12	5.98
750	0.240	0.415	1.2027	1.0671	2.15	5.40
800	0.268	0.416	1.1947	1.0742	2.19	4.87
850	0.300	0.411	1.1840	1.0840	2.26	4.30
900	0.345	0.403	1.1640	1.1030	2.42	3.66
925	0.380	0.380	1.133	1.133	2.91	2.91

250.0°F

Pressure psia	Composition mole frac. CO_2		Refractive Index		Molar Volume cu.ft./lb-mole	
	Liquid	Vapor	Liquid	Vapor	Liquid	Vapor
450	0.015	0.039	1.2090	1.0575	2.51	8.48
500	0.044	0.113	1.2039	1.0618	2.51	7.69
550	0.072	0.168	1.1979	1.0664	2.52	6.89
600	0.100	0.202	1.1908	1.0722	2.53	6.04
650	0.128	0.230	1.1817	1.0819	2.59	5.21
700	0.158	0.237	1.1658	1.0958	2.77	4.34
738	0.202	0.202	1.129	1.129	3.36	3.36
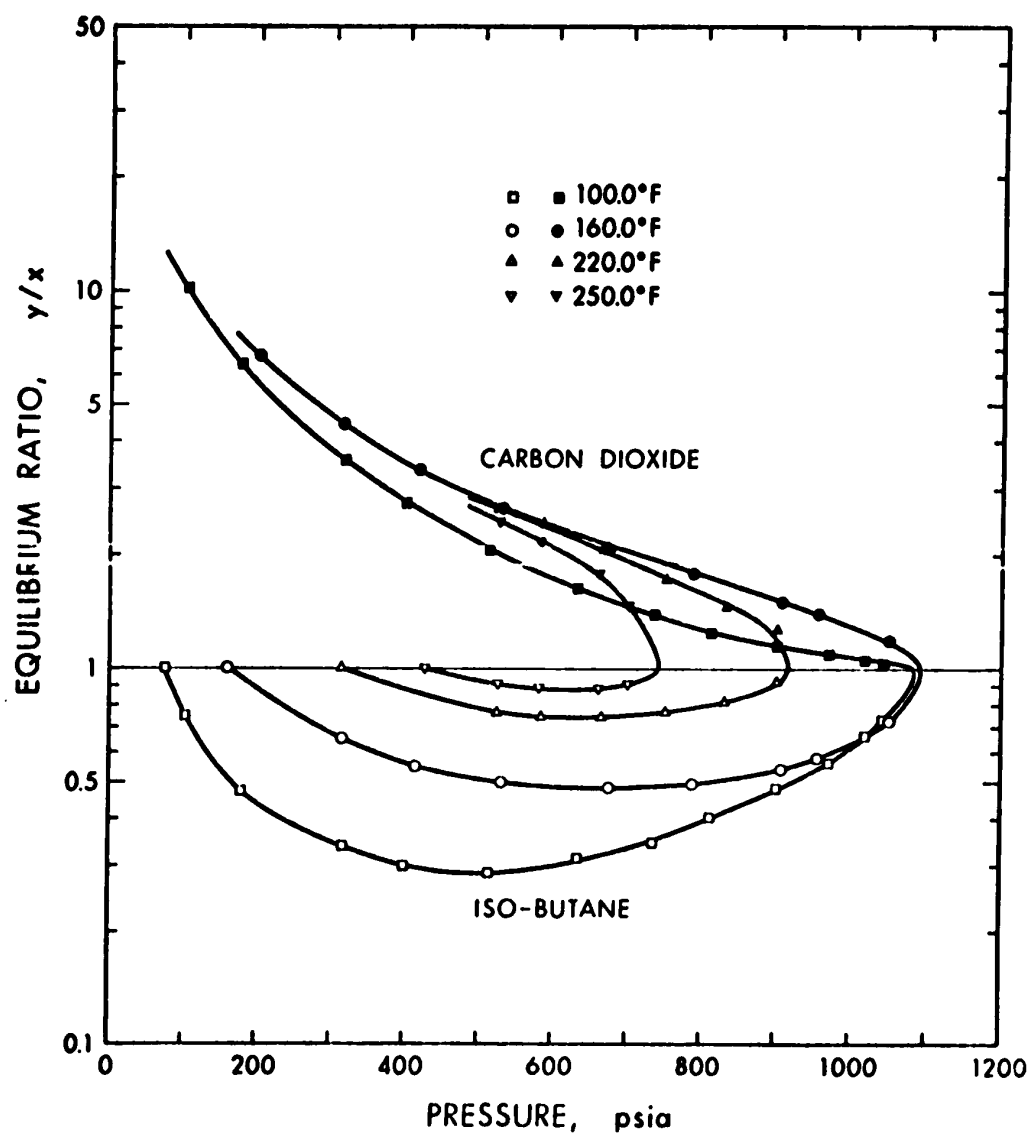
FIG. 19 EQUILIBRIUM RATIOS FOR i-BUTANE AND CARBON DIOXIDE
IN THE i-BUTANE-CARBON DIOXIDE SYSTEM
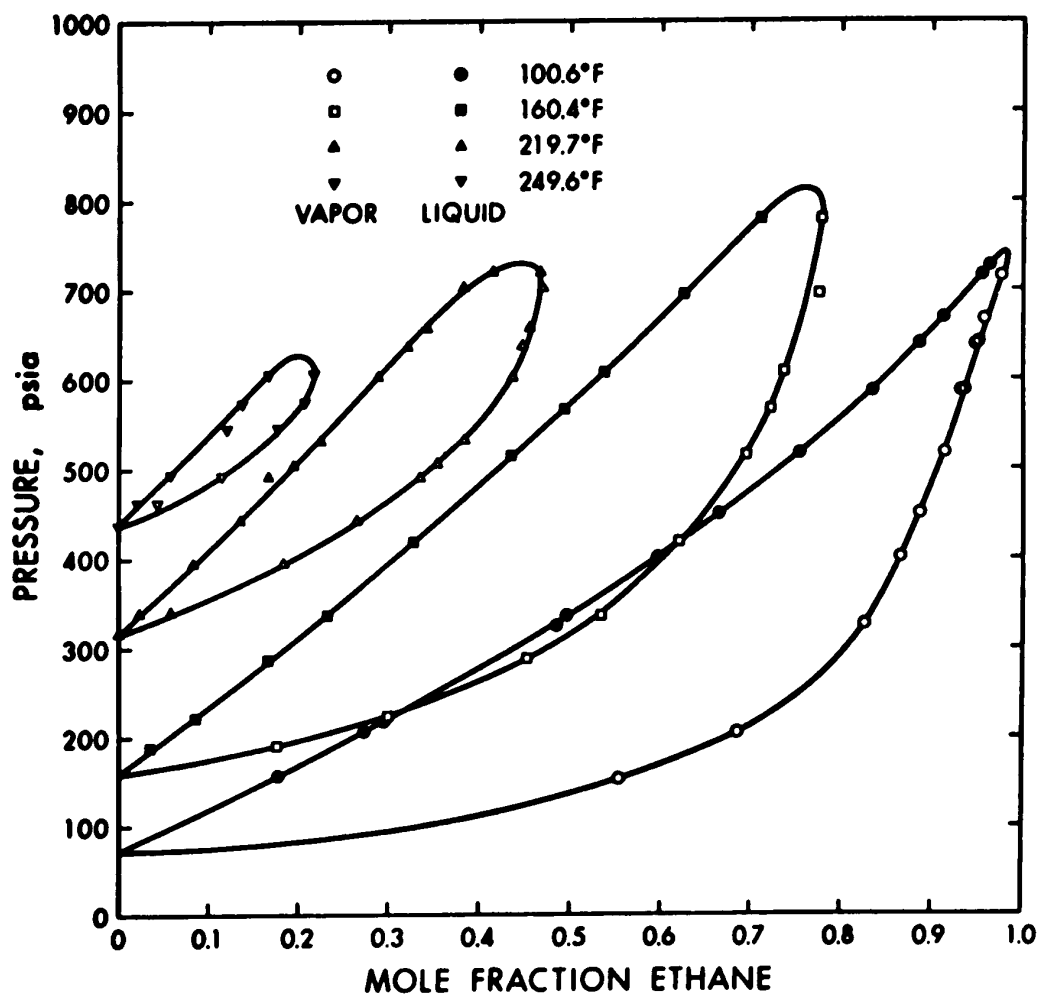
FIG. 20   PRESSURE-EQUILIBRIUM PHASE COMPOSITION DIAGRAM
FOR THE i-BUTANE-ETHANE SYSTEM
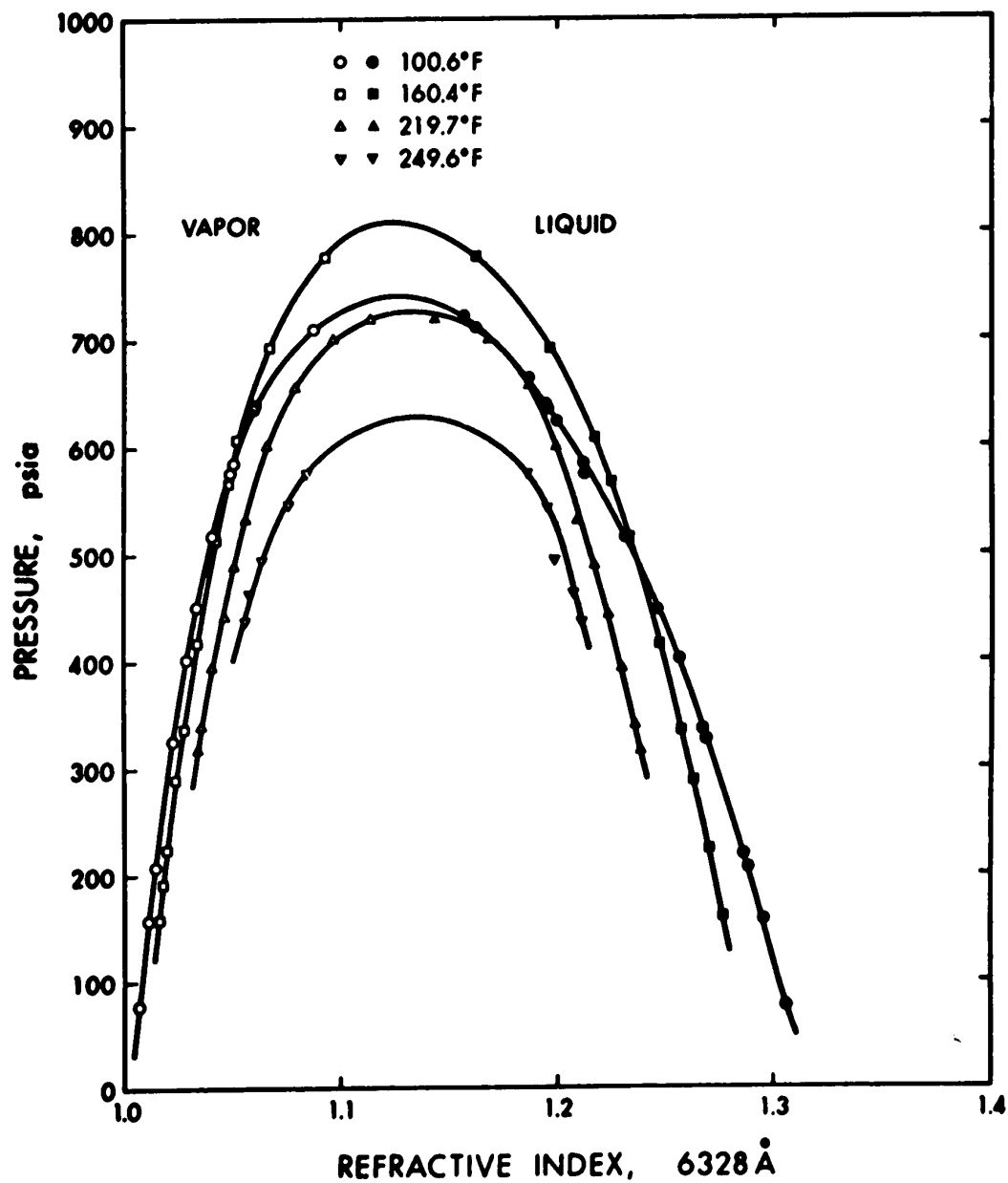
FIG. 21   PRESSURE-EQUILIBRIUM PHASE REFRACTIVE INDEX
DIAGRAM FOR THE i-BUTANE-ETHANE SYSTEM
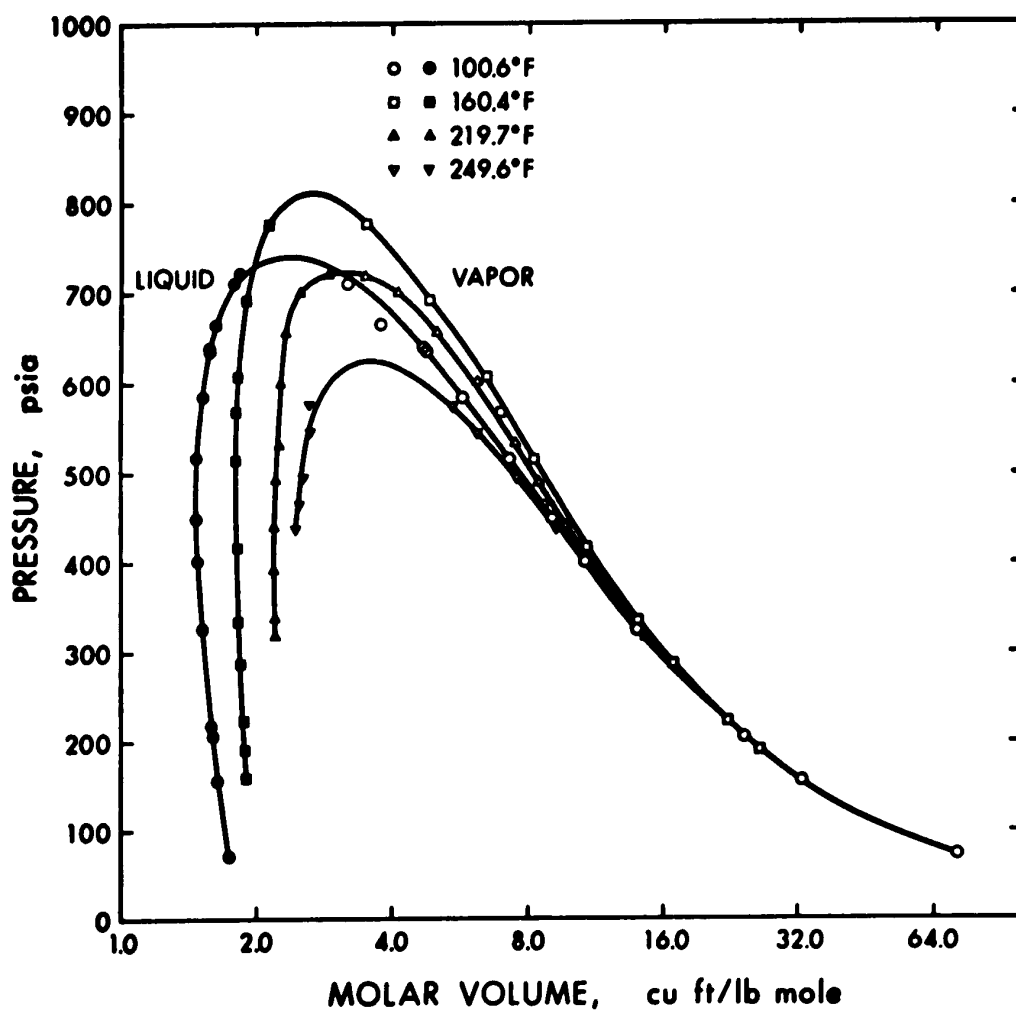
FIG. 22 PRESSURE-EQULIBRIUM PHASE MOLAR VOLUME DIAGRAM
FOR THE i-BUTANE-ETHANE SYSTEM

Table 7. Smoothed Vapor Liquid Equilibria Data

for the i-Butane-Ethane System

100.6°F

Pressure psia	Composition mole frac. ethane		Refractive Index		Molar Volume cu.ft./lb-mole	
	Liquid	Vapor	Liquid	Vapor	Liquid	Vapor
100	0.057	0.334	1.3045	1.0083	1.71	51.1
150	0.161	0.545	1.2970	1.0111	1.65	33.9
200	0.261	0.676	1.2892	1.0141	1.61	24.8
250	0.355	0.755	1.2811	1.0171	1.57	19.2
300	0.443	0.809	1.2728	1.0205	1.54	15.4
350	0.523	0.840	1.2640	1.0243	1.51	12.7
400	0.597	0.864	1.2546	1.0286	1.49	10.6
450	0.667	0.887	1.2450	1.0331	1.48	9.00
500	0.734	0.907	1.2343	1.0385	1.47	7.57
550	0.794	0.923	1.2222	1.0447	1.49	6.39
600	0.850	0.940	1.2083	1.0522	1.53	5.39
650	0.900	0.952	1.1915	1.0624	1.60	4.48
700	0.943	0.971	1.1695	1.0791	1.74	3.55
740	0.980	0.980	1.128	1.128	2.33	2.33

160.4°F

Pressure psia	Composition mole frac. ethane		Refractive Index		Molar Volume cu.ft./lb-mole	
	Liquid	Vapor	Liquid	Vapor	Liquid	Vapor
200	0.056	0.213	1.2730	1.0179	1.89	25.0
250	0.123	0.370	1.2678	1.0211	1.86	19.6
300	0.189	0.475	1.2620	1.0247	1.84	15.9
350	0.249	0.550	1.2555	1.0281	1.82	13.3
400	0.308	0.603	1.2490	1.0321	1.81	11.3
450	0.364	0.650	1.2420	1.0364	1.80	9.75
500	0.420	0.687	1.2341	1.0411	1.80	8.51
550	0.475	0.713	1.2260	1.0465	1.80	7.45
600	0.530	0.734	1.2165	1.0526	1.81	6.45
650	0.581	0.751	1.2063	1.0599	1.85	5.54
700	0.633	0.763	1.1942	1.0690	1.92	4.68
750	0.683	0.773	1.1773	1.0818	2.02	3.89
800	0.738	0.778	1.1450	1.1050		3.05
810	0.760	0.760	1.126	1.126	2.60	2.60

Table 7. (continued)

219.7°F

Pressure psia	Composition mole frac. ethane		Refractive Index		Molar Volume cu.ft./lb-mole	
	Liquid	Vapor	Liquid	Vapor	Liquid	Vapor
350	0.037	0.088	1.2341	1.0371	2.20	12.8
400	0.091	0.197	1.2284	1.0416	2.19	10.8
450	0.144	0.280	1.2225	1.0465	2.19	9.35
500	0.195	0.348	1.2160	1.0520	2.20	8.16
550	0.242	0.399	1.2085	1.0585	2.22	7.07
600	0.290	0.433	1.2000	1.0663	2.27	6.08
650	0.334	0.457	1.1890	1.0764	2.32	5.16
700	0.386	0.466	1.1700	1.0960	2.49	4.10
730	0.450	0.450	1.13	1.13	3.14	3.14

249.6°F

Pressure psia	Composition mole frac. ethane		Refractive Index		Molar Volume cu.ft./lb-mole	
	Liquid	Vapor	Liquid	Vapor	Liquid	Vapor
450	0.013	0.037	1.2090	1.0570	2.47	8.80
500	0.064	0.128	1.2045	1.0645	2.52	7.42
550	0.115	0.187	1.1940	1.0751	2.64	6.00
600	0.164	0.217	1.1725	1.0950	2.92	4.70
625	0.200	0.200	1.13	1.13	3.52	3.52
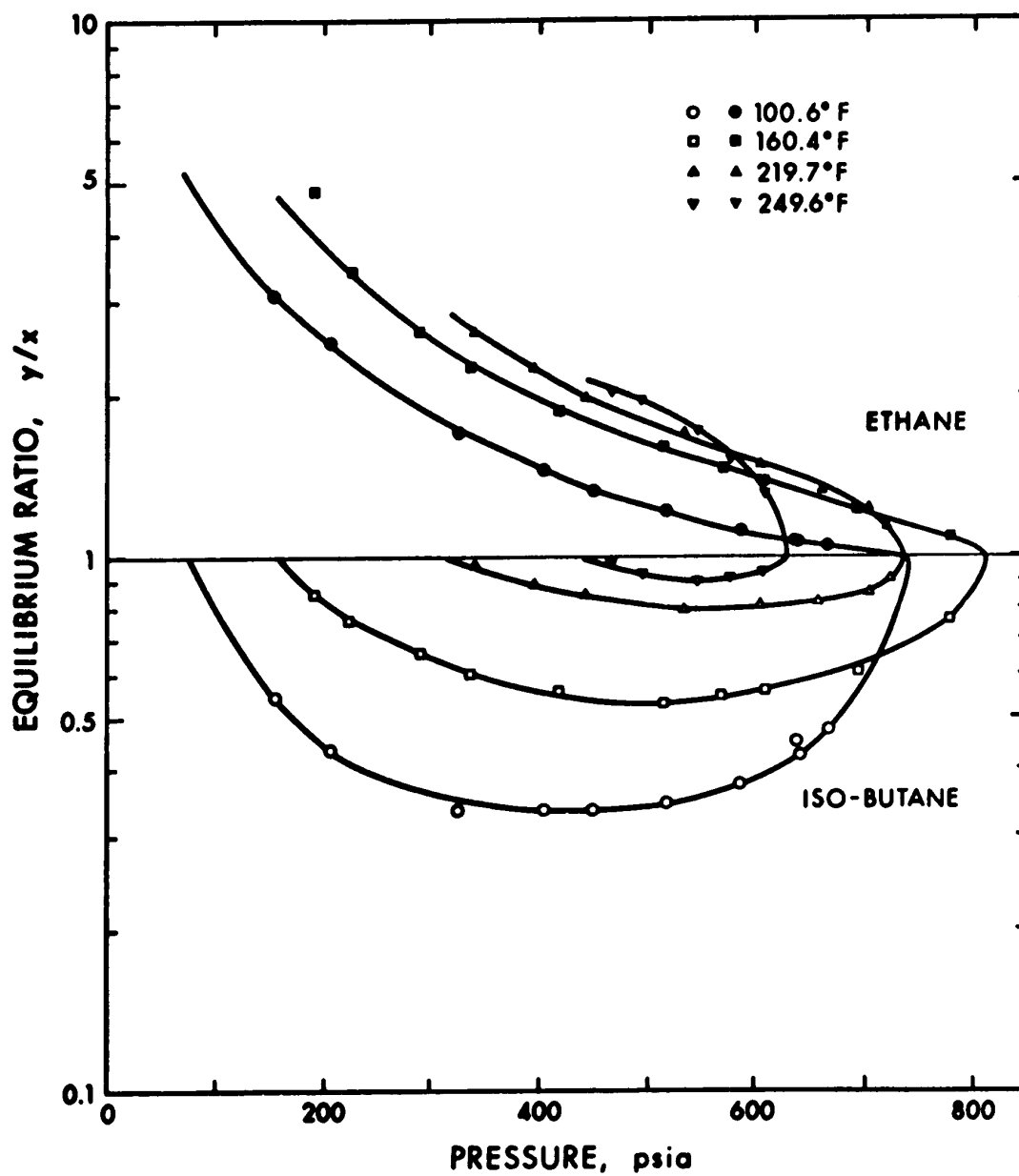
FIG. 23   EQUILIBRIUM RATIOS FOR I-BUTANE AND ETHANE
IN THE ETHANE-I-BUTANE SYSTEM.

X - THERMODYNAMIC CONSISTENCY AND PREDICTION
OF THE DATA

Chueh-Prausnitz Parameters

The smoothed experimental pressure-composition data were processed with slightly modified Chueh-Prausnitz[70] Henry's and Fitting programs. The resulting parameters are given in Table 8.

The low temperature i-butane-ethane data of Skripa et al[68] were processed with the Chueh-Prausnitz Symfit program. All of the α_{12} parameters obtained from this data were negative suggesting a possible thermodynamic inconsistency.

Prediction of the Equilibrium Data

The K-factor data were predicted with the Chueh-Prausnitz[70] method using the above tabulated parameters and also with the NGPA version of the Chao-Seader[71] method. The predictions for the i-butane-carbon dioxide system and the i-butane-ethane system are given along with the smoothed experimental equilibrium constants in Tables 9 and 10, respectively.

Thermodynamic Consistency Test

The smoothed experimental data were tested for thermodynamic consistency using a method presented by Chueh, Muirbrook, and Prausnitz[72]. The test is based on the Gibbs-Duhem equation which for a binary system at constant temperature is

$$x_1 \, d \ln f_1 + x_2 \, d \ln f_2 = v^L \, dP/RT \qquad 10.01$$

By the appropriate substitutions and integration the following point

59

by point consistency test was arrived at.

Area I + Area II + Area III =

$$[\ln K_1 + \frac{\ln \phi_1 \, P}{\phi_1^s \, P_1^s} + x_2(\ln \frac{\phi_2}{\phi_1} + \ln \frac{K_2}{K_1})]_{at \; x=x_2} \qquad 10.02$$

where

$$\text{Area I} = \int_0^{x_2} \ln K_2/K_1 \; dx_2 \qquad 10.03$$

$$\text{Area II} = \int_0^{x_2} \ln \phi_2/\phi_1 \; dx_2 \qquad 10.04$$

$$\text{Area III} = \int_0^{P \; at \; x_2} V^L \; dP \qquad 10.05$$

The three areas were found numerically using the method of assigned sample points at unequal intervals[73]. A comparison of the sum of the three areas, the left hand side of the equation, with the right hand side of the equation for the i-butane-carbon dioxide system and the i-butane-ethane system are given in Tables 11 and 12 respectively.

The fugacity coefficients, ϕ_i, were calculated using the Redlich-Kwong equation of state with binary interaction parameters and in view of this uncertainty Chueh et al judged that a disagreement of less than about five percent constituted very good thermodynamic consistency.

The data at 220°F and below are certainly consistent and it is felt that the large inconsistency of the 250°F data may be due in part to the inability of the equation of state to predict fugacities when the solvent component is in a near-critical situation, and in part to the data themselves.

Table 8. Chueh-Prausnitz Parameters for the

1-Butane-Carbon Dioxide and 1-Butane-Ethane Systems

System	Temperature °F	$H^{p=0}$ psia	α_{12} lb.-mole/cu.ft.
$1\text{-}C_4H_{10}\text{-}CO_2$	100	1105	0.3267
$k_{ij} = 0.14$	160	1380	0.5969
	220	1450	1.2807
	250	1030	0.9542
$1\text{-}C_4H_{10}\text{-}C_2H_6$	100	463	0.0342
$k_{ij} = 0.00$	160	695	0.1000
	220	938	0.3220
	250	940	0.7519

Table 9. Comparison of the Chueh-Prausnitz and Chao-Seader
Predictions of the i-Butane-Carbon Dioxide System

100.2°F

Pressure psia	i-Butane K_{exp}	% Deviation C-S	% Deviation C-P	Carbon Dioxide K_{exp}	% Deviation C-S	% Deviation C-P
200	0.4479	-4.1	-0.3	5.607	- 1.6	2.0
300	0.3441	-1.8	0.2	3.708	- 0.2	5.1
400	0.3001	0.1	0.6	2.739	2.3	8.2
500	0.2896	-0.5	-1.1	2.149	5.5	11.3
700	0.3333	-3.7	-4.5	1.471	13.3	16.2
900	0.4817	-	-	1.145	-	-
1000	0.6164	-	-	1.066	-	-

160.0°F

Pressure psia	i-Butane K_{exp}	% Deviation C-S	% Deviation C-P	Carbon Dioxide K_{exp}	% Deviation C-S	% Deviation C-P
200	0.8659	-4.4	-1.2	6.696	10.1	3.4
300	0.6579	-3.2	-0.7	4.545	8.0	4.2
400	0.5523	-0.4	1.2	3.557	3.0	1.5
500	0.5083	0.4	1.0	2.817	3.5	3.1
700	0.4864	-	4.0	2.006	-	2.0
900	0.5341	-	-	1.521	-	-
1000	0.6378	-	-	1.283	-	-

Table 9. (continued)

220.0°F

Pressure psia	1-Butane			Carbon Dioxide		
	K_{exp}	% Deviation		K_{exp}	% Deviation	
		C-S	C-P		C-S	C-P
400	0.8642	0.5	1.3	3.580	- 5.3	0.9
500	0.7752	1.6	3.1	2.896	- 7.3	- 1.1
600	0.7408	0.5	3.3	2.371	- 6.6	- 2.1
700	0.7497	-3.3	2.4	1.925	- 2.2	- 2.2
800	0.7978	-9.8	-	1.552	5.9	-
900	0.9115	-	-	1.168	-	-

250.0°F

Pressure psia	1-Butane			Carbon Dioxide		
	K_{exp}	% Deviation		K_{exp}	% Deviation	
		C-S	C-P		C-S	C-P
450	0.9756	-0.4	0.5	2.600	- 5.3	- 8.3
500	0.9278	-	1.6	2.568	-	-12.3
600	0.8867	-	4.1	2.020	-	-10.1
700	0.9062	-	-	1.500	-	-

Table 10. Comparison of the Chueh-Prausnitz and Chao-Seader
Predictions for the 1-Butane-Ethane System

100.6°F

Pressure psia	1-Butane K_{exp}	% Deviation C-S	C-P	Ethane K_{exp}	% Deviation C-S	C-P
200	0.4384	- 0.1	5.8	2.590	2.7	0.1
300	0.3429	2.3	9.1	1.826	2.9	0.2
400	0.3375	- 5.3	3.0	1.447	3.4	0.5
500	0.3496	- 9.3	2.0	1.236	3.2	0.1
600	0.4000	-15.6	0.0	1.106	2.8	0.2
700	0.5088	-21.3	-	1.030	1.9	-

160.4°F

Pressure psia	1-Butane K_{exp}	% Deviation C-S	C-P	Ethane K_{exp}	% Deviation C-S	C-P
200	0.8337	- 0.2	3.2	3.804	2.9	- 1.1
300	0.6473	- 0.5	3.6	2.513	7.9	3.6
400	0.5737	- 2.0	3.7	1.958	7.5	2.8
500	0.5397	- 2.2	6.8	1.636	6.4	0.7
600	0.5660	- 7.8	9.5	1.385	8.3	- 0.5
700	0.6458	-16.2	-	1.205	10.3	-
800	0.8473	-31.2	-	1.054	14.3	-

Table 10. (continued)

219.7°F

Pressure psia	1-Butane			Ethane		
	K_{exp}	% Deviation		K_{exp}	% Deviation	
		C-S	C-P		C-S	C-P
400	0.8834	- 1.5	-0.2	2.165	21.9	21.0
500	0.8099	- 1.6	4.2	1.785	18.9	9.0
600	0.7986	- 3.7	6.8	1.493	17.9	3.2
700	0.8697	- 9.2	-	1.207	21.1	-

249.6°F

Pressure psia	1-Butane			Ethane		
	K_{exp}	% Deviation		K_{exp}	% Deviation	
		C-S	C-P		C-S	C-P
450	0.9757	- 0.5	0.6	2.846	-13.3	-16.0
500	0.9316	0.2	-	2.000	9.4	-
600	0.9366	-	-	1.323	-	-

Table 11. Thermodynamic Consistency of the

1-Butane-Carbon Dioxide System

100.2°F

Pressure psia	X_{CO_2} mole frac.	R.H.S.	L.H.S.	% Deviation
300	0.195	0.627	0.598	4.8
500	0.382	1.151	1.131	1.7
900	0.782	2.082	2.088	- 0.3
1075	0.915	2.335	2.319	0.7

160.0°F

Pressure psia	X_{CO_2} mole frac.	R.H.S.	L.H.S.	% Deviation
400	0.149	0.407	0.405	0.5
600	0.275	0.732	0.734	- 0.4
800	0.403	1.024	1.051	- 2.6
1082	0.678	1.556	1.608	- 3.2

220.0°F

Pressure psia	X_{CO_2} mole frac.	R.H.S.	L.H.S.	% Deviation
600	0.159	0.347	0.381	- 9.3
800	0.268	0.588	0.626	- 6.2
918	0.380	0.793	0.832	- 4.8

250.0°F

Pressure psia	X_{CO_2} mole frac.	R.H.S.	L.H.S.	% Deviation
600	0.072	0.184	0.228	-21.2
700	0.128	0.302	0.352	-15.4
738	0.202	0.393	0.427	- 8.3

Table 12. Thermodynamic Consistency Test of the

1-Butane-Ethane System

100.6°F

Pressure psia	$X_{C_2H_6}$ mole frac.	R.H.S.	L.H.S.	% Deviation
200	0.261	0.540	0.539	0.2
400	0.597	1.253	1.248	0.4
600	0.850	1.769	1.760	0.5
740	0.980	2.011	2.018	- 0.3

160.4°F

Pressure psia	$X_{C_2H_6}$ mole frac.	R.H.S.	L.H.S.	% Deviation
400	0.308	0.553	0.578	- 4.3
600	0.530	0.943	0.980	- 3.8
800	0.738	1.281	1.334	- 4.1

219.7°F

Pressure psia	$X_{C_2H_6}$ mole frac.	R.H.S.	L.H.S.	% Deviation
400	0.091	0.135	0.140	- 3.9
550	0.242	0.353	0.376	- 6.4
700	0.386	0.561	0.599	- 6.6

249.3°F

Pressure psia	$X_{C_2H_6}$ mole frac.	R.H.S.	L.H.S.	% Deviation
550	0.115	0.136	0.196	-36.5
625	0.200	0.249	0.321	-25.3

XI - CONCLUSION

This work has shown that in high pressure vapor-liquid equilibrium studies the densities of the coexisting phases can be obtained conveniently and with reasonable accuracy by measuring their refractive indices and compositions. The designed equilibrium cell proved to be convenient to use and easy to assemble. The measurement of the refractive indices was simple and rapid and the measurement of the compositions was routine.

Although the refractive indices of the phases can be measured with high accuracy, there are some limitations to the accuracy of the obtained densities. These limitations are caused by the variation of the Lorentz-Lorenz molar refractivity with density for both pure components and mixtures and also by the existence of non-additive terms which are ignored when calculating mixture refractivities. In general, these limitations seldom cause inaccuracies greater than one or two percent in the calculated density. The experimental uncertainty in the composition of the phases can also lead to slight inaccuracies in the calculated refractivities.

When data of higher precision are required the nature and magnitude of the variation of the refractivity with density and composition must be considered. This information can best be obtained by measuring the refractive index and density in single phase regions where it is much less difficult to obtain accurate volumetric data. The information obtained will prove equally valid in the two phase region and improve the accuracy of the obtained densities.

The use of refractive index, therefore, has the possibility of becoming a very powerful aid in the experimental determination of

densities in high pressure two phase systems and in single phase systems in the near critical regions.

NOMENCLATURE

d	distance between two plates of an interferometer
f	fugacity
k	number of interference fringe shifts
i	angle of incidence
m	induced electrical moment
n	refractive index
r	angle of refraction
x	composition, mole fraction
α	polarizability
α_{12}	van Laar interaction parameter
β	angle of refraction in the window
γ	minimum deviation angle measured by autocollimation
δ	prism angle
ϵ	permittivity
ρ	density
λ	wavelength
ϕ	fugacity coefficient
A	prism angle
B	critical angle of refraction
B	second refractivity virial coefficient
C	third refractivity virial coefficient
D	minimum deviation angle
F	electric field strength
H	Henry's law constant
K	vapor-liquid equilibrium constant

M	molecular weight
N	Avogadro's number
P	pressure
R_{LL}	Lorentz-Lorenz refractivity
R_{LL}^{o}	zero density limit of the Lorentz-Lorenz molar refractivity
T	temperature
V	molar volume

REFERENCES

1. Batsanov, S.S., Refractometry and Chemical Structure, Trans. P.P. Sutton, New York: Consultants Bureau, 1961.

2. Partington, J.R., Advanced Treatise on Physical Chemistry, Vol. 4, London: Longmans Green & Co. Ltd., 1953.

3. Hill, N.E., Vaughan, W.E., Price, A.H., and Davies, M., Dielectric Properties and Molecular Behavior, London: Van Nostrand Reinhold Co., 1969.

4. Michels, A., Botzen, A., and DeGroot, S.R., Physica 13, 343 (1947).

5. Michels, A., and Hamers, J., Physica 4, 995 (1937).

6. Michels, A., Lebesque, H., Lebesque, L., and deGroot, S.R., Physica 13, 337 (1947).

7. Raman, C.V., and Krishnan, K.S., Proc. Royal Soc. (London), A177, 589 (1928).

8. Kirkwood, J.G., J. Chem. Phys. 4, 592 (1936).

9. Yvon, J., Recherches sur la Theorie Cinetique des Liquids, Paris: Herman and Cie, 1937.

10. Mazur, P. and Mandel, M., Physica 22, 299 (1956).

11. Jansen, L., and Mazur, P., Physica 21, 139 (1955).

12. Buckingham, A.D., and Pople, J.A., Disc. of Faraday Soc. 22, 17 (1956).

13. Stoll, E., Ann. Physik 69, 81 (1922).

14. Lyons, W.J., and Poindexter, F.E., J. Opt. Soc. Amer. 26, 146 (1936).

15. Poulter, T.C., Ritchey, C., and Benz, C.A., Phys. Rev. 41, 366 (1932).

16. Smith, B.L., Rev. of Sci. Instr. 34, 19 (1963).

17. Schmidt, E., and Thomas, W., Forch. Gebiete Ingenieurw 20B, 161 (1954).

18. Teague, R.K., and Pings, C.J., J. Chem. Phys. 48, 4973 (1968).

19. Siertsema, L.H., Z. Physik 14, 574 (1914).

20. Ayres, H.O., Phys. Rev. 2, 161 (1913).

21. Phillips, P., Proc. Roy. Soc. (London) 97A, 225 (1920).

22. Himstedt, F., and Wertheimer, I., Ann. Physik 67, 395 (1922).

23. Eisele, I., Ann. Physik 76, 396 (1925).

24. Opladen, M., Z. Physik 42, 160 (1927).

25. Belonogov, A.V., and Gorbunkov, V.M., Pribory i Tekhn. Eksperim 10, 188 (1965).

26. Belonogov, A.V., and Gorbunkov, V.M., Opt. i Spektroskopeya 14, 438 (1963).

27. Diller, D.E., J. Chem. Phys. 49, 3096 (1968).

28. Childs, G.E., and Diller, D.E., Advan. Cryog. Eng. 15, 65 (1969).

29. Sliwinski, P., Z. Phys. Chem., Newe Folge, 63, 263 (1969).

30. Francis, A.W., J. Chem. Eng. Data 5, 534 (1960).

31. Melville, H.W., and Watson, W.F., Trans. Faraday Soc. 44, 68 (1948).

32. Deryagin, B.V., Zorin, Z.M., and Churaev, N.V., Dokl. Akad. Nauk SSSR 182, 811 (1968).

33. Konstantinov, B.P., Lyaclov, N.W., and Oskurkova, O.V., Zh. Tekh. Fiz 38, 2117 (1968).

34. Shaw, R.F., and Johnson, G.A., U.S. Patent 3282149, Nov. 1, 1966.

35. Vukalovich, M.P., Kobelev, V.P., and Timoshenko, N.I., Teploener getika 15 (6), 80 (1968).

36. Edwards, M.H., Tr. Mezhdunar Kont. Fiz. Nizkikh Temp. 10th, 1966.

37. Knobler, C.M., Abbiss, C.P., and Pings, C.J., J. Chem. Phys. 41, 2200 (1964).

38. Miedziejko, E., Poznon Tow. Przyjaciol Nauk. Wydz. Mot. Przyr. Prkom Mat. Przyr. 11, 511 (1966).

39. Marcoux, J.E., J. Opt. Soc. Am. 59, 998 (1969).

40. Marcoux, J.E., Can. J. Phys. 48, 1947 (1970).

41. Michels, A., and Botzen, A., Physica 15, 769 (1949).

42. Jones, G.O., and Smith, B.L., Phil. Mag. 5, 355 (1960).

43. Garside, D.H., Moelgaard, H.V., and Smith, B.L., Proc. Phys. Soc., London, At. Mol. Physics 1, 449 (1968).

44. Posejpal, V., J. Phys. Radium 4, 451 (1923).

45. Schmidt, E., and Traube, K., Proc. Intern. Res. Thermodyn. Transport Properties, 2nd, Princeton, N.J., 1962, p. 193.

46. Schmidt, E.H.W., Critical Phenomena, Proc. of Conference, Washington, D.C., April 1965.

47. Timoshenko, N.I., Kobelev, V.P., and Kholodov, E.P., Teploenergetika 17, 64 (1970).

48. Ashton, H.M. and Halberstadt, E.S., Proc. Roy. Soc. (London) A245, 373 (1958).

49. Loria, S., Ann. der Physik, Ser. 4, 29, 605 (1909).

50. Rosen, J.S., J. Optical Soc. Am. 37, 932 (1947).

51. Sato, M., Proc. Japan Acad. 26, 36 (1950).

52. Beaume, R., and Couton, R., C.R. Acad. Sci. Paris, Ser. AB, 265B, 309 (1967).

53. Fousse, H., and Grange, J., Cahiers Phys. 13, 34 (1959).

54. Gross, A.V., J. Am. Chem. Soc. 59, 2739 (1937).

55. Gamalie, A.F., Gorbunkov, V.M., and Soloven, M.I., Opt. Spectrosh 23, 633 (1967).

56. Langer, D.W., Mohtalvo, R.A., J. Chem. Phys. 49, 2836 (1968).

57. Timmermans, J., Physico Chemical Constants of Pure Organic Compounds, Vol. 1, Amsterdam: Elsevier Publishing Co., 1958.

58. Timmermans, J., Physico Chemical Constants of Pure Organic Compounds, Vol. 2, Amsterdam: Elsevier Publishing Co., 1965.

59. Smyth, C.P., Engel, E.W., and Wilson, Jr., E.G., J.A.C.S. 51, 1736 (1929).

60. Bloom, H., and Rhodes, A., J. Phys. Chem. 60, 791 (1956).

61. Young, J., and Finn, A., J. Research Nat. Bur. Stand. 25, 759 (1940).

62. Burfield, D.W., Richardson, H.P., and Guereca, R.A., A.I.Ch.E. J. 16, 97 (1970).

63. Kielich, S., Physica 28, 1116 (1962).

64. Brower, W., "Matrix Methods in Optical Instrument Design", New York: W.A. Benjamin Inc., pp. 227, 235, 1964.

65. Olds, R.H., Reamer, H.H., Sage, B.H., and Lacey, W.N., Ind. Eng. Chem. 41, 475 (1949).

66. Poettmann, F.H., and Katz, D.L., Ind. Eng. Chem. 37, 847 (1945).

67. Sage, B.H., Webster, D.C., and Lacey, W.N., Ind. Eng. Chem. 29, 1188 (1937).

68. Skripa, V.G., Nikitina, I.E., Zhdanovich, L.A., Sirotin, A.G., and Benyaminovich, O.A., Gazov. Prom. 15 (12), 35 (1970).

69. Sage, B.H., and Lacey, W.N., Ind. Eng. Chem. 30, 673 (1938).

70. Prausnitz, J.M., and Chueh, P.L., Computer Calculations for High Pressure Vapor-Liquid Equilibria, Englewood Cliffs, N.J.: Prentice-Hall Inc., 1968.

71. Erbar, J.H., NGPA K and H Value Program 1962.

72. Chueh, P.L., Muirbrook, N.K., and Prausnitz, J.M., A.I.Ch.E. J. 11, 1097 (1965).

73. Hamming, R.W., Numerical Methods For Scientists and Engineers, Ch. 10, Toronto: McGraw Hill Book Co., 1962.

APPENDIX A

DERIVATION OF THE LORENTZ-LORENZ EQUATION

In a parallel plate condenser across which a potential
difference, V, is maintained, the field, F, acting on a single mole-
cule in the dielectric can be calculated by placing an imaginary
sphere around the molecule. The radius being small compared with
the dimensions of the condenser but large compared with the molecular
dimensions. Outside the sphere the material is treated as homogeneous
while inside the sphere it is treated as if it were made up of
individual molecules.

The field acting on the molecule is due to three sources.

1. The charge on the condenser plates and the dielectric surfaces
   adjacent to them giving rise to a field equal to the applied
   field

$$F_1 = \frac{4\pi Q}{\epsilon} = E \qquad\qquad A-1$$

2. The polarization charges on the spherical surface around the
   molecule

$$F_2 = \int_0^\pi \frac{\text{Surface Charge Density} \cdot \cos\theta \cdot d\,\text{Area}}{\epsilon(\text{Distance})^2}$$

$$F_2 = \int_0^\pi \frac{P\cos\theta \cdot \cos\theta \cdot 2\pi r^2 \sin\theta\, d\theta}{\epsilon\, r^2}$$

$$F_2 = \frac{2\pi}{\epsilon} \int_0^\pi P\cos^2\theta \sin\theta\, d\theta \qquad\qquad A-2$$

77

$$F_2 = \frac{4\pi P}{3\epsilon} \qquad \text{A-3}$$

3. The molecules inside the spherical region assumed to be in a spherically symmetric arrangement thereby providing no net field.

$$F_3 = 0 \qquad \text{A-4}$$

Therefore, the field acting on a molecule in the dielectric is

$$F = F_1 + F_2 + F_3 = E + \frac{4\pi P}{3\epsilon} \qquad \text{A-5}$$

The permittivity or dielectric constant, ϵ_0, of an isotropic material is related to the polarization, P, the product of the average induced moment per molecule produced by an applied field, E, and the number of molecules per unit volume, by

$$P = \frac{\epsilon}{4\pi} E(\epsilon_0 - 1) \qquad \text{A-6}$$

where ϵ is the permittivity of free space in rationalized units. Substituting into Equation A-5 for P and simplifying we have

$$F = (\epsilon_0 + 2) E/3 \qquad \text{A-7}$$

By definition, the molar polarization at visible frequencies is

$$P = N_1 \alpha_e F \qquad \text{A-8}$$

and the number of molecules per unit volume, N_1, is

$$N_1 = N\rho/M \qquad \text{A-9}$$

Combining Equations A-6, A-7, A-8, and A-9,
and simplifying we have the Clausius-Mossitti equation applicable at
visible frequencies.

$$\frac{\epsilon_0 - 1}{\epsilon_0 + 2} \frac{M}{\rho} = \frac{4\pi N}{3\epsilon} \alpha_e \qquad \text{A-10}$$

From Maxwell's electromagnetic theory it follows that the permittivity
of a material, ϵ_0, is equal to the square of the refractive index, n^2,
measured at the same frequency. Therefore we have the Lorentz-Lorenz
equation

$$\frac{n^2 - 1}{n^2 + 2} \frac{M}{\rho} = \frac{4\pi N}{3\epsilon} \alpha_e \qquad \text{A-11}$$

APPENDIX B

COMPARISON OF THE CHAO-SEADER AND CHUEH-PRAUSNITZ
APPROACHES TO VAPOR-LIQUID EQUILIBRIUM PREDICTIONS

Computers have significantly reduced the time and effort required to calculate the vapor-liquid equilibrium data needed in the design of contacting equipment. In general, the prediction methods are semi-empirical, being based on a thermodynamic foundation with a significant amount of experimental data for the evaluation of parameters.

Two such methods, one recent, the Chueh-Prausnitz[1], and the other relatively old, the Chao-Seader[2,3,4,5], have a similar thermodynamic foundation but differ mainly in the amount of experimental data used in the evaluation of parameters.

The Thermodynamic Method

The thermodynamic method has been presented in detail by Prausnitz[6] and only an outline of its basic features will be given here. The thermodynamic criteria which determine the state of equilibrium between two phases of a multicomponent system are equality of temperature and pressure in both phases and for each component equality of its fugacity in both phases. In order to find the conditions which satisfy these criteria, it is necessary to have some method for evaluating the fugacity of each component in each phase.

The fugacity of any component can be obtained from the volumetric data for the mixture in question by integrating according to Equation B-1 from a pressure of zero to the operating pressure. This equation applies to both the vapor and the liquid phases. For the liquid phase, x replaces y.

$$\ln f_1 = \ln y_1 P + \frac{1}{RT} \int_0^P [(\frac{\partial V}{\partial n_1})_{T,P,n_j} - \frac{RT}{P}] \, dP \qquad \text{B-1}$$

This relatively simple equation involves a presupposed knowledge of the behavior at constant temperature of the total volume of the mixture, with respect to a slight compositional change, from zero to the operating pressure. For the vapor phase this knowledge can be provided by an equation of state. However, for the liquid phase the necessary density range over which the integration is to be performed is usually beyond the scope of any equation of state. Some success with the Redlich-Kwong and Benedict-Webb-Rubin equations have been reported[7,8,9,10].

An alternative method for obtaining liquid phase fugacities is by defining an ideal solution and using a solutions theory to determine deviations from this ideal behavior. This technique has been used in both the Chao-Seader and Chueh-Prausnitz methods to determine the liquid phase fugacities. Also, both methods determine vapor phase fugacities using a form of the Redlich-Kwong equation of state.

Once methods for calculating liquid and vapor fugacities are available, an iterative procedure can be set up to satisfy the thermodynamic criteria with the restriction that the liquid and vapor compositions both sum to 1.000.

Vapor Phase Fugacities

In both the Chao-Seader and the Chueh-Prausnitz methods the vapor phase fugacities are calculated with the Redlich-Kwong equation of state.

$$\frac{PV}{RT} = \frac{V}{V-b} - \frac{a}{RT^{3/2} (V+b)}$$
B-2

A vapor-phase fugacity coefficient, ϕ_i, is defined by rewriting
Equation B-1 as follows

$$\ln f_i^V = \ln y_i P + \ln \phi_i$$
B-3

Performing the required integration on the R-K equation gives

$$\ln \phi_i = \frac{V}{V-b} + \frac{b_i}{V-b} - \frac{a_i}{RT^{2/3} b} \ln \left(\frac{V+b}{V}\right)$$
B-4

To calculate ϕ_i a value of V, the total volume, is obtained
by solving the R-K equation at a given T, P, and y. This value is
then substituted into equation B-4 adhering to the mixing rules for
the constants as given below.

$a = \Sigma y_i a_i$ $a_i = \dfrac{0.4278 \, R^2 \, T_{c_i}^{2.5}}{P_{c_i}}$ B-5

$b = \Sigma y_i b_i$ $b_i = \dfrac{0.0867}{P_{c_i} T_{c_i}}$ B-6

Chueh and Prausnitz modified the mixing rules to include a binary
interaction parameter, k_{ij}, and substituted specific component para-
meters for the universal constants. Their mixing rules are given in
equations B-7 to B-13

$a = \sum_i \sum_j y_i y_j a_{ij}$ $a_{ij} = \dfrac{(\Omega_{a_i} + \Omega_{a_j})}{2} \dfrac{R^2 T_{c_{ij}}^{2.5}}{P_{c_{ij}}}$ B-7

$$b = \sum_i y_i b_i \qquad , \quad b_i = \frac{\Omega_{b_i}}{P_{c_i} T_{c_i}} \qquad \text{B-8}$$

$$a_i = 2 \sum y_k a_{ki} \qquad \text{B-9}$$

where

$$P_{c_{ij}} = \frac{Z_{c_{ij}} R T_{c_{ij}}}{V_{c_{ij}}} \qquad \text{B-10}$$

$$V_{c_{ij}} = 1/2(V_{c_i}^{1/3} + V_{c_j}^{1/3})^3 \qquad \text{B-11}$$

$$Z_{c_{ij}} = 0.291 - 0.08 \left(\frac{w_i + w_j}{2}\right) \qquad \text{B-12}$$

$$T_{c_{ij}} = \sqrt{T_{c_i} T_{c_j}} \, (1 - k_{ij}) \qquad \text{B-13}$$

Liquid Phase Fugacities

An ideal solution can be defined as one in which the fugacity of a component in the solution is equal to the product of its mole fraction and the fugacity of the pure component at the same temperature and pressure over the entire composition range and a non-zero range of temperature and pressure.

Chao-Seader Pure Component Fugacities

The pure component fugacity in the Chao-Seader correlation is obtained by multiplying the operating pressure by a fugacity

coefficient, v_i^0. This fugacity coefficient is calculated from a corresponding states correlation in Pitzer's modified form,

$$\ln v_i^0 = \ln v^{(o)} + w_i \ln v^{(1)} \qquad \text{B-14}$$

where $v^{(o)}$ and $v^{(1)}$ are functions of the reduced temperature and pressure only.

Chao-Seader Deviation From Ideal Solution Behavior

The deviation from ideal solution behavior is represented by the activity coefficient, γ_i, obtained from Hildebrand's[11] regular solution model.

$$\ln \gamma_i = \frac{V_i(\delta_i - \bar{\delta})^2}{RT} \qquad \text{B-15}$$

where V_i is the pure liquid molar volume at 25°C and its vapor pressure and δ is free energy density function defined by

$$\delta = \left(\frac{\Delta E_v}{V}\right)^{1/2} \simeq \left[\frac{\lambda_v - RT}{V}\right]^{1/2} \qquad \text{B-16}$$

where λ_v is the latent heat of vaporization at 25°C.

The total solution solubility parameter, $\bar{\delta}$, is defined by

$$\bar{\delta} = \frac{\Sigma x_i V_i \delta_i}{\Sigma x_i V_i} \qquad \text{B-17}$$

For components which are super-critical or near critical at 25°C such as methane, ethane and propane the δ_i and V_i parameters can be evaluated from a best fit of binary vapor-liquid equilibrium data for the light component with several of the heavier components.

All the necessary terms are defined and the liquid phase fugacity is given by equation B-18.

$$\ln f_i^L = \ln (x_i P) + \ln v_i^o + \ln \gamma_i^o \qquad \text{B-18}$$

Chueh-Prausnitz Pure Component Fugacities

In the Chueh-Prausnitz method a distinction is made between solvents and solutes, a solute being defined as any component whose reduced temperature is greater than 0.93, and a solvent being any component whose reduced temperature is less than 0.93.

A solvent pure component fugacity is obtained by calculating the fugacity of the vapor at the solvent's vapor pressure with the R-K equation of state and reducing it to zero pressure by a Poynting correction according to equation B-19.

$$\ln f_i^{o,P=0} = \ln f_i^{o,P=P_s} - \frac{V_L^{P=P_s} P_s}{RT} \qquad \text{B-19}$$

This correction is necessarily hypothetical because the saturated liquid molar volume, V_L, is assumed constant from the saturation pressure, P_s, to zero pressure and in fact no liquid can exist below its saturation pressure.

A solute pure component fugacity is calculated from its Henry's Law constant in a solvent, and is also reduced to zero pressure by a Poynting correction

$$\ln f_{ij}^{o,P=0} = \ln H_{ij}^{o,P=P_{sj}} \left(\frac{V_{L_i}^{P=P_{sj}} P_{sj}}{RT} \right) \qquad \text{B-20}$$

where V_{L_i} is the partial molar volume of the solute i in the solvent j at infinite dilution. The use of Henry's Law constants has two advantages over 'hypothetical liquid' fugacities. It is an experimentally measurable quantity and the pure solute fugacity is a function of the solvent in which it is dissolved. However, the Poynting correction is

still hypothetical.

Chueh-Prausnitz Deviations From Ideal Solution Behavior

The deviations from ideal solution behavior are calculated using the van Laar equation with a dilation parameter, n.

$$\ln \gamma_i^{P=0} = \alpha_{ij} \, V_{c_i} \, q_i^2 \, [1 + 3n_i \, q_i^2] \qquad\qquad \text{B-21}$$

where

$$q_i = \frac{x_i V_{c_i}}{\Sigma x_i V_{c_i}}$$

n_i = dilation parameter for solutes in the form of an empirical function of T but is set equal to zero for solvents.

α_{ij} = the van Laar interaction constant which must be obtained from binary vapor-liquid equilibrium data.

Partial Molar Volumes

The partial molar volumes in all of the Poynting corrections are calculated using the modified Redlich-Kwong equation of state.

$$\bar{V}_k = \frac{\frac{RT}{V-b}\left(1 + \frac{b_k}{V-b}\right) - \frac{2\left(\sum\limits_{i=1}^{n} x_i a_{ki}\right) - \frac{ab_k}{(V+b)}}{V(V+b)\, T^{1/2}}}{\frac{RT}{(V-b)^2} - \frac{a}{T^{1/2}}\left[\frac{2V+b}{V^2(V+b)^2}\right]} \qquad\qquad \text{B-22}$$

The liquid molar volume, V, is not, however, obtained from the equation of state but rather from the corresponding states correlation of Lyckman and Eckert[12]. The mixing rules are the same as those used for the vapor phase fugacity.

Having defined all of the necessary terms the liquid phase fugacities can be written according to equation B-23

$$\ln f_i^L = \ln(x_i f_i^{0,P=0}) + \ln \gamma_i^{P=0} + \frac{\overline{V}_i P}{RT} \qquad \text{B-23}$$

Chueh-Prausnitz Program

For convenient use in the program the following properties are fitted to polynomials in temperature:

1. The pure component zero pressure solvent fugacities.

2. The Henry's law constants reduced to zero pressure as determined from solubility data are fitted to a polynomial for each binary solvent-solute pair.

3. The zero pressure Van Laar interaction constants as determined from binary vapor-liquid equilibrium data are fitted to a polynomial for each solvent-solvent pair and solvent-solute pair.

Nomenclature

f	fugacity
y	vapor phase mole fraction
P	pressure
R	gas constant
T	absolute temperature
V	molar volume
n	number of moles
a, b, Ω_a, Ω_b	Redlich-Kwong constants
ϕ	vapor phase fugacity coefficient
T_c	critical temperature
P_c	critical pressure
V_c	critical volume
Z_c	critical compressibility factor
k_{ij}	binary interaction parameter
v^0	pure component fugacity coefficient
γ	activity coefficient
δ	solubility parameter
λ_V	heat of vaporization
ΔE_V	free energy of vaporization
H	Henry's law constant
α	van Laar interaction parameter
q	critical volume fraction
η	dilation parameter
ω	accentric factor

Bibliography

1. Prausnitz, J.M., Chueh, P.L., Computer Calculations for High Pressure Vapor-Liquid Equilibria, Englewood Cliffs, N.J.: Prentice-Hall, Inc. (1968).

2. Prausnitz, J.M., Edmister, W.C., Chao, K.C., A.I.Ch.E. J. 6, 214 (1960).

3. Chao, K.C., Seader, J.D., A.I.Ch.E. J. 7, 598 (1961).

4. Cavett, R.H., American Petroleum Institute, Division of Refining, 42, 351 (1962).

5. Erbar, J.H., NGPA K and H Program (1962).

6. Prausnitz, J.M., Thermodynamics of Fluid Phase Equilibria, Englewood Cliffs, N.J.: Prentice-Hall, Inc., (1970).

7. Benedict, M., Webb, G.B., Rubin, L.C., Friend, L., Chem. Eng. Prog. 47, 609 (1951).

8. Bishnoi, P.R., Robinson, D.B., submitted to Can. J. Chem. Eng., November 1971.

9. Hsi, C., Lu, B.C.Y., Can. J. Chem. Eng. 49 (1), 134 (1971).

10. Zudkevitch, D., Joffe, J., A.I.Ch.E. J. 16 (1), 113 (1970).

11. Hildebrand, J.H., Scott, R.L., Regular Solutions, Englewood Cliffs, N.J.: Prentice-Hall Inc., 1962.

12. Lyckman, E.W., Eckert, C.A., Prausnitz, J.M., Chem. Eng. Sci. 20, 703 (1965).

APPENDIX C

EQUILIBRIUM CELL DIMENSIONS

NOTE: ALL DIMENSIONS ARE IN INCHES
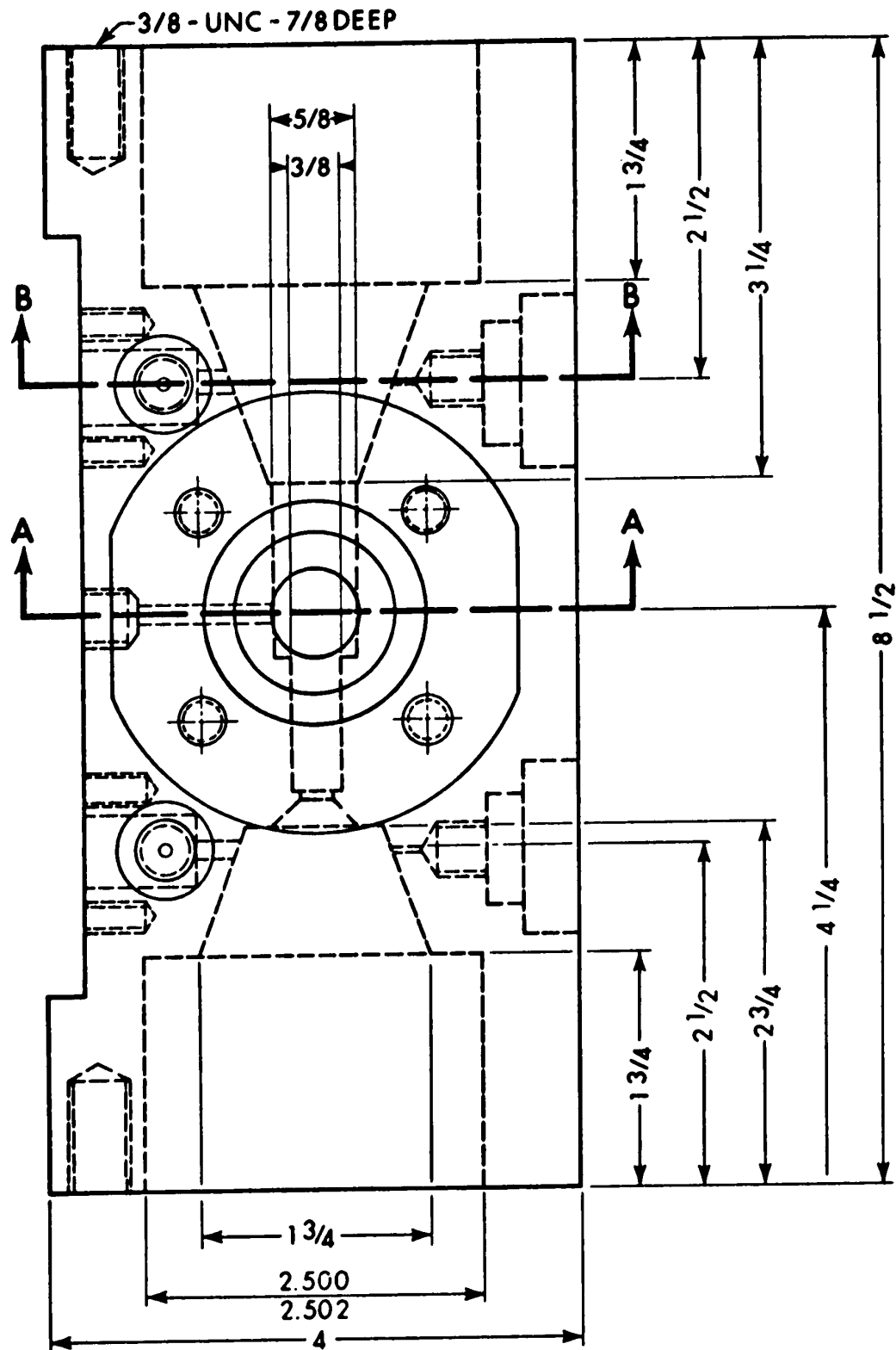
FIG. 24   DIMENSIONS OF THE CELL MAIN BODY
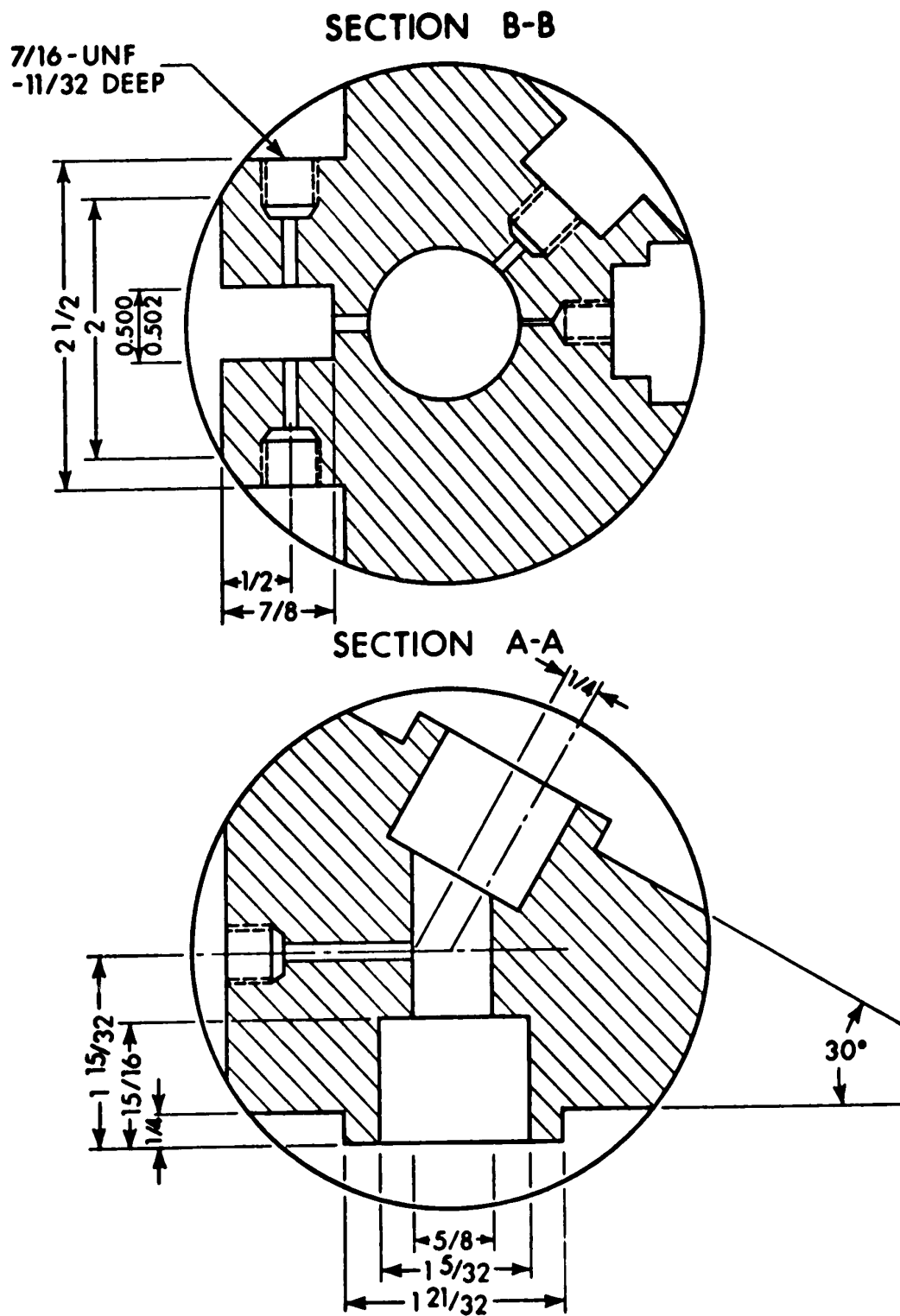
FIG. 25   CROSS-SECTIONS OF THE CELL MAIN BODY
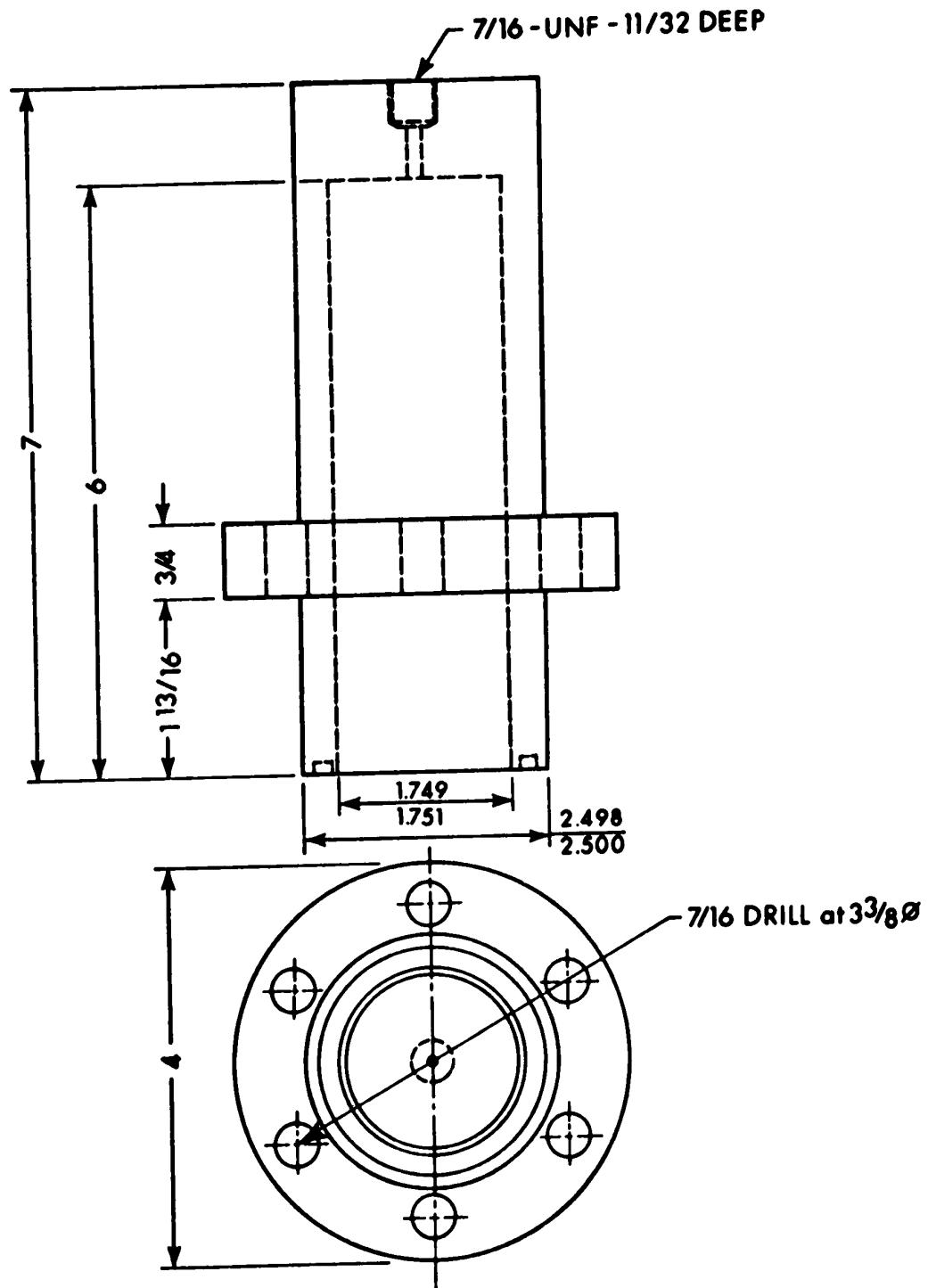
FIG. 26   DIMENSIONS OF THE END CYLINDERS
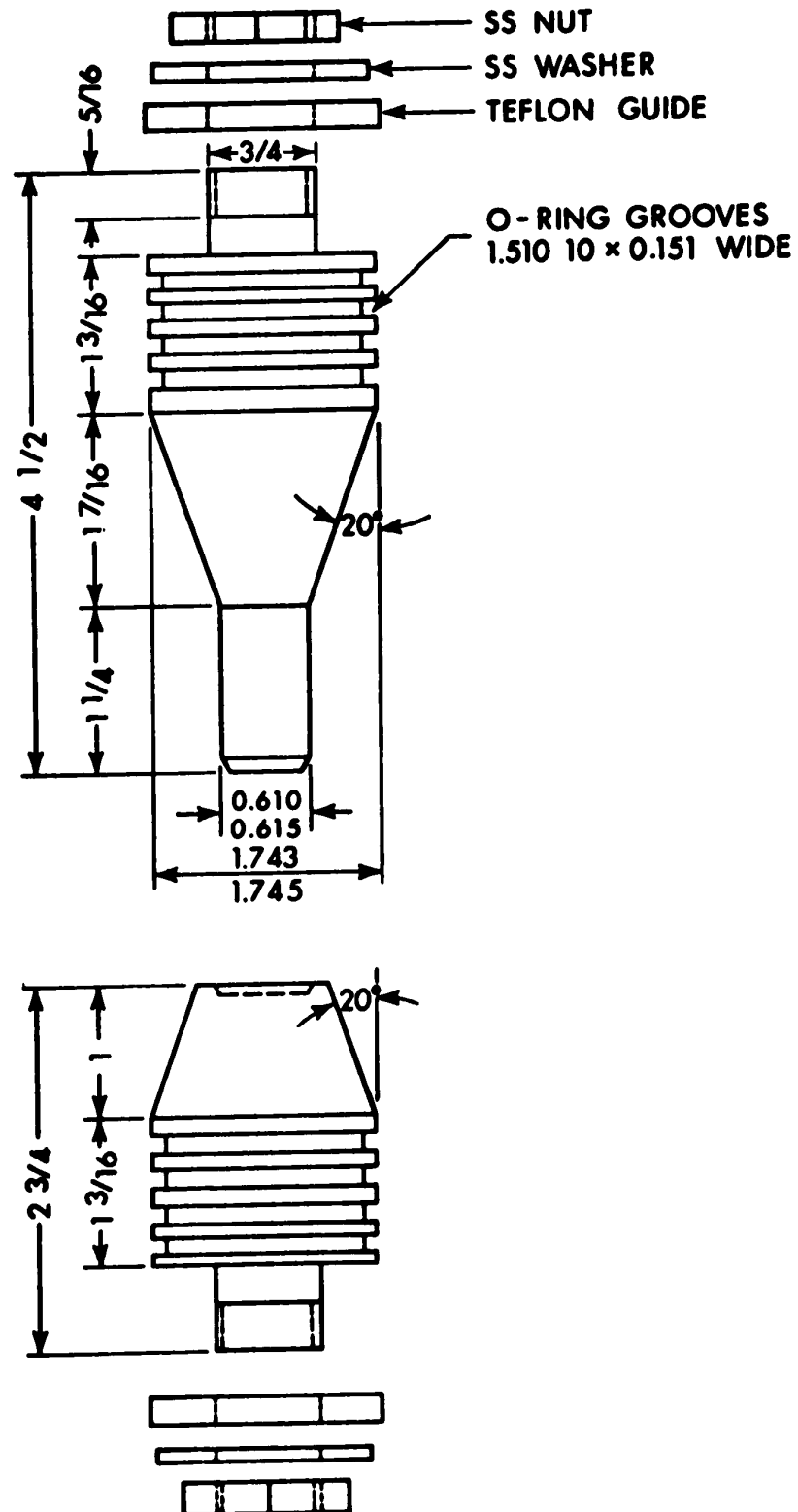
FIG. 27   DIMENSIONS OF THE PISTONS

APPENDIX D

EXPERIMENTAL DATA

This Appendix lists the experimental data points taken during the course of this work. The actual experimental data on the pure substances consists of three parameters only: the temperature, the pressure, and the refractive index at the wavelength 6328Å.

In Table 13: the figures in the column headed by 'Specific Volume Exp.' are interpolated data taken from Sage, Webster and Lacey (Ref. 67 main text);
the figures in the column headed by 'Molar Refractivity Exp.' are the values of the Lorentz-Lorenz molar refractivity,

$$R_{LL} = \frac{n^2-1}{n^2+2} \frac{m}{\rho}$$

the refractive index is the experimental data point and the density is that obtained from Sage, Webster and Lacey;
the figures in the column headed by 'Molar Refractivity Calc.' are the values obtained from the virial refractivity expansion where

$$R_{LL} = R_{LL_0} + B/V + C/V^2$$

V has units of cc/g-mole. The values of B and C were calculated so as to give a best fit in the least squares sense of the data in the column headed 'Molar Refractivity Exp.' and are given in Appendix E;
the figures in the column headed 'Specific Volume Calc.' were obtained by substituting the experimental refractive index into the values listed in the column 'Molar Refractivity Calc.'.

In Table 14: the headings have a similar connotation to those in Table 13 except that the figures in the column headed by 'Specific Volume Exp.' were interpolated from the volumetric data of Sage and Lacey (Reference 69 main text).

In Tables 15 and 16 the figures in the column headed by 'RLL' were obtained from the virial expansion using the coefficients listed in Appendix E and the figures in the column headed by 'Spec. Vol.' have the same connotation as those in the column headed 'Specific Volume Calc.' in Tables 14 and 15.

In Tables 17 and 18 the actual experimental data consists of the temperature, the pressure, and the liquid and vapor compositions and refractive indices. The figures listed under the column headed by V* were calculated as outlined on page 37 of the main text.

95

TABLE 13. EXPERIMENTAL REFRACTIVE INDEX DATA FOR N-BUTANE LIQUID

TEMPERATURE DEG. F	PRESSURE PSIA	N	MOLAR REFRACTIVITY CC/G-MOLE		SPECIFIC VOLUME CU.FT./LB.	
			CALC.	EXP.	CALC.	EXP.
100.34	62.3	1.31854	20.427	20.471	0.02849	0.02856
100.17	133.1	1.31915	20.421	20.457	0.02844	0.02849
100.27	260.0	1.32015	20.412	20.436	0.02834	0.02838
100.34	362.6	1.32066	20.407	20.408	0.02829	0.02830
100.27	474.9	1.32157	20.399	20.411	0.02821	0.02823
100.27	596.2	1.32245	20.391	20.404	0.02813	0.02815
100.27	697.3	1.32318	20.384	20.402	0.02806	0.02809
100.27	849.1	1.32419	20.374	20.395	0.02797	0.02800
100.27	964.4	1.32560	20.361	20.424	0.02784	0.02793
100.27	1080.1	1.32593	20.358	20.384	0.02781	0.02785
100.27	1193.5	1.32667	20.351	20.375	0.02774	0.02778
100.27	1304.7	1.32739	20.344	20.372	0.02768	0.02772
100.24	1433.0	1.32817	20.337	20.364	0.02761	0.02765

TABLE 14. EXPERIMENTAL REFRACTIVE INDEX DATA FOR I-BUTANE LIQUID

TEMPERATURE DEG. F	PRESSURE PSIA	N	MOLAR REFRACTIVITY CC/G-MOLE		SPECIFIC VOLUME CU.FT./LB.	
			CALC.	EXP.	CALC.	EXP.
100.00	93.1	1.30656	20.647	20.631	0.02983	0.02981
100.00	128.2	1.30704	20.643	20.647	0.02978	0.02979
99.96	221.6	1.30802	20.636	20.624	0.02968	0.02967
99.96	341.5	1.30920	20.626	20.620	0.02956	0.02956
99.82	484.8	1.31065	20.614	20.617	0.02942	0.02943
99.96	588.0	1.31149	20.607	20.605	0.02934	0.02934
100.00	716.7	1.31256	20.599	20.592	0.02923	0.02923
100.00	833.5	1.31342	20.591	20.582	0.02915	0.02910
100.00	936.8	1.31438	20.583	20.574	0.02906	0.02905
100.10	1025.7	1.31519	20.576	20.573	0.02898	0.02898
100.17	1195.7	1.31652	20.565	20.559	0.02885	0.02885
100.17	1308.0	1.31737	20.558	20.553	0.02877	0.02877
100.10	1378.2	1.31794	20.553	20.551	0.02872	0.02872
100.06	1522.8	1.31912	20.543	20.548	0.02861	0.02862

TABLE 14. (CONTINUED)

TEMPERATURE DEG. F	PRESSURE PSIA	N	MOLAR REFRACTIVITY CC/G-MOLE		SPECIFIC VOLUME CU.FT./LB.	
			CALC.	EXP.	CALC.	EXP.
159.82	172.6	1.27733	20.719	20.717	0.03283	0.03283
159.79	198.2	1.27766	20.718	20.695	0.03279	0.03276
159.72	364.9	1.28088	20.703	20.675	0.03242	0.03238
159.75	525.3	1.28355	20.691	20.676	0.03212	0.03210
159.79	631.5	1.28584	20.680	20.727	0.03186	0.03194
159.75	744.4	1.28678	20.675	20.659	0.03176	0.03174
159.79	856.9	1.28828	20.668	20.661	0.03160	0.03159
159.89	974.6	1.28985	20.660	20.653	0.03143	0.03142
159.86	1090.8	1.29135	20.653	20.646	0.03127	0.03126
159.89	1184.8	1.29244	20.647	20.638	0.03115	0.03114
159.96	1301.7	1.29371	20.641	20.620	0.03102	0.03099
160.03	1381.6	1.29464	20.636	20.620	0.03092	0.03090
160.10	1459.9	1.29557	20.631	20.620	0.03082	0.03081

TABLE 14. (CONTINUED)

TEMPERATURE DEG. F	PRESSURE PSIA	N	MOLAR REFRACTIVITY CC/G-MOLE		SPECIFIC VOLUME CU.FT./LB.	
			CALC.	EXP.	CALC.	EXP.
219.96	328.8	1.23681	20.819	20.627	0.03823	0.03788
219.93	441.1	1.24269	20.807	20.672	0.03734	0.03710
220.00	521.7	1.24585	20.800	20.665	0.03687	0.03664
220.10	632.9	1.24982	20.791	20.685	0.03631	0.03613
220.03	754.8	1.25345	20.782	20.676	0.03581	0.03563
219.96	815.4	1.25525	20.778	20.691	0.03556	0.03542
220.00	874.6	1.25686	20.774	20.700	0.03535	0.03523
219.93	1034.2	1.26064	20.764	20.716	0.03485	0.03478
220.10	1159.8	1.26318	20.757	20.677	0.03453	0.03440
220.20	1285.1	1.26564	20.751	20.686	0.03422	0.03412
220.03	1528.6	1.27000	20.739	20.681	0.03369	0.03360

TABLE 14. (CONTINUED)

TEMPERATURE DEG. F	PRESSURE PSIA	N	MOLAR REFRACTIVITY CC/G-MOLE		SPECIFIC VOLUME CU.FT./LB.	
			CALC.	EXP.	CALC.	EXP.
249.96	527.8	1.21871	20.785	20.611	0.04114	0.04080
249.96	583.1	1.22276	20.780	20.715	0.04042	0.04030
249.96	638.4	1.22642	20.776	20.666	0.03980	0.03959
249.96	693.7	1.23005	20.772	20.771	0.03920	0.03920
249.96	748.9	1.23234	20.769	20.731	0.03883	0.03876
249.96	804.2	1.23485	20.766	20.736	0.03843	0.03838
249.96	859.5	1.23723	20.763	20.743	0.03806	0.03803
249.96	914.8	1.23931	20.760	20.737	0.03775	0.03771
249.96	970.1	1.24123	20.757	20.739	0.03746	0.03743
249.96	1025.4	1.24297	20.755	20.745	0.03720	0.03719
249.96	1080.7	1.24427	20.753	20.703	0.03701	0.03693
249.96	1136.0	1.24637	20.750	20.740	0.03671	0.03670
249.96	1228.1	1.24894	20.746	20.737	0.03635	0.03634

TABLE 14. (CONTINUED)

TEMPERATURE DEG. F	PRESSURE PSIA	N	MOLAR REFRACTIVITY CC/G-MOLE		SPECIFIC VOLUME CU.FT./LB.	
			CALC.	EXP.	CALC.	EXP.
249.96	1283.4	1.25034	20.744	20.743	0.03616	0.03616
249.96	1338.7	1.25177	20.742	20.732	0.03596	0.03595
249.96	1394.0	1.25344	20.739	20.774	0.03574	0.03580
249.96	1449.3	1.25422	20.738	20.729	0.03563	0.03562
249.96	1486.1	1.25506	20.737	20.752	0.03552	0.03555

TABLE 15. EXPERIMENTAL REFRACTIVE INDEX DATA FOR CARBON DIOXIDE

TEMPERATURE DEG. F	PRESSURE PSIA	N	RLL CC/G-MOLE	SPEC. VOL. CU.FT./LB.
100.17	14.9	1.00040	6.645	9.85785
100.17	97.0	1.00263	6.645	1.51382
100.17	168.6	1.00468	6.645	0.85285
100.17	244.7	1.00697	6.645	0.57246
100.17	321.2	1.00942	6.645	0.42408
100.13	395.4	1.01197	6.646	0.33408
100.17	474.2	1.01478	6.646	0.27068
99.96	547.7	1.01764	6.646	0.22682
99.96	694.3	1.02427	6.646	0.16508
100.10	767.0	1.02806	6.646	0.14291
100.17	818.9	1.03104	6.646	0.12926
100.17	883.5	1.03518	6.646	0.11412
100.17	933.8	1.03894	6.645	0.13318
100.17	1011.1	1.04694	6.645	0.08572
100.17	1078.8	1.05364	6.644	0.07509
100.00	1133.8	1.06275	6.642	0.06428
100.00	1177.8	1.07331	6.640	0.05512
100.00	1202.1	1.08319	6.637	0.04865
100.06	1224.5	1.09438	6.633	0.04296
100.10	1245.4	1.10738	6.628	0.03783

TABLE 15. (CONTINUED)

TEMPERATURE DEG. F	PRESSURE PSIA	N	RLL CC/G-MOLE	SPEC. VOL. CU.FT./LB.
100.17	1263.6	1.11778	6.623	0.03454
100.03	1293.1	1.13061	6.617	0.03120
99.86	1308.8	1.13541	6.614	0.03012
100.00	1343.5	1.14212	6.610	0.02872
99.93	1370.3	1.14685	6.607	0.02781
100.10	1403.2	1.15061	6.605	0.02713
100.10	1443.5	1.15431	6.603	0.02649
100.20	1470.3	1.15654	6.601	0.02612
100.27	1476.7	1.15667	6.601	0.02610
100.17	1480.4	1.15706	6.601	0.02604

TABLE 15. (CONTINUED)

TEMPERATURE DEG. F	PRESSURE PSIA	N	RLL CC/G-MOLE	SPEC. VOL. CU.FT./LB.
100.06	139.5	1.00382	6.645	1.04463
100.00	262.2	1.00737	6.645	0.54211
100.00	429.0	1.01294	6.646	0.30896
100.17	627.5	1.02081	6.646	0.19248
99.86	719.7	1.02540	6.646	0.15777
99.75	812.2	1.03041	6.646	0.13193
99.79	940.9	1.03932	6.645	0.10218
99.82	1093.1	1.05569	6.643	0.07235
99.82	1162.9	1.06938	6.641	0.05821
99.93	1192.8	1.07883	6.638	0.05130
100.03	1214.0	1.08816	6.635	0.04594
100.13	1236.8	1.10160	6.630	0.03995
100.41	1267.0	1.11757	6.623	0.03460
100.41	1299.5	1.13059	6.617	0.03121
100.03	1359.9	1.14463	6.609	0.02823
99.82	1350.2	1.14426	6.609	0.02830
99.65	1412.9	1.15241	6.604	0.02682
100.17	1488.6	1.15797	6.600	0.02589
100.34	1499.1	1.15817	6.600	0.02586

TABLE 15. (CONTINUED)

TEMPERATURE DEG. F	PRESSURE PSIA	N	RLL CC/G-MOLE	SPEC. VOL. CU.FT./LB.
159.89	63.1	1.00160	6.645	2.48115
159.89	178.9	1.00450	6.645	0.88714
159.93	294.4	1.00749	6.645	0.53334
159.93	411.4	1.01074	6.646	0.37205
160.03	632.6	1.01759	6.646	0.22754
159.93	743.7	1.02150	6.646	0.18631
160.03	839.8	1.02503	6.646	0.16009
160.03	949.7	1.02938	6.646	0.13652
160.06	1051.1	1.03372	6.646	0.11905
160.10	1175.9	1.03960	6.645	0.10146
160.13	1294.3	1.04582	6.645	0.08779
160.10	1420.5	1.05331	6.644	0.07556
160.10	1421.3	1.05336	6.644	0.07549
160.06	1480.3	1.05721	6.643	0.07044
160.06	1482.0	1.05748	6.643	0.07012

TABLE 15. (CONTINUED)

TEMPERATURE DEG. F	PRESSURE PSIA	N	RLL CC/G-MOLE	SPEC. VOL. CU.FT./LB.
219.72	89.4	1.00200	6.645	1.98643
219.72	126.3	1.00286	6.645	1.39487
219.68	163.3	1.00369	6.645	1.07980
219.68	200.2	1.00456	6.645	0.87449
219.72	237.2	1.00541	6.645	0.73712
219.72	274.1	1.00627	6.645	0.63710
219.65	311.1	1.00715	6.645	0.55840
219.72	348.0	1.00804	6.645	0.49705
219.72	385.0	1.00900	6.645	0.44372
219.72	421.9	1.00985	6.645	0.40550
219.72	458.9	1.01079	6.645	0.37047
219.65	495.8	1.01172	6.646	0.34104
219.65	532.8	1.01267	6.646	0.31554
219.65	569.7	1.01369	6.646	0.29217
219.65	606.7	1.01467	6.646	0.27266
219.65	643.6	1.01562	6.646	0.25614
219.62	680.6	1.01662	6.646	0.24080
219.72	717.5	1.01762	6.646	0.22720
219.72	754.5	1.01870	6.646	0.21410
219.72	791.4	1.01978	6.646	0.20245
219.72	828.4	1.02081	6.646	0.19246
219.68	852.4	1.02159	6.646	0.18553

TABLE 15. (CONTINUED)

TEMPERATURE DEG. F	PRESSURE PSIA	N	RLL CC/G-MOLE	SPEC. VOL. CU.FT./LB.
219.68	865.3	1.02189	6.650	0.18312
219.68	902.3	1.02313	6.650	0.17331
219.79	976.2	1.02526	6.651	0.15880
219.79	939.2	1.02429	6.651	0.16506
219.82	1013.1	1.02643	6.651	0.15177
219.82	1050.1	1.02764	6.651	0.14516
219.82	1087.0	1.02872	6.651	0.13975
219.93	1124.0	1.02998	6.651	0.13391
219.86	1160.9	1.03112	6.652	0.12903
219.89	1197.9	1.03241	6.652	0.12392
219.86	1234.8	1.03364	6.652	0.11944
219.93	1271.8	1.03494	6.652	0.11500
219.89	1308.7	1.03617	6.652	0.11114
219.93	1327.2	1.03688	6.652	0.10902
219.96	1345.7	1.03749	6.652	0.10725
219.96	1364.1	1.03817	6.652	0.10536
219.96	1382.6	1.03886	6.652	0.10350
219.96	1401.1	1.03950	6.652	0.10182
220.00	1419.6	1.04021	6.652	0.10004
220.00	1438.0	1.04092	6.653	0.09832
220.00	1456.5	1.04150	6.653	0.09696
220.00	1475.0	1.04221	6.653	0.09535

TABLE 15. (CONTINUED)

TEMPERATURE DEG. F	PRESSURE PSIA	N	RLL CC/G-MOLE	SPEC. VOL. CU.FT./LB.
249.82	232.9	1.00500	6.645	0.79869
249.79	340.5	1.00743	6.645	0.53719
249.79	456.6	1.01007	6.645	0.39683
249.86	633.9	1.01433	6.646	0.27900
249.82	895.3	1.02112	6.646	0.18962
249.82	761.1	1.01756	6.646	0.22786
249.86	868.0	1.02046	6.646	0.19575
249.93	980.4	1.02349	6.646	0.17053
249.96	1087.0	1.02645	6.646	0.15157
249.96	1183.9	1.02931	6.646	0.13682
250.20	1337.2	1.03396	6.646	0.11818
250.20	1444.9	1.03732	6.645	0.10762
250.20	1580.9	1.04173	6.645	0.09633

TABLE 16. EXPERIMENTAL REFRACTIVE INDEX DATA FOR ETHANE

TEMPERATURE DEG. F	PRESSURE PSIA	N	RLL CC/G-MOLE	SPEC. VOL. CU.FT./LB.
100.55	29.7	1.00143	11.231	6.26607
100.55	59.9	1.00282	11.233	3.17966
100.55	152.2	1.00746	11.239	1.20653
100.55	244.4	1.01274	11.246	0.70762
100.58	304.6	1.01635	11.250	0.55206
100.58	392.0	1.02256	11.257	0.40082
100.58	487.6	1.03051	11.266	0.29704
100.58	576.5	1.04008	11.275	0.22667
100.58	668.8	1.05441	11.286	0.16762
100.58	705.7	1.06289	11.292	0.14533
100.58	733.4	1.07192	11.297	0.12737
100.58	751.8	1.08072	11.302	0.11372
100.55	770.3	1.09371	11.306	0.09826
100.55	781.0	1.10480	11.309	0.08808

TABLE 16. (CONTINUED)

TEMPERATURE DEG. F	PRESSURE PSIA	N	RLL CC/G-MOLE	SPEC. VOL. CU.FT./LB.
100.55	788.7	1.11696	11.310	0.07914
100.27	797.9	1.13329	11.309	0.06968
100.51	816.4	1.14620	11.307	0.06370
100.41	853.3	1.16277	11.301	0.05740
100.41	908.6	1.17192	11.296	0.05444
100.41	945.5	1.17778	11.293	0.05271
100.41	1037.8	1.18669	11.288	0.05027
99.48	1037.8	1.18669	11.288	0.05027
99.48	1111.6	1.19221	11.284	0.04888
99.65	1168.8	1.19548	11.281	0.04809
99.48	1185.4	1.19662	11.280	0.04782
99.65	1277.6	1.20128	11.277	0.04675
99.65	1462.1	1.20869	11.270	0.04514
99.65	1554.4	1.21188	11.268	0.04449

TABLE 16. (CONTINUED)

TEMPERATURE DEG. F	PRESSURE PSIA	N	RLL CC/G-MOLE	SPEC. VOL. CU.FT./LB.
160.44	13.2	1.00053	11.230	16.88352
160.44	38.3	1.00164	11.232	5.45853
160.44	69.2	1.00295	11.234	3.04059
160.44	84.7	1.00356	11.234	2.52396
160.44	143.0	1.00623	11.238	1.44441
160.44	253.5	1.01144	11.244	0.78755
160.44	345.7	1.01623	11.250	0.55626
160.44	437.8	1.02142	11.256	0.42196
160.44	561.3	1.02914	11.264	0.31085
160.44	677.4	1.03776	11.273	0.24045
160.44	762.2	1.04503	11.279	0.20202
160.44	854.4	1.05412	11.286	0.16851
160.44	898.6	1.05884	11.290	0.15517
160.44	972.3	1.06762	11.295	0.13532
160.44	1046.0	1.07779	11.300	0.11792
160.44	1119.8	1.08941	11.305	0.10288
160.44	1156.6	1.09541	11.307	0.09655
160.44	1248.8	1.11037	11.310	0.08374
160.44	1322.5	1.12179	11.310	0.07608
160.44	1377.8	1.12960	11.310	0.07162
160.44	1411.7	1.13424	11.309	0.06921
160.44	1451.5	1.13837	11.308	0.06720
160.44	1469.9	1.14048	11.308	0.06622
160.44	1543.6	1.14804	11.306	0.06293

TABLE 16. (CONTINUED)

TEMPERATURE DEG. F	PRESSURE PSIA	N	RLL CC/G-MOLE	SPEC. VOL. CU.FT./LB.
219.48	41.2	1.00153	11.232	5.86831
219.51	115.0	1.00439	11.235	2.04578
219.65	188.7	1.00740	11.239	1.21553
219.93	299.3	1.01213	11.245	0.74337
219.86	409.8	1.01704	11.251	0.52992
219.31	520.4	1.02254	11.257	0.40117
219.44	612.6	1.02720	11.262	0.33283
219.51	723.1	1.03340	11.269	0.27155
219.51	815.3	1.03892	11.274	0.23339
219.48	903.8	1.04452	11.279	0.20431
219.48	977.5	1.04966	11.283	0.18341
219.31	1051.2	1.05516	11.287	0.16535
219.44	1124.9	1.06041	11.291	0.15119
219.51	1198.6	1.06618	11.294	0.13821
219.65	1272.4	1.07241	11.298	0.12651
219.89	1346.1	1.07844	11.301	0.11697
220.00	1419.8	1.08494	11.303	0.10818
220.00	1493.5	1.09146	11.306	0.10062
219.65	1567.2	1.09801	11.307	0.09404

TABLE 16. (CONTINUED)

TEMPERATURE DEG. F	PRESSURE PSIA	N	RLL CC/G-MOLE	SPEC. VOL. CU.FT./LB.
249.79	84.0	1.00303	11.234	2.95480
249.44	301.8	1.01157	11.245	0.77767
249.55	506.0	1.02021	11.255	0.44636
249.55	696.6	1.02933	11.265	0.30839
249.55	872.1	1.03877	11.274	0.23389
249.55	1024.7	1.04759	11.281	0.19101
249.55	1163.6	1.05629	11.288	0.16184
249.55	1293.4	1.06493	11.293	0.14061
249.58	1426.1	1.07409	11.298	0.12351
249.48	1507.5	1.07960	11.301	0.11511
249.48	1565.8	1.08370	11.303	0.10957

Table 17. Experimental Equilibrium Phase Properties for the i-Butane-Carbon Dioxide System

100°F

Pressure psia	Liquid x_{CO_2}	Liquid n	Liquid v^*	Vapor y_{CO_2}	Vapor n	Vapor v^*	K_{CO_2}	K_{i-C_4}
105	.0251	1.30420	1.716	.2657	1.00795	51.17	10.586	0.7532
179	.0881	1.30038	1.660	.5668	1.01040	29.38	6.434	0.4751
309	.2056	1.28606	1.588	.7297	1.01517	16.55	3.549	0.3403
401	.2891	1.27653	1.531	.7872	1.01929	12.02	2.723	0.2993
514	.3991	1.26249	1.458	.8267	1.02469	8.858	2.071	0.2884
632	.5195	1.24473	1.382	.8480	1.03133	6.758	1.632	0.3163
733	.6205	1.22691	1.327	.8690	1.03813	5.374	1.400	0.3452
811	.7073	1.21096	1.277	.8822	1.04444	4.515	1.247	0.4025
902	.7828	1.19010	1.271	.8959	1.05405	3.634	1.144	0.4793
971	.8324	1.17053	1.310	.9058	1.06474	2.988	1.088	0.5621
1018	.8694	1.15554	1.349	.9125	1.07501	2.554	1.050	0.6700
1042	.8845	1.14372	1.419	.9154	1.08533	2.238	1.035	0.7325

160°F

Pressure psia	Liquid x_{CO_2}	Liquid n	Liquid v^*	Vapor y_{CO_2}	Vapor n	Vapor v^*	K_{CO_2}	K_{i-C_4}
314	.0946	1.26685	1.849	.4154	1.02165	16.55	4.391	0.6457
414	.1573	1.25900	1.814	.5481	1.02598	12.07	3.484	0.5363
530	.2320	1.24895	1.775	.6166	1.03168	9.170	2.658	0.4992
673	.3227	1.23420	1.741	.6706	1.04012	6.794	2.078	0.4863
787	.3930	1.22230	1.717	.7006	1.04862	5.404	1.783	0.4932
908	.4814	1.20202	1.726	.7177	1.06155	4.184	1.491	0.5444
956	.5191	1.19130	1.748	.7209	1.06833	3.757	1.389	0.5804

114

Table 17   (continued)

220°F

Pressure psia	x_{CO_2}	Liquid n	v*	y_{CO_2}	Vapor n	v*	K_{CO_2}	K_{i-C_4}
525	.1242	1.23276	2.061	.3288	1.04537	8.600	2.647	0.7664
583	.1490	1.22061	2.127	.3638	1.04013	9.414	2.442	0.7476
663	.1960	1.21307	2.120	.4054	1.05766	6.251	2.068	0.7396
749	.2390	1.20236	2.150	.4160	1.06696	5.402	1.741	0.7674
830	.2833	1.18891	2.213	.4149	1.08035	4.517	1.465	0.8164
899	.3419	1.16501	2.395	.4369	1.10169	3.509	1.278	0.8556

250°F

Pressure psia	x_{CO_2}	Liquid n	v*	y_{CO_2}	Vapor n	v*	K_{CO_2}	K_{i-C_4}
524	.0597	1.19677	2.536	.1464	1.06502	6.998	2.45	.908
579	.0856	1.19361	2.528	.1865	1.06814	6.478	2.18	.890
659	.1308	1.18092	2.608	.2345	1.08533	4.996	1.79	.881
701	.1601	1.16034	2.865	.2361	1.09833	4.338	1.47	.910

* cu.ft./lb.-mole

Table 18. Experimental Equilibrium Phase Properties for the i-Butane-Ethane System

100.6°F

Pressure psia	Liquid			Vapor			$K_{C_2H_6}$	K_{i-C_4}
	$x_{C_2H_6}$	n	v^*	$y_{C_2H_6}$	n	v^*		
155	.1782	1.29515	1.649	.5524	1.01137	32.68	3.100	0.5447
207	.2742	1.28789	1.606	.6863	1.01418	24.08	2.503	0.4322
219	.2951	1.28616	1.598	—	—	—	—	—
326	.4841	1.26889	1.524	.8277	1.02225	13.92	1.710	0.3340
334	.4978	1.26747	1.519	—	—	—	—	—
401	.5955	1.25551	1.494	.8639	1.02842	10.63	1.451	0.3365
449	.6648	1.24521	1.485	.8879	1.03306	8.977	1.336	0.3344
516	.7536	1.23012	1.485	.9152	1.04032	7.218	1.214	0.3442
584	.8314	1.21232	1.516	.9267	1.05041	5.686	1.127	0.3761
585	.8318	1.21247	1.514	.9370	1.04949	5.590	1.127	0.375
636	.8858	1.19536	1.576	.9481	1.05938	4.792	1.071	0.4529
639	.8875	1.19484	1.577	.9524	1.06075	4.669	1.072	0.423
664	.9135	1.18652	1.611	.9588	—	—	1.050	0.4763
712	.9541	1.16210	1.785	.9788	1.08755	3.188	1.026	0.4619
723	.9626	1.15736	1.825	—	—	—	—	—

160.4°F

Pressure psia	Liquid			Vapor			$K_{C_2H_6}$	K_{i-C_4}
	$x_{C_2H_6}$	n	v^*	$y_{C_2H_6}$	n	v^*		
191	.0367	1.27364	1.899	.1771	1.01750	26.20	4.826	0.8543
224	.0867	1.27060	1.876	.2999	1.01954	22.04	3.459	0.7666
289	.1697	1.26309	1.847	.4513	1.02372	16.71	2.659	0.6609
336	.2328	1.25712	1.827	.5330	1.02704	13.97	2.290	0.6087
418	.3285	1.24638	1.808	.6201	1.03349	10.70	1.888	0.5657
513	.4333	1.23282	1.799	.6962	1.04181	8.164	1.607	0.5361
569	.4931	1.22414	1.801	.7194	1.04860	6.922	1.459	0.5536

Table 18 (cont'd)

Pressure psia	Liquid x_C_2H_6	Liquid n	Liquid v*	y_C_2H_6	Vapor n	Vapor v*	K_C_2H_6	K_$1-C_4$
608	.5366	1.21672	1.811	.7382	–	–	1.376	0.5650
693	.6240	1.19654	1.908	.7766	1.06721	4.827	1.225	0.6104
779	.7118	1.16279	2.127	.7792	1.09324	3.491	1.095	0.7661

219.7°F

Pressure psia	Liquid x_C_2H_6	Liquid n	Liquid v*	y_C_2H_6	Vapor n	Vapor v*	K_C_2H_6	K_$1-C_4$
340	.0226	1.23535	2.206	.0593	1.03640	13.42	2.624	0.9625
394	.0812	1.22958	2.195	.1827	1.04049	11.37	2.250	0.8895
441	.1345	1.22281	2.201	.2657	1.04583	9.631	1.975	0.8582
489	.1638	1.21691	2.225	.3342	1.05073	8.396	2.040	0.7962
532	.2269	1.20801	2.242	.3854	1.05552	7.465	1.699	0.7950
602	.2742	1.20034	2.267	.4048	1.06728	6.106	1.476	0.820
657	.3421	1.18770	2.326	.4554	1.07972	5.019	1.333	0.827
701	.3811	1.16936	2.512	.4694	1.09690	4.109	1.232	0.858
720	.4169	1.14289	2.901	.4690	1.11448	3.492	1.124	0.910

249.6°F

Pressure psia	Liquid x_C_2H_y	Liquid n	Liquid v*	y_C_2H_6	Vapor n	Vapor v*	K_C_2H_6	K_$1-C_4$
464	.0211	1.20680	2.498	.0431	1.05702	8.676	2.043	0.9775

117

Table 18 (cont'd)

Pressure psia	$x_{C_2H_6}$	Liquid n	V*	$y_{C_2H_6}$	Vapor n	V*	$K_{C_2H_6}$	K_{i-C_4}
493	.0583	1.19938	2.541	.1153	1.06390	7.488	1.978	0.9395
545	.1183	–	–	.2031	–	–	1.717	0.9038
574	.1372	1.18525	2.623	.2082	1.08420	5.447	1.517	0.9177
607	.1672	–	–	.2197	1.09064	5.037	1.314	0.9370

* cu.ft./lb.-mole

APPENDIX E

PURE COMPONENT REFRACTIVITIES

Table 19. Pure Component Refractivities

Compound	R_{LL_0} cc/g-mole		Temperature Range deg. F	B cc/g-mole	C/B cc/g-mole
	Na_D	He-Ne			
n-Butane	20.62[1]	20.56	100.24	254±30	-109
			30 - 200	141± 4	- 99[1]
i-Butane	20.68[1]	20.62	100.0	260±25	-107
			159.9	174±25	-111
			220.0	125±25	-108
			250.0	85±25	-106
			100 - 250	66± 6	-109
			30 - 200	143± 4	- 69[1]
Propane	15.92[1]	15.87	30 - 200	83.5± 3	- 77[1]
Ethane	11.26[1]	11.23	30 - 200	27.8± 1	- 72[1]
			30 - 70	23.2± 1	- 72[1]
CO_2	6.663[3]	6.645	77.1	1.30±.3	-211[2]
			121.5	1.25±.3	-211[2]
			211.6	1.17±.3	-211[2]

[1] Sliwinski, P., Z. Physik. Chem., Newe Folge, 63, 263 (1969).

[2] High Density Data, Michels, A., Hamers, J., Physica 4, 995 (1937).

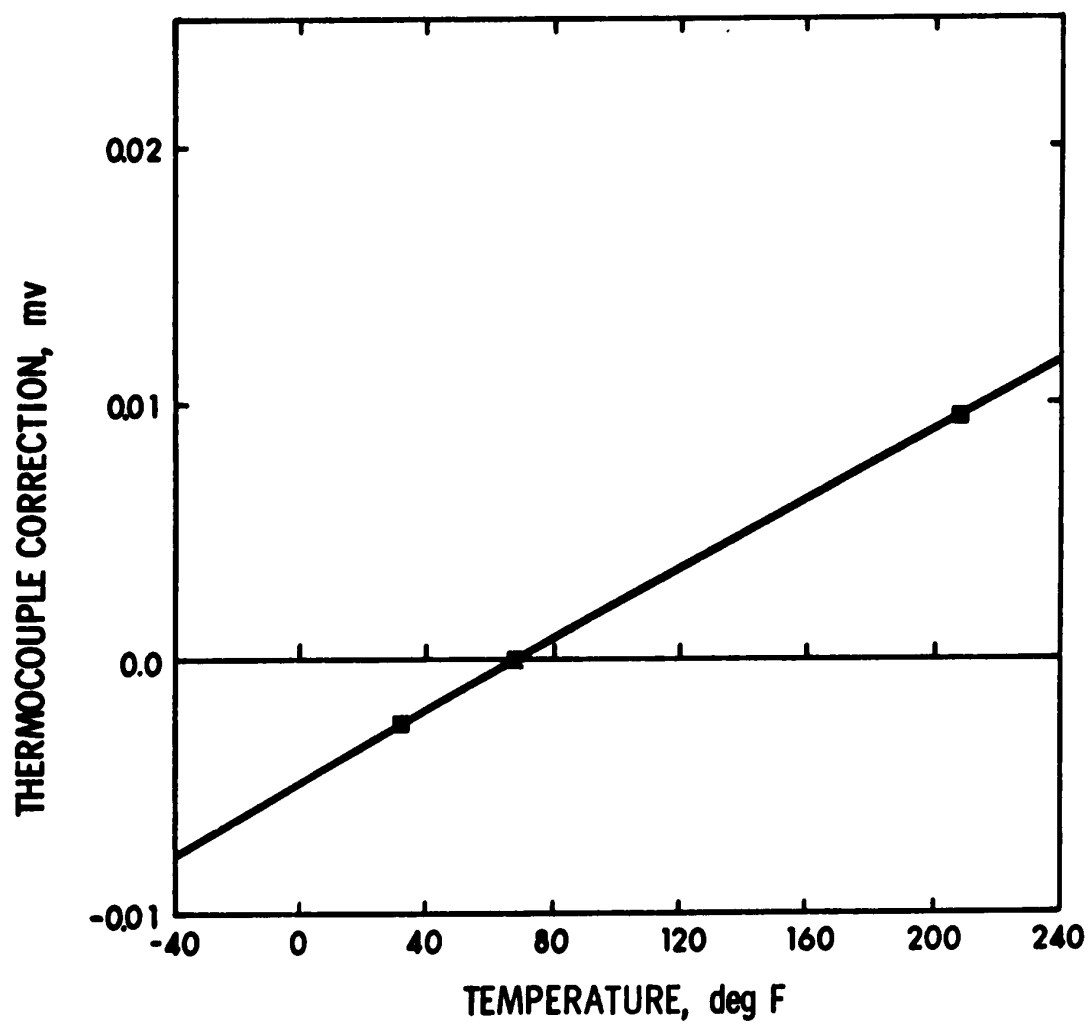[3] Stoll, E., Ann. Physik 69, 81 (1922).

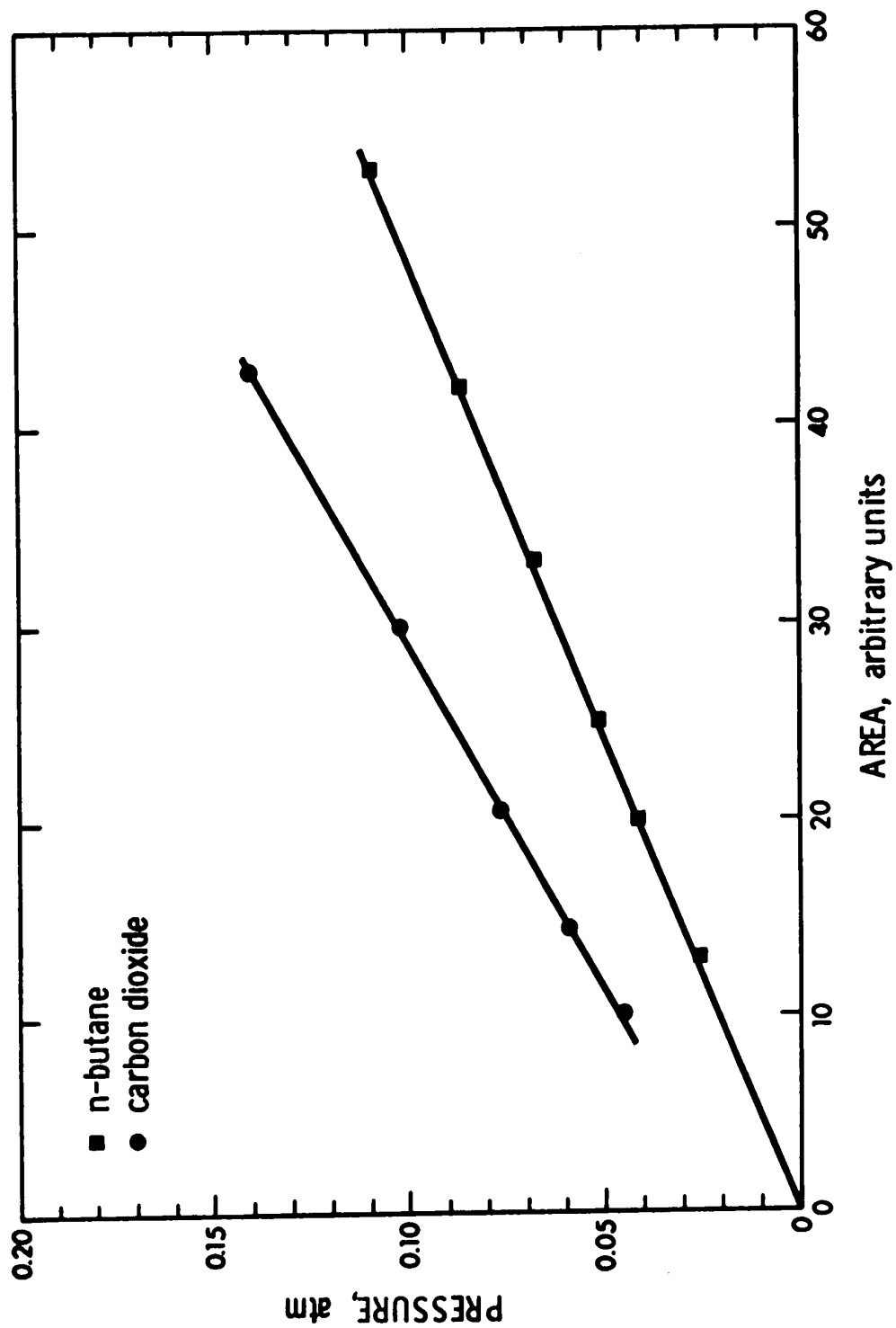# APPENDIX F

CALIBRATIONS

FIG. 28   THERMOCOUPLE CORRECTION

FIG. 29 GAS CHROMATOGRAPH CALIBRATION FOR n-BUTANE-CARBON DIOXIDE

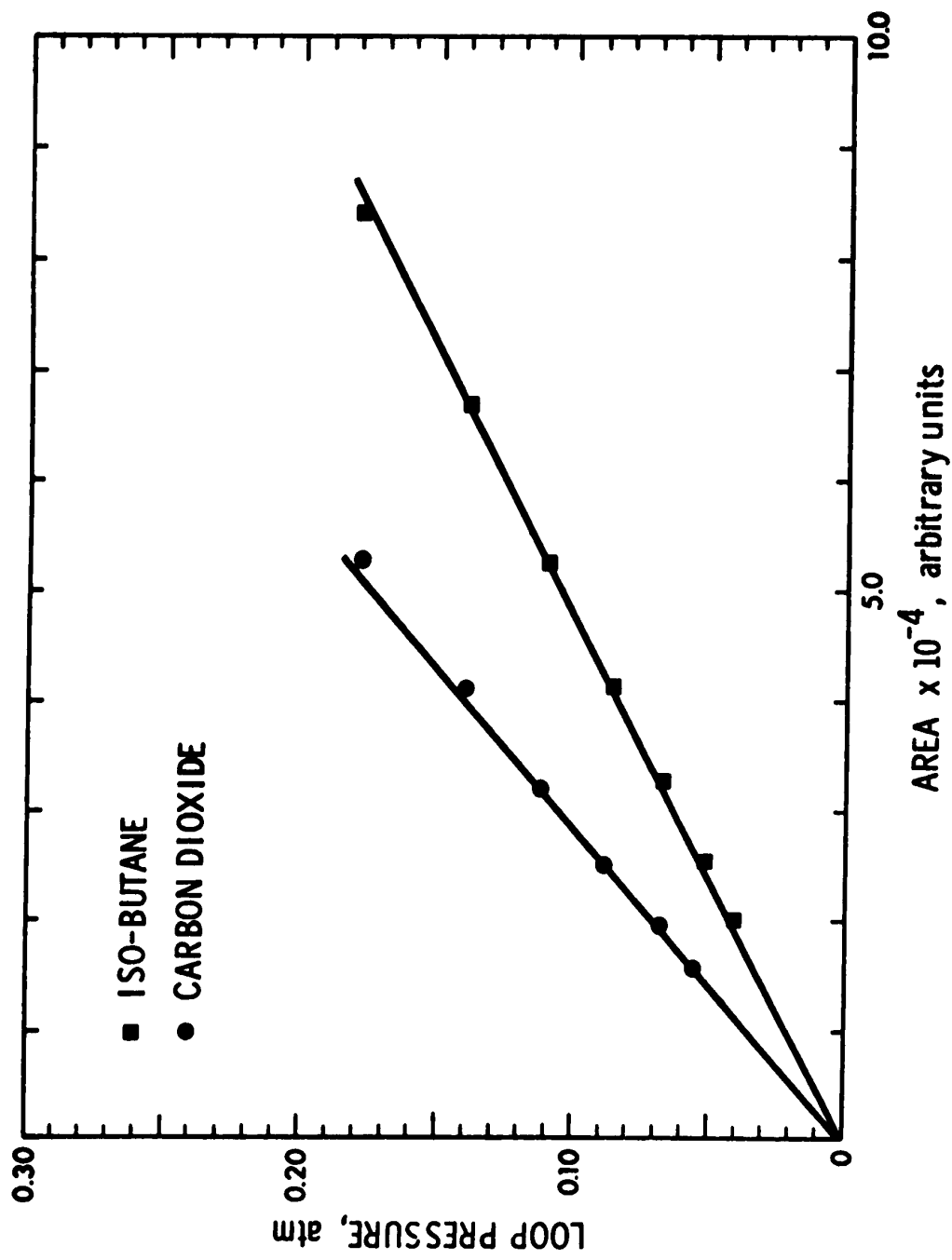

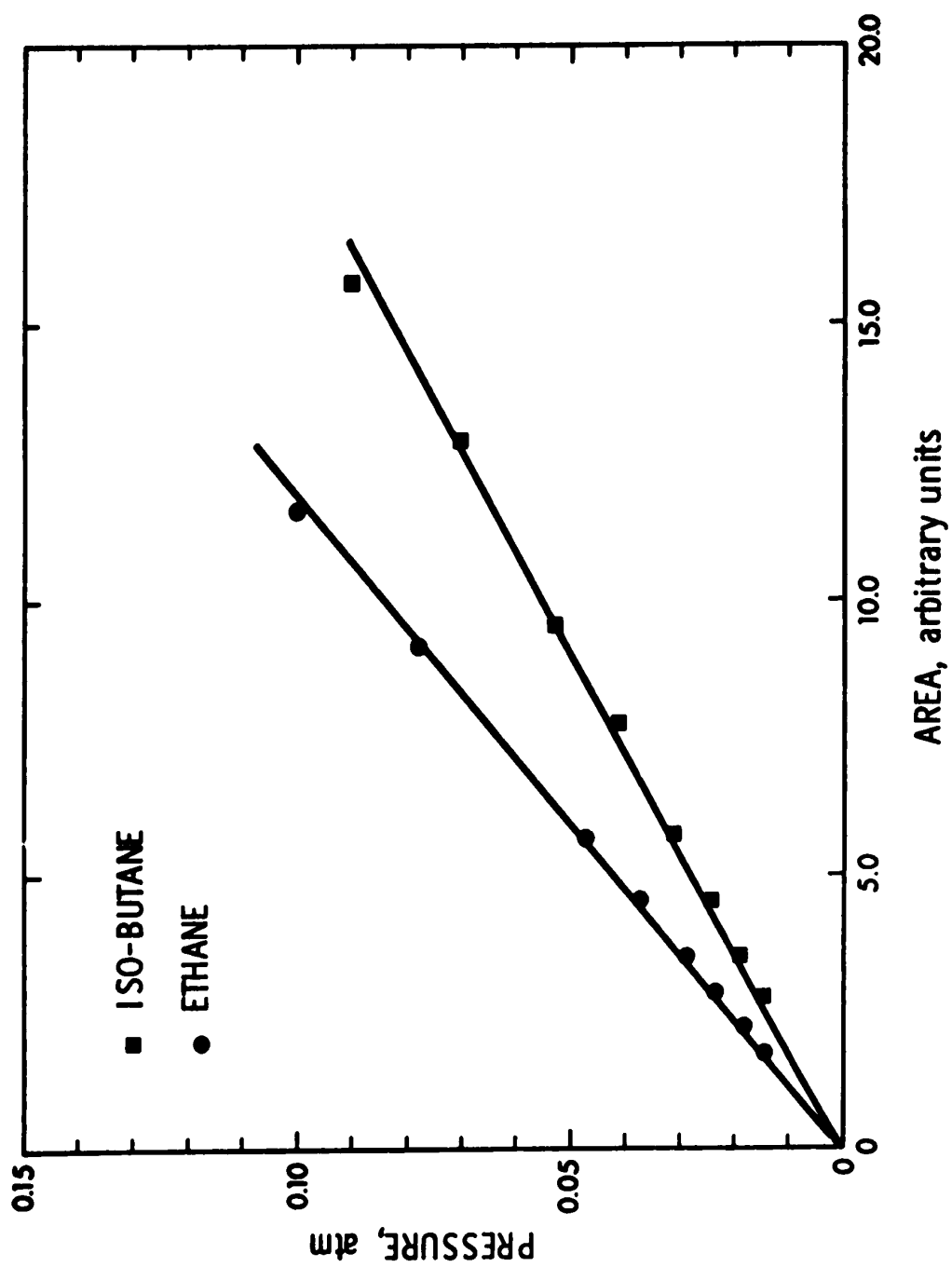FIG. 30   GAS CHROMATOGRAPH CALIBRATION FOR i-BUTANE-CARBON DIOXIDE

FIG. 31   GAS CHROMATOGRAPH CALIBRATION FOR i-BUTANE-ETHANE